

# Aerodynamics of airfoils with leading edge roughness



**Philipp Janoff**  
**DTU Wind-M-0631**  
July 2023

**Author:** Philipp Janoff

**Title:**  
Aerodynamics of airfoils with leading edge roughness

**DTU Wind-M-0631**  
**July 2023**

**Project period:**  
November 2022 - July 2023

**ECTS: 45**

**Education: Master of Science**

**Supervisor(s):**

Anders Smærup Olsen  
Christian Bak

**DTU Wind and Energy Systems**

Rolf Hansen

**LM Wind Power**

Delphine de Tavernier

**TU Delft**

**Remarks:**

This report is submitted as partial fulfillment of the requirements for graduation in the above education at the Technical University of Denmark.

DTU Wind and Energy Systems is a department of the Technical University of Denmark with a unique integration of research, education, innovation and public/private sector consulting in the field of wind and energy. Our activities develop new opportunities and technology for the global and Danish exploitation of wind and energy. Research focuses on key technical-scientific fields, which are central for the development, innovation and use of wind energy and provides the basis for advanced education.

**Technical University of Denmark**  
Department of Wind and Energy Systems  
Frederiksborgvej 399  
DK-4000 Roskilde  
[www.wind.dtu.dk](http://www.wind.dtu.dk)



# Aerodynamics of Airfoils with Leading Edge Roughness

European Wind Energy Master

M.Sc. Thesis Report

by

Philipp Janoff

to obtain the degrees: Master of Science in

Aerospace Engineering · Wind Energy Engineering  
at Delft University of Technology · at Denmark's Technical University

to be defended publicly on August 21, 2023 at 09:00 CET.

*Thesis committee:*

---

|                    |                             |
|--------------------|-----------------------------|
| DTU Supervisor:    | Christian Bak               |
| LMWP Supervisor:   | Rolf Hansen                 |
| TUD Supervisor:    | Delphine de Tavernier       |
| TUD Chair:         | Daniele Ragni               |
| External examiner: | Roland Schmehl              |
| Project Duration:  | November, 2022 - July, 2023 |
| Student numbers    | TUD:5208254 / DTU:203272    |

An electronic version of this thesis is available at <http://repository.tudelft.nl/>.



Danmarks  
Tekniske  
Universitet



Copyright © Philipp Janoff, 2023  
All rights reserved.

# Acknowledgement

With this thesis concluding the final part of my study career, I would like to thank several greatly influential parties. First of all greatest thank goes to my partner Amber who has carried me through all steps in this challenging program through 4 locations in 4 semesters and before, this would have never been as successful without you. Further thanks goes to my family in Germany that have enabled me to start this path to begin with and have been motivating me since early school days. My family in the Netherlands also deserves great thanks for the extraordinary support for and the frequent and well needed breaks from studies even if only for a day. Thank you all for getting me through this and to this point!

The project has been supported by many parties, starting with my supervisor team Delphine de Tavernier, Christian Bak and Rolf Hansen that not only helped defining the project scope, but have also been most frequent meeting group during the project phase to listen to my progresses and plans. Especially great thanks to Rolf for giving me the chance to work in the wind tunnel during this project and to get many unique insights. Related to this, many thanks to Marc Canal for allowing the project to be started in the first place and to Jesper Madsen for jumping in temporarily as daily supervisor when needed. Further great help has been provided by Arun Kumar with simulation runs for which I am thankful. Also, many thanks to Hans Norgaard Paulsen for setting up a large amount of tests and having to go through plenty of airfoil cleaning sessions - tusind tak! Lastly, greatest thanks to my buddy Sergio Flores Perez at LM Wind Power for going above and beyond to introduce me to every aspect besides my own wind tunnel tasks to teach about and introduce to manufacturing, workshop works, protection tapes and rain erosion - I am thankful for our friendship.

# Abstract

Leading edge roughness is an important challenge for the wind energy industry as blades are permanently exposed to the damaging impacts of the environment. The contamination due to impact of insects, ice accretion and dust; as well as the erosion of the blade due to rain, debris and abrasive airborne particles increase roughness upon the surface. Leading edge roughness leads to the deterioration of aerodynamic performance, including early transition from laminar to turbulent flow, increased drag, and reduced lift. These performance losses directly translate into a decreased annual energy production (AEP) and increased levelized costs of energy (LCoE).

The aim of this study is to enhance the understanding of airfoil aerodynamics with LER, specifically focusing on the usage and impact of tripping tapes as a standard representation of LER in wind tunnel campaigns by deviating proven zigzag tapes in non-standard setups. The research objectives include investigating critical roughness height, analyzing the impact of different tripping tape setups, studying drag generation in the boundary layer, and exploring the effects of real erosion.

Contrary to expected reference values, the critical height was found to be traceable with the Roughness Reynolds number for zigzag tape usage as  $Re_k = 125$ , opposing to expected critical Reynolds number  $Re_k = 200$  in current literature. Most interesting application parameter after critical condition, often related to height, is found as tape location. Drag and lift performance penalties behave as linear function of tape location for pre-stall drag bucket and linear lift region. In stall, the performance penalty is heavily related to locations closer to the leading edge with increased importance of tape height. Additionally, real roughness of reference studies has been more closely resembled by tripping tapes closest to the leading edge in terms of magnitude and as function of pitching angles when compared to industry standards. The boundary layer measurements have indicated that panel code simulation data has errors connected to transition location rather than boundary layer development, which reflects in polar data and transition location.

Overall, this study emphasized that ZZT is more versatile than the industry standard setup, highlighting the importance of considering different application variations for accurate assessments of LER impact, while indicating possible panel code improvements related to transition location as observed in performance polars and boundary layer thickness.

**Keywords:**

experimental aerodynamics, airfoil, wind tunnel, leading edge roughness, zig zag tape, critical roughness height, boundary layer, flow transition

# Contents

|   |           |
|---|-----------|
| <b>List of Figures</b>                                    | <b>7</b>  |
| <b>List of Tables</b>                                     | <b>10</b> |
| <b>I The Project</b>                                      | <b>1</b>  |
| <b>1 Introduction</b>                                     | <b>2</b>  |
| 1.1 Report Outline . . . . .                              | 2         |
| 1.2 Relevance of the study . . . . .                      | 3         |
| 1.3 Review of Previous LER Studies . . . . .              | 5         |
| 1.4 Research Question and Objectives . . . . .            | 8         |
| <b>2 Experimental Setup</b>                               | <b>11</b> |
| 2.1 The Wind Tunnel Facility . . . . .                    | 11        |
| 2.2 Airfoil Choice . . . . .                              | 11        |
| 2.3 Roughness Setup . . . . .                             | 12        |
| 2.4 Data Acquisition . . . . .                            | 14        |
| 2.5 Data Correction . . . . .                             | 16        |
| 2.6 Test Matrix . . . . .                                 | 18        |
| <b>II The Research Objectives</b>                         | <b>21</b> |
| <b>3 RO1: Critical Roughness Height</b>                   | <b>22</b> |
| 3.1 Reference Paper Correction . . . . .                  | 22        |
| 3.2 Roughness Reynolds Number Approach . . . . .          | 23        |
| <b>4 RO2: Wind Tunnel Measurements</b>                    | <b>28</b> |
| 4.1 Clean Airfoil. . . . .                                | 28        |
| 4.2 Pressure Distribution Analysis. . . . .               | 31        |
| 4.3 Isolated Deviations from Standard ZZT Setup . . . . . | 32        |
| 4.4 Overview of Performance Penalty Polars . . . . .      | 35        |
| 4.5 Statistics . . . . .                                  | 37        |
| 4.6 Additional Impact of Tape Application . . . . .       | 45        |
| 4.7 Pressure Distribution . . . . .                       | 47        |
| <b>5 RO3: Boundary Layer Rake</b>                         | <b>50</b> |
| 5.1 The BLR Design . . . . .                              | 50        |
| 5.2 Boundary Layer Rake Testing . . . . .                 | 54        |
| 5.3 Results . . . . .                                     | 56        |
| 5.4 Limitations and Improvements. . . . .                 | 57        |
| <b>6 RO4: Step Orientation</b>                            | <b>61</b> |
| <b>7 RO5: Reference Roughness Data</b>                    | <b>63</b> |
| 7.1 Detachable Leading Edge . . . . .                     | 63        |

---

|            |  |           |
|------------|--|-----------|
| 7.2        | Roughness Profiles by Gaudern et al. . . . . | 65        |
| <b>III</b> | <b>The Conclusions</b>                       | <b>68</b> |
| <b>8</b>   | <b>Post Project Reflection</b>               | <b>69</b> |
| 8.1        | Challenges . . . . .                         | 69        |
| 8.2        | Lessons Learned . . . . .                    | 69        |
| <b>9</b>   | <b>Results</b>                               | <b>70</b> |
| 9.1        | Conclusions . . . . .                        | 70        |
| 9.2        | Future Work . . . . .                        | 71        |
| <b>A</b>   | <b>Appendix</b>                              | <b>72</b> |
| A.1        | CL over CD . . . . .                         | 73        |
| A.2        | Polars . . . . .                             | 79        |
| A.3        | 3 Regions for $\Delta CP$ . . . . .          | 89        |
| A.4        | FW vs BW Step . . . . .                      | 92        |
| A.5        | Reference Roughness . . . . .                | 93        |
|            | <b>References</b>                            | <b>98</b> |

# Nomenclature

## List of Abbreviations

|         |   |
|---------|---|
| AEP     | Annual Energy Production                                    |
| AOA     | Angle of Attack   |
| BL      | Boundary Layer  |
| BLMT    | Boundary Layer Momentum Thickness                           |
| BLR     | Boundary Layer Rake   |
| BLT     | Boundary Layer Thickness                                    |
| BW Step | Backward Step   |
| CD      | Drag Coefficient  |
| CFD     | Computational Fluid Dynamics                                |
| CL      | Lift Coefficient  |
| CP      | Pressure Coefficient  |
| DLE     | Detachable Leading Edge (Airfoil Model)                     |
| FW Step | Forward Step  |
| HWA     | Hot Wire Anemometry   |
| LCoE    | Levelized Cost of Energy                                    |
| LE      | Leading Edge  |
| LER     | Leading Edge Roughness                                      |
| LERcat  | LERcat DTU Project on Leading Edge Roughness Categorization |
| PIV     | Particle Image Velocimetry                                  |
| PS      | Pressure Side   |

|        |                               |
|--------|-------------------------------|
| Re     | Reynolds Number               |
| SS     | Suction Side                  |
| WR     | Wake Rake                     |
| WT     | Wind Turbine                  |
| ZZT    | Zigzag Tape with width 12mm   |
| ZZT c5 | ZZT at 5% chord-wise location |
| ZZT w6 | ZZT with width 6mm            |
| ZZT125 | ZZT with height 0.125mm       |
| ZZT205 | ZZT with height 0.205mm       |
| ZZT400 | ZZT with height 0.400mm       |

## List of Symbols

|               |   |
|---------------|---|
| $\beta$       | ZZT angle                                   |
| $x/c$         | Chord-wise airfoil location [%]             |
| $\alpha$      | Angle of Attack                             |
| $\alpha_0$    | Zero Lift Angle of Attack                   |
| $\Delta$      | Difference                                  |
| $\delta_{99}$ | Boundary Layer Thickness                    |
| $\Theta$      | Pressure Tube Directional Sensitivity Angle |
| $f_{vec}$     | Vector Scaling Factor                       |
| $h_{BLR}$     | Boundary Layer Rake Height                  |
| $Re_k$        | Roughness Reynolds Number                   |
| $Re_{k,crit}$ | Critical Roughness Reynolds Number          |

# List of Figures

|      |  |    |
|------|--|----|
| 2.1  | Moving average wake rake drag for ZZT and combined ZZT plus bumptape . . . . .   | 13 |
| 2.2  | Polars and pressure distribution: ZZT with $125\mu m$ height at chord-wise location<br>$x/c = 1\%$ for $Re=2e6$ for $\alpha = [-5, 0, 5, 10]^\circ$ . . . . .        | 14 |
| 2.3  | Pressure tap locations on the DU00-W-212 airfoil model . . . . .   | 15 |
| 2.4  | DU00-W-212 airfoil model imperfections from inspection . . . . .   | 17 |
| 2.5  | Wake rake drag filter mask for data correction on DU00-W-212 experiments . . . . .   | 18 |
| 3.1  | Boundary layer momentum thickness over lift coefficient: data correction from<br>present study simulations and confirmation data from reference author [3] . . . . . | 23 |
| 3.2  | Roughness Reynolds number estimation based on panel code friction coefficient<br>[7] for selected ZZT setups . . . . .   | 24 |
| 3.3  | CL over CD for all tape heights at $Re = [2, 4, 6] \times 10^6$ at $x/c = 1\%$ . . . . .   | 25 |
| 3.4  | CL over CD for all tape heights at $Re = [2, 4, 6] \times 10^6$ at $x/c = 2\%$ . . . . .   | 25 |
| 3.5  | Identified critical height setups in relation to clean airfoil stagnation points . . . . .   | 26 |
| 3.6  | $Re_k$ and $TH/BLMT$ for observed jump response in ZZT setups . . . . .  | 26 |
| 4.1  | Stagnation Point for raw pressure taps and interpolated data . . . . .   | 28 |
| 4.2  | Natural Transition locations from stethoscope measurements and simulation data . . . . .   | 30 |
| 4.3  | ZZT impact on the pressure distribution for ZZT400 at $x/c = [2, 5, 20]\%$ at $AOA=6^\circ$ . . . . .  | 31 |
| 4.4  | Polar data for isolated variation type 1: tape height . . . . .  | 33 |
| 4.5  | POlar data for isolated variation type 2: tape width . . . . .   | 34 |
| 4.6  | POlar data for isolated variation type 3: tape location . . . . .  | 35 |
| 4.7  | Colormap of $\Delta CL/CL_{clean}$ . . . . .   | 36 |
| 4.8  | Colormap of $\Delta CD/CD_{clean}$ . . . . .   | 36 |
| 4.9  | $\Delta$ Lift Slope in the linear region of the Lift Coefficient over the angle of attack,<br>typically $-5^\circ \leq \alpha \leq 8^\circ$ . . . . .                | 37 |
| 4.10 | Angle of Attack for maximum Lift coefficient for the lift polar . . . . .  | 38 |
| 4.11 | Angle of Attack for maximum Lift coefficient for the lift polar at $Re=4e6$ for clean<br>and different zig zag tape setups . . . . .                                 | 39 |
| 4.12 | Maximum Lift coefficient values for the lift polar . . . . .   | 40 |
| 4.13 | Lift coefficient and stall behavior for the lift polar at $Re=4e6$ . . . . .   | 40 |
| 4.14 | $\Delta CL$ over tape location for full range of $\alpha$ . . . . .  | 41 |
| 4.15 | $\Delta CL$ over tape location for positive lift $\alpha \geq -3^\circ$ . . . . .  | 42 |
| 4.16 | $\Delta CL$ over tape location for positive lift pre stall $-3^\circ \leq \alpha \leq 9^\circ$ . . . . .   | 42 |
| 4.17 | $\Delta CL$ over tape location for positive lift in stall $\alpha \geq 9^\circ$ . . . . .  | 43 |
| 4.18 | $\Delta CD$ over tape location for full range of $\alpha$ . . . . .  | 43 |
| 4.19 | $\Delta CD$ over tape location for positive lift $\alpha \geq -3^\circ$ . . . . .  | 44 |
| 4.20 | $\Delta CD$ over tape location for positive lift pre stall $-3^\circ \leq \alpha \leq 9^\circ$ . . . . .   | 44 |
| 4.21 | $\Delta CD$ over tape location for positive lift in stall $\alpha \geq 9^\circ$ . . . . .  | 45 |
| 4.22 | Mean Shifting of the aerodynamic center location due to zigzag tape application<br>normalized by the chord length. . . . .   | 46 |
| 4.23 | Mean Shifting of the Stagnation point in arch length for $\alpha \geq -3$ . Positive values<br>indicate aft shifting over the suction side. . . . .                  | 47 |

|      |  |    |
|------|--|----|
| 4.24 | DU00-W-212 airfoil shape, derivative and curvature . . . . .   | 48 |
| 4.25 | Three identified regions from analysis of $\Delta CP$ force vectors . . . . .  | 49 |
| 5.1  | Conceptual idea of the BLR measurement plane on the DU00-W-212 at $\alpha = 8^\circ$ . . .   | 50 |
| 5.2  | Simulated BLT at $x/c = 0.95$ for 2D-CFD EllipSys and panel code Rfoil over angle of attack . . . . .                                  | 51 |
| 5.3  | U-shaped BLR Pressure Tube Layout with effective 2.5 Diameter distances . . . . .  | 52 |
| 5.4  | Visualization of the CAD design, final BLR instrument with attachment adapter and installation on the DU00-W-212 airfoil . . . . .     | 54 |
| 5.5  | Uncorrected and corrected velocity profile for $Re=6e6$ at $\alpha = 2^\circ$ . . . . .  | 56 |
| 5.6  | BLR Intrusiveness of WR Drag and CP Distribution . . . . .   | 57 |
| 5.7  | Comparison of BLT measurements and simulation cases including proposed Panel Code modification . . . . .                               | 59 |
| 5.8  | Wind Tunnel Tests compared to Simulation Data for polars, BLT and transition location . . . . .  | 60 |
| 6.1  | Forward vs Backward step of 6mm ZTZ wrt. shared reference of 12mm ZTZ . . . . .  | 61 |
| 7.1  | CL,CD comparison with the detachable leading edge model [33] at $Re=6e6$ . . . . .   | 65 |
| 7.2  | CD comparison with Gaudern et al. [7] at $Re=2e6$ . . . . .  | 66 |
| 7.3  | CL comparison with Gaudern et al. [7] at $Re=2e6$ . . . . .  | 67 |
| A.1  | CL over CD at $x/c = -1\%$ . . . . .   | 73 |
| A.2  | CL over CD at $x/c = 0\%$ . . . . .  | 73 |
| A.3  | CL over CD at $x/c = 1\%$ . . . . .  | 74 |
| A.4  | CL over CD at $x/c = 2\%$ . . . . .  | 74 |
| A.5  | CL over CD at $x/c = 3\%$ . . . . .  | 75 |
| A.6  | CL over CD at $x/c = 5\%$ . . . . .  | 75 |
| A.7  | CL over CD at $x/c = 7\%$ . . . . .  | 76 |
| A.8  | CL over CD at $x/c = 8\%$ . . . . .  | 76 |
| A.9  | CL over CD at $x/c = 9\%$ . . . . .  | 77 |
| A.10 | CL over CD at $x/c = 12\%$ . . . . .   | 77 |
| A.11 | CL over CD at $x/c = 20\%$ . . . . .   | 78 |
| A.12 | CL over CD at $x/c = 40\%$ . . . . .   | 78 |
| A.13 | CL,CD,CM Polars for ZTZ with $400\mu m$ height and $12mm$ width at $Re=6m$ and for Locations= $[-1,1,2,3,5,7] \%x/c_{ss}$ . . . . .    | 80 |
| A.14 | CL,CD,CM Polars for ZTZ with $400\mu m$ height and $12mm$ width at $Re=6m$ and for Locations= $[8,9,12,20,40] \%x/c_{ss}$ . . . . .    | 80 |
| A.15 | CL,CD,CM Polars for ZTZ with $400\mu m$ height and $12mm$ width at $Re=4m$ and for Locations= $[-1,1,2,3,5,7] \%x/c_{ss}$ . . . . .    | 81 |
| A.16 | CL,CD,CM Polars for ZTZ with $400\mu m$ height and $12mm$ width at $Re=4m$ and for Locations= $[8,9,12,20,40] \%x/c_{ss}$ . . . . .    | 81 |
| A.17 | CL,CD,CM Polars for ZTZ with $400\mu m$ height and $12mm$ width at $Re=2m$ and for Locations= $[-1,1,2,3,5,7] \%x/c_{ss}$ . . . . .    | 82 |
| A.18 | CL,CD,CM Polars for ZTZ with $400\mu m$ height and $12mm$ width at $Re=2m$ and for Locations= $[8,9,12,20,40] \%x/c_{ss}$ . . . . .    | 82 |
| A.19 | CL,CD,CM Polars for ZTZ with $205\mu m$ height and $12mm$ width at $Re=6m$ and for Locations= $[-1,0,1,2,3,5,7] \%x/c_{ss}$ . . . . .  | 83 |
| A.20 | CL,CD,CM Polars for ZTZ with $205\mu m$ height and $12mm$ width at $Re=6m$ and for Locations= $[8,9,12,20,40,50] \%x/c_{ss}$ . . . . . | 83 |

|  |    |
|--|----|
| A.21 CL,CD,CM Polars for ZTT with $205\mu m$ height and $12mm$ width at $Re=4m$ and for Locations= $[-1,0,1,2,3,5,7] \%x/c_{ss}$ . . . . .     | 84 |
| A.22 CL,CD,CM Polars for ZTT with $205\mu m$ height and $12mm$ width at $Re=4m$ and for Locations= $[8,9,12,20,40,50] \%x/c_{ss}$ . . . . .    | 84 |
| A.23 CL,CD,CM Polars for ZTT with $205\mu m$ height and $12mm$ width at $Re=2m$ and for Locations= $[-1,0,1,2,3,5,7] \%x/c_{ss}$ . . . . .     | 85 |
| A.24 CL,CD,CM Polars for ZTT with $205\mu m$ height and $12mm$ width at $Re=2m$ and for Locations= $[8,9,12,20,40,50] \%x/c_{ss}$ . . . . .    | 85 |
| A.25 CL,CD,CM Polars for ZTT with $125\mu m$ height and $12mm$ width at $Re=6m$ and for Locations= $[-1,0,1,2,3,5,7] \%x/c_{ss}$ . . . . .     | 86 |
| A.26 CL,CD,CM Polars for ZTT with $125\mu m$ height and $12mm$ width at $Re=6m$ and for Locations= $[8,9,12,20,30,40,50] \%x/c_{ss}$ . . . . . | 86 |
| A.27 CL,CD,CM Polars for ZTT with $125\mu m$ height and $12mm$ width at $Re=4m$ and for Locations= $[-1,0,1,2,3,5,7] \%x/c_{ss}$ . . . . .     | 87 |
| A.28 CL,CD,CM Polars for ZTT with $125\mu m$ height and $12mm$ width at $Re=4m$ and for Locations= $[8,9,12,20,30,40] \%x/c_{ss}$ . . . . .    | 87 |
| A.29 CL,CD,CM Polars for ZTT with $125\mu m$ height and $12mm$ width at $Re=2m$ and for Locations= $[-1,0,1,2,3,5,7] \%x/c_{ss}$ . . . . .     | 88 |
| A.30 CL,CD,CM Polars for ZTT with $125\mu m$ height and $12mm$ width at $Re=2m$ and for Locations= $[8,9,12,20,30,40] \%x/c_{ss}$ . . . . .    | 88 |
| A.31 3 Regions at $Re=2e6$ at $\alpha = 6^\circ$ . . . . .   | 89 |
| A.32 3 Regions at $Re=4e6$ at $\alpha = 6^\circ$ . . . . .   | 90 |
| A.33 3 Regions at $Re=6e6$ at $\alpha = 6^\circ$ . . . . .   | 91 |
| A.34 Forward vs Backward step $x/c=1\%$ . . . . .  | 92 |
| A.35 Forward vs Backward step $x/c=12\%$ . . . . .   | 92 |
| A.36 DLE comparison ZTT205c0 . . . . .   | 93 |
| A.37 DLE comparison ZTT400c5 . . . . .   | 94 |
| A.38 CD comparison with Gaudern et al. [7] at $Re=2e6$ . . . . .   | 94 |
| A.39 CL comparison with Gaudern et al. [7] at $Re=2e6$ . . . . .   | 95 |

# List of Tables

|     |  |    |
|-----|--|----|
| 2.1 | Testmatrix for ZZT application on the DU00-W-212 airfoil. 'x' indicates single tape usage on the suction side, while 'o' indicates symmetric application on suction and pressure side. . . . . | 19 |
| 2.2 | Resulting amount of data points from the conducted test series in Table 2.1 . . . .  | 20 |
| 3.1 | Reference paper table as relation of TH/BLMT by Bak et al. [3] with original and corrected data . . . . .  | 23 |
| 4.1 | Standard ZZT Setup Parameters with * indicating frequently used optional combined pressure side application . . . . .  | 32 |
| 4.2 | Three identified regions to vary clearly in pressure impact due to ZZT application within these regions. Starred values indicate the boundaries of tested conditions. .                        | 48 |
| 5.1 | Boundary Layer Rake Design Parameters . . . . .  | 53 |
| 5.2 | Test Matrix of the BLR applied on the DU00-W-212 trailing edge at $x/c = 95\%$ . .   | 55 |
| 7.1 | Ranking the DLE heavy erosion with roughness stages by Sareen et al. [6] and Gaudern et al. [7] . . . . .  | 64 |
| 7.2 | Alternative ZZT setups to resemble DLE erosion patterns . . . . .  | 66 |

# Part I

## The Project

*Roughness on the edge ...*

# Introduction

This document gathers all results and knowledge gathered within the "Aerodynamics of Airfoils with Leading Edge Roughness" graduation project by Philipp Janoff within the "European Wind Energy Master - Rotor Design Aerodynamics" M.Sc. master program by DTU and TUDelft, while collaborating with industry partner LM Wind Power, a GE Renewable Energy business. The general topics and respective chapters are introduced and structured as report outline within a classical 5-7-5 haiku by connecting major aspects of this study, where each row is linked to the coming main chapters as described in Section 1.1:

Roughness on the edge,  
the airfoil performance drops,  
crucial 'LER' impact.  
- Philipp Janoff

Starting with an introduction on ***Roughness on the edge***, as it is described in literature and used within this project on airfoils in wind tunnel testing. Followed by an analysis of measurement campaigns, it can be stated how ***the airfoil performance drops***. Finally, the conclusions rate applications and whether a ***crucial 'LER' impact*** is observed, what makes it crucial and what can be learned from the present study.

## 1.1. Report Outline

This Chapter 1 aims to set the basis to understanding the setup of the report, the importance of this study and the underlying theories that revolve around solving the research questions that are finally presented to kick-off the goals of the present study.

Major aspects of this experimental study are described in Part I, referring to the first row of the haiku stating "***Roughness on the edge***". This section includes the description of the wind tunnel, the airfoil choice, the leading edge roughness setup, available data acquisition channels and the data processing - in summary clarifying, how "***Roughness on the edge***" is to be understood within this study.

The second row "***the airfoil performance drops,***" roughly summarizes the findings and expectations in the following two sections, that are based on experimental and numerical studies considering airfoils. First Part II presents the different experimental work that has been conducted in the wind tunnel at LM Wind Power to provide a detailed measurement campaign with insights on several variables.

Finally, Part III addresses the final row of the haiku stating "*crucial LER impact.*" including analysis and conclusions based on the results of this study, delivering an outline of relevant results, limitations based on assumptions and proposed future work.

## 1.2. Relevance of the study

Leading edge roughness is an important challenge for the wind energy industry [1]. Blades are permanently exposed to the damaging impacts of the environment as they operate in conditions that cause increasing roughness, predominantly chord-wise on the leading edge and span-wise in the high-speed outer board region towards the tip. This rotor tip region is essential to the energy capture and rotational effects are assumed negligible, thus allowing this study to be performed as 2D experimental study, assuming span-wise invariant roughness over an airfoil section in a wind tunnel. The contamination due to impact of insects, ice accretion and dust; as well as the erosion of the blade due to rain, debris and abrasive airborne particles increase roughness upon the surface. Roughness results in the degradation of the aerodynamic performance, mainly coupled with a shift of the transition location towards the leading edge thus early transition from laminar to turbulent flow, a significant increase in drag and a loss in lift. This loss in performance is directly linked with a reduced annual energy production (AEP) and therefore with increasing levelized costs of Energy (LCoE).

The importance of LER research was motivated in the past as the development of pitch-regulated turbines has highly increased the performance of turbines with contaminated surfaces, as stall-regulated turbines are more pronounced to performance penalties due to LER [2], due to the shift in the stall angle of attack. Additionally, the upscaling of wind turbines in the past has caused larger chord lengths and therefore larger Reynolds numbers, resulting in a thinner relative boundary layer (BL) thickness with respect to the chord length. Equally sized roughness patterns are relatively larger in the boundary layer, which is in an important relation observed by Bak et al. [3].

The present importance to optimize wind turbines can be indicated with an estimation in the total cash flow due to production percentage-related losses per MW capacity: combining a total of 30GW installed offshore wind power capacity in 2022 in Europe [4] and an estimated loss of  $5kEur/yr/MW/\%$  [5] results in a yearly loss of 1.5 Million Euros when operating at a production loss of 0.01%. Trends are increasing with additional 116 GW of expected capacity until 2026 [4].

As observed by Sareen et al. [6], roughness highly contributes to AEP losses as high as 5% for light erosion levels due to pits on the blade surface and as high as 25% for heavy erosion due to deeper gorges and chordwise delamination from the LE. The design of blades should therefore be optimized with regards to LER, which is achieved by roughness insensitivity studies and measurement campaigns in the design phase. The typical approach is tripping the flow over an airfoil from laminar to turbulent with the application of turbulator tapes such as zigzag tape. Deviations between design and operational conditions, i.e. tape applications versus real roughness, require improvements to simulate LER within wind tunnel campaigns to optimize the performance of blades in their operational phase. This study therefore aims to improve the understanding regarding aerodynamics of airfoils with LER. The industry standard regarding LER in wind tunnel campaigns is the usage of zigzag tape which is observed to be unrepresentative for real roughness when moving towards high angles of attack or towards heavier erosion, while even light erosion can not be conservatively rated with tripping tapes [7]. Especially the knowledge of drag generation in the boundary layer in the wind tunnel tests is limited and therefore a common question is if standard setups of zigzag tape is representing LER properly for roughness insensitivity design phases.

No basic study on the impact of different tripping tape setups is known to the supervisor team, which is the main motivation to propose this work. This projects aims to experimentally measure and study the impact of leading edge roughness on the aerodynamics of airfoils, with interest within the wind energy sector. This shall be achieved by varying the experimental setup with respect to inflow and tape parameters to simulate effects of real leading edge roughness (LER), while focussing on the usage of tripping tape as it is the industry standard to further understand the process of applying these standards to provide better understanding towards roughness insensitivity studies. Especially a more detailed study of tape locations based on the relative height with respect to the BL thickness will be tested and analyzed as its relevance was requested by Bak et al. [3]. Finally, a detailed study on the drag generation is conducted by investigating the velocity gradient for different setups from the design and construction of an elliptical boundary layer rake in the shape of a winglet, as motivated by Bui et al. [8].

### 1.2.1. Boundary Layer

Forsting et al. [9] concluded that viscous effects are largely negligible for wind turbine blade sections outside of the root region as  $Re_c$  usually exceeds  $1 \times 10^6$  and the flow can therefore be assumed to be inviscid, whereas this is untrue for the surface region where viscous forces are dominant leading towards a thin layer of reduced velocity magnitudes. This region is called the boundary layer. The no-slip condition gives rise to a zero magnitude velocity at the very surface which describes that viscosity leads to a wall shear stress that acts on the flow to yield a velocity gradient/profile as the flow approaches the free stream velocity with increasing distance  $y$  to the surface. The displacement thickness  $\delta^*$  of the BL describes the region where  $u_y/U_\infty \leq 0.99 \times U_\infty$  is true. The BL is driven by the outer inviscid flow and the inside pressure is constant and equal to the pressure on the BL edge. The drag is found to be a function of viscosity  $\mu$  and velocity gradient at the wall  $du/dy$ , with the former only varying slightly thus leading to the latter being the dominant driver of the drag. This raises importance to studying the boundary layer as described in Chapter 5 by usage of a BL rake that was designed for the purposes of this project.

### 1.2.2. Aerodynamic Influence of Roughness

This subsection aims to summarize the influence of roughness elements in the BL and their resulting influence on the aerodynamic performance, though most research focuses on distributed roughness particles within the BL. Roughness types are generally categorized as three types: 2D spanwise strips, isolated 3D elements and distributed 3D roughness. For all types, the main non-dimensional parameters are the relative height with respect to the BL  $k/\delta^*$  and the roughness Reynolds Number  $Re_k$ . For each roughness type, the influence varies providing a unique alteration of the transition process with their respective variations in critical roughness Reynolds number  $Re_{k,crit}$ .

Bragg et al. [10] identified different impacts while documenting the related critical roughness Reynolds Numbers  $Re_k$  for 3D roughness. At the absence of roughness, Tollmien-Schlichting waves cause transition for a clean airfoil at low Mach numbers, by introducing originally linear waves that break down into nonlinear 3D instabilities to form turbulent spots that form the turbulent BL. This process develops within a finite distance that can greatly be decreased with the introduction of roughness as turbulence growth rises rapidly. 3D roughness elements introduce horseshoe vortices at  $Re_k = 300$  and hairpin vortices at  $Re_k = 450$ . The transition bypass process occurs for a further increase in  $Re_k$  that bypasses known linear transition processes as turbulent wedges downstream of the roughness element are formed at larger frequencies than the Tollmien-Schlichting waves. For distributed roughness, the typical values are reported as  $Re_k = 600$ .

Opposing the introduction of flow structures for 3D roughness, Langel et al. [11] observed

2D roughness to rather amplify the naturally occurring transition process by the introduction of Rayleigh instabilities to move the transition point upstream towards the roughness location. The fundamental difference in the phenomena leads to the conclusion that 2D roughness behaves less critically than its 3D equivalent.

### 1.3. Review of Previous LER Studies

The introduction has introduced the general problem of LER impact on airfoils for wind turbine blades. This chapter aims to establish the foundation to perform the research successfully by reviewing previous work to identify the state-of-the-art methodologies, possible objectives and thus the sample. The state of the art in wind power industry and academia regarding the testing of aerodynamics of airfoils with leading edge roughness to investigate roughness insensitivity is tripping tape. It is important to understand methods of the most relevant previous work that was mainly focused on testing actual rough blades, measuring wind turbines in roughness promoting conditions, and especially standard roughness by applying tripping tape due to its easy yet efficient application - as reviewed in this chapter. Only specific focused setups were considered and while important, these are unable to rate the inter-correlation of tripping tape setups, which is being studied in this work. The most relevant influences on aerodynamics with LER as studied as state of the art are mentioned below are critically analyzed per paper and as new setup variations are to be studied, it is of greatest importance to view detailed setup specifics regarding tape choice and location.

Rooij et al. [12] and [13] studied the roughness intensity of several thick airfoils, focussing mostly on mid-span to inner board blade sections close to the root where aerodynamic parameters as a high lift-to-drag ratio are dominating for relative thicknesses above 25 %. 3D flow regime has to be considered close to the root as radial flow is found due to the significant impact of rotational effects, which favors the roughness insensitivity. Earlier transition is found for rotating blades which outweighs the aerodynamic performance penalties due to LER allowing stronger focus on high lift and structural demands, rather than roughness sensitivity as design driver. Increased pressure gradients over the aft part of the suction-side (SS) are found for thick airfoils, leading to premature turbulent separation and therefore reducing the maximum lift coefficient  $C_{L,max}$ . The roughness sensitivity was found to be a function of nose radius and maximum thickness location and designs should aim for lower SS velocities by limiting the SS thickness. For inboard sections, the performance penalties are reduced by rotational effects such that only negligible differences between the clean and rough setup are measured. Problematic is the discrepancy of deviating wind tunnel measurement setups for the different airfoil types as inflow parameters and roughness considerations do not match, thus finally comparing a very broad field of possible influence variables besides the target of researching the individual airfoils. Finally, the test matrix results in only one matching pair of equivalent testing parameters to compare different airfoils with same setup. This motivates the following study to focus on equal test setups for each airfoil. Higher turbulence intensity of the VELUX wind tunnel of 1% opposing 0.1% in test facilities in Delft and Stuttgart causes earlier transition and adversely affects the lift-to-drag ratio. Additionally, different Reynolds Numbers (Re) between  $1.6 \times 10^6$  and  $3.0 \times 10^6$  were considered. Finally, different roughness considerations were used to simulate LER. Some tests based roughness on usage of grit roughness at  $x/c_{SS} = 0.02$  on the suction side (SS) and  $x/c_{PS} = 0.10$  on the pressure side (PS), while zigzag tape (ZZT) of  $0.35mm$  height was used at  $x/c_{SS} = 0.05$  and at  $x/c_{PS} = 0.10$ .

Sareen et al. [6] studied the DU96W180 airfoil for outer board blade region at 75% span with a relative thickness of  $t/c = 18\%$  for three different Re between  $10^6$  and  $1.85 \times 10^6$ . LER was studied by identifying different erosion levels from photographs that were applied to the model in a workshop; additionally insects were simulated by adding discrete particles to both clean and rough

models. Pits and gorges were worked into the model for small, medium and heavy erosion. From photographs it was found that magnitude and chord-wise extent of erosion features is distributed at a ratio of 1 : 1.3 for  $SS : PS$ , which is expected and motivates the tape location in a similar variation between SS and PS. An AEP analysis has been done to conclude that AEP loss due to LER is predominantly due to the outer span region, at a magnitude of up to 5% AEP loss for small erosion with 80% drag increase and up to 25% AEP loss with 500% drag increase for heavy erosion. AEP losses will also be considered but at higher Reynolds number than it was done by Sareen et al.

The NACA 633 418 airfoil has heavily been tested for roughness purposes. White et al. [14] compared a deliberately roughened attachable LE spanning  $0 < x/c < 0.15$  with standard ZYT configuration at  $x/c_{SS} = 0.05$  and at  $x/c_{PS} = 0.10$  for Re between  $1.6 \times 10^6$  and  $3.0 \times 10^6$ . The standard ZYT configuration was found to be unrepresentative for low and high roughness results. The roughness impact upon aerodynamic performance of an airfoil can be summarized with the two main principles of separation and transition due to LER. Separation causes a reduction in  $C_{L,max}$ , increases drag and represents a source of unsteadiness which can cause vibrations in the blade. Premature transition is mostly linked to an increase in drag. The attachable rough nose models 3D roughness that is varying span-wise, while the trip tape represents span-wise invariant 2D roughness. It was mainly found that at deviations in angle of attack (AOA) above or below  $\alpha = 0$ , the rough LE has a more significant impact than the trip tape. Problematic for this study is the low Re and choice of airfoil as it is not a dedicated airfoil for wind turbines and the roughness insensitivity is therefore expected to be rather low. A similar attachable nose setup will be considered in this study as described in Section 1.4.

Ehrmann et al. [15] did a follow-up study as proposed in the previous paper with the same airfoil at  $Re = 3.6 \times 10^6$  with  $60^\circ$  pattern ZYT with an amplitude of  $7mm$  at a turbulence intensity of 0.25%. It is observed that isolated 3D roughness is more critical than 2D roughness and ZYT as well as sandpaper are unrepresentative.

Kruse et al. [16] also tested the NACA 633 418 airfoil with a comparable setup of an attachable rough nose and same tape configurations, but at larger Re that are more representative for wind turbine applications with 3,5 and  $7 \times 10^6$ . The turbulence intensity in the Poul la Cour wind tunnel is 0.1%. Additionally, coarse and fine sandpaper was tested with P40, P400 sandpaper, respectively, where the number denotes particles per square inch. The ZYT was used at same (standard) positions as the previous experiments but with different heights of 0.2, 0.4 and  $0.8mm$ . The variation in tape height gave an almost linear relation to the decrease in maximum lift coefficient  $C_{L,max}$  and as expected the drag coefficient rises with tape height. This is opposite for the sandpaper, where a continuous increase of drag is observed while  $C_{L,max}$  remains almost constant. Unexpectedly, the coarse sandpaper yields the better value for  $C_{L,max}$  compared to the fine sandpaper, but overall higher losses than for the ZYT are found. This results in an over prediction of airfoil performance when considering ZYT results as the loss can be estimated as  $P_{loss} = 1.5\lambda_{local}(C_l/C_d)$ . Results for the attachable nose should be considered critically as the gap in the model is expected to heavily impact the aerodynamic performance and forms a source of errors.

Ozcakmak et al. [17] studied the same NACA 633 418 airfoil for different inflow turbulence and LER effects wrt. transition of the flow. These tests were conducted at the same facility as the present study with a turbulence intensity of 0.1%. This study was conducted at Re between 1.6 and  $6 \times 10^6$ . The measurement setup causes a problem as flush-mounted surface microphones are used that caused a slight deviation from the theoretical airfoil shape. It was observed that the impact of roughness depends upon the size wrt. the boundary layer (BL) thickness, type of roughness, airfoil shape and Reynolds number. The transition location was tracked by observing

a sudden increase in the Sound Pressure Level (SPL). In a second method, the standard deviation increase over the chord was tracked, but this method was ruled out as inflow turbulence results in misleading transition locations. For an increasing velocity, a lower roughness height is required to trigger transition, which can be explained as critical roughness height. The transition point was moved forward towards the LE with an increasing turbulence intensity, coupled with a larger skin friction drag as the turbulent flow covers more parts in the chord-wise direction. Larger turbulence intensity also causes more interaction between single microphones, requiring larger distances between individual microphones.

Bak et al. [3] studied this critical roughness height on several airfoils (NACA0015, Risoe-B1-18, Risoe-C2-18) in the LMWind LSWT in Lunderskov at different Reynolds numbers: 1.6, 3 and  $6 \times 10^6$  for different tapes. Bump tape with a height of  $0.1\text{mm}$  and ZTT with a height of  $0.4\text{mm}$  are mounted at  $x/c = 0.02$  on the SS. It was found that there is a critical roughness height in relation to boundary layer momentum thickness, below which there is no impact of LER upon the aerodynamic performance. This threshold scales related to the chord  $c$  as  $Re_{crit} \propto c^{0.5} < x < c^{0.8}$ . This states that performance penalties due to (constant sized) LER will decrease with increasing chord lengths, which is the industry trend for the upscaling of wind turbines. However, if LER is upscaled equivalent to the chord length, then LER related performance penalties will increase. The relation found in this study is though only valid up to  $Re = 6 \times 10^6$ .

Gaudern et al. [7] studied LE erosion by creating 5 stages of LE nose profiles to model small to heavy erosion at  $Re = 2.2 \times 10^6$  and tested results with ZTT with height  $h_{ZTT} = 0.38\text{mm}$  with a pattern of  $60^\circ$  at  $x/c_{SS} = 0.05$ . The trip tape results in larger performance penalties than the first two stages of erosion. Unexpectedly, the largest drag penalty was observed for stage 4, pointing out the problem that stage 5 (delamination) is probably too clean within and outside of the roughness step that resembles the delamination of the LE. Tripping tape represents low stages well, but overpredicts performance wrt. heavier erosion stages and is therefore not a conservative choice to test roughness impact upon aerodynamic performance. The overprediction of performance by the ZTT case rises with higher AOA. It should be critically seen in this study, that the 5 profiles are created somewhat homogeneous along the span and might not be fully representative of real roughness, as a rather small amount of random roughness elements are used and the step denotes the roughness, the general surface is still rather clean.

Soltani et al. [18] studied the impact of surface contamination upon performance of wind turbine blades by utilizing a contamination model and different tapes at  $x/c_{SS} = 0.05$  with a height  $h_{ZTT} = 0.07\text{mm}$  and very low Reynolds numbers of 0.43, 0.85 and  $1.15 \times 10^6$ . Smooth stall behaviour is observed for the contaminated airfoil and  $C_{L,max}$  is observed to rise with Re. A transition bubble is observed for the clean airfoil (not for the tripped airfoil) at mid-chord. The effect of trip tape upon  $C_{L,max}$  is decreased with increasing Re from a reduction of 29% at low Re to a reduction of 11% at high Re. The ZTT with a pattern of  $60^\circ$  causes a stronger and earlier decrease wrt. AOA in lift, compared to the ZTT with a  $90^\circ$  pattern. The strip tape causes a sharper and slightly earlier stalling behaviour than the  $90^\circ$  ZTT.

Timmer et al. [19] tested the DU97W300 airfoil at very high Re of 1,3 and  $10 \times 10^6$  in the cryogenic wind tunnel of DNW in Cologne, Germany. Wrap around roughness was tested as well as ZTT with height  $h_{ZTT} = 0.4\text{mm}$ . A larger performance decrease of the wrap-around roughness was observed compared to the case with ZTT, but both performances improved significantly with increasing Re. As the transition location moves closer to the LE with LER, the favourable effect of the increasing Re is counterbalanced wrt. boundary layer thickness and stability. For the clean airfoil, there was no clear variation when increasing Re.

Khafallah et al. [2] measured impact of dust on an operating turbine in a dust-heavy site, thus delivering real-life data. Stall- and pitch-regulated turbines are tested and a stall regulated turbine has larger performance penalties approximately by factor 3. Several periods were simulated

with an initial cleaning of the blades: after 1 day a mean power loss of 2.5% is measured, which develops to a mean power loss of 57% after 9 months. Critically, this field study could also be affected by other factors as it is not conducted in a controlled surrounding, but this study shows a trend of the impact of LER from dust.

## 1.4. Research Question and Objectives

From Section 1.3 it can be concluded that LER on airfoils was studied in different variations for wind turbine applications but there is a missing and also by literature proposed sample required to be studied regarding different turbulator tape setups, as turbulator tapes are the established method to simulate LER but its known impact is mainly limited to the standard setup. This chapter aims to introduce the research design of the current study. Zigzag tape has been widely used to force early transition in order to simulate rough airfoil characteristics and it has been found to be unrepresentative for light or heavy roughness levels. Thus it remains unresolved, whether the tape usage in wind tunnel testing is unrepresentative in general or what improvements in the setup can be made to yield better results. The setup by Gaudern et al. [7] was observed to be representative for light roughness stages, but how do the results change with a variation in the setup of the tripping tape? A basic study of the tripping tape is required and is motivated as future work by Bak et al. [3] - and realized within this project - by identifying a trend of the critical roughness height which is to be further researched by a more detailed study on tripping tape in larger variations of the experimental setup that impact the aerodynamic performance of airfoils. This is the starting point of this by Bak et al. proposed thesis project as base research for the parallel running LERcat project on real reference roughness data. Furthermore, the author identified a lack of discussion on the tripping tape usage, as an industry standard method is being cited by various studies while neglecting to question the variation that originate from varying the application parameters.

### 1.4.1. Research Questions

#### Research Objective

To deliver and analyze a detailed data set from various tripping tape applications and therefore improve the understanding of zigzag tape usage in wind tunnel testing when estimating leading edge roughness to simulate aerodynamic performance of rough airfoils. Wind industry importance is motivated as these estimations are the baseline for the roughness-insensitivity design of wind turbine blades. The industry standard application shall be compared and rated with respect to possibilities from variations. Finally, limitations shall be stated when utilizing tripping tapes.

#### Research Question 1

What is the critical roughness height as related to critical Reynolds number  $Re_k$  and to boundary layer momentum thickness ?

#### Research Question 2

What is the influence of varying zig zag tape testing parameters upon performance polars ?

This includes the following sub-tasks:

1. **RQ 2.1** Varying tape height
2. **RQ 2.2** Varying tape width
3. **RQ 2.3** Varying tape location

#### Research Question 3

How does the boundary layer vary for tripping applications as studied by designing, constructing and testing a new measurement instrument?

#### Research Question 4

Which step orientation, as introduced by roughness, is more critical: forward or backward step ?

#### Research Question 5

How do zig zag tape variations compare to real roughness, what setups can more accurately resemble real erosion patterns and what are identified possibilities and limits ?

### 1.4.2. Research Question Focus

However, due to the boundaries of the project, that are heavily dominated by availability of the testing facility and the equipment, a large focus was put on the testing of tape locations. While different airfoils were originally targeted, it became clear that industry partner had a large interest towards the RQ-3, which was given priority as wind tunnel availability was not controlled by the author. To dedicate the study with an increased focus, the tape application with respect to location is prioritized in this study.

When covering roughness studies, it is important to follow the differentiation by White et al. [14], stating to distinguish between either experimental testing to focus on either gross aerodynamic performance such as polars for various configurations, or investigating on underlying phenomena of important observations. This study focuses on the former, motivated to yield more detailed information of tripping tape usage as proposed by Bak et al. [3].

### 1.4.3. Research Objectives

The main objective of this thesis is:

"To deliver a detailed data set from various tripping tape applications and therefore improve the understanding of zigzag tape usage in wind tunnel testing when estimating leading edge roughness to simulate aerodynamic performance of rough airfoils as baseline for the roughness-insensitivity design of wind turbine blades.

The industry standard application shall be rated with respect to variation possibilities and limitations shall be stated when utilizing tripping tapes."

The main research objective (RO) is divided into sub-objectives (RSO) that are related to the process of answering the research questions above. First of all, **RSO 1** describes the proposed future work by Bak et al. to improve study on critical roughness conditions by investigating tripping tape impact close to expected critical conditions and to validate with the literature. **RSO 2** describes the wind tunnel measurement campaign as described in Chapter 2 and the initial usage

of panel code simulations (RFOIL within this publication) to determine the stagnation point of the airfoil for various angles of attack to separate suction and pressure side of the airfoil. This allows to determine boundaries of the variation of tape locations. It should be avoided to place pressure and suction side tape too close to the leading edge, as the stagnation point moves towards the lower surface when pitch angle increases, which results in two tape strips effectively impacting the flow over the upper surface. **RSO 3** is the design, construction and testing of an innovative measurement instrument to study boundary layer for different tripping setups and to validate and conclude findings with respect to simulation data. **RSO 4** is to study whether a FW or BW step is more critical. The chosen airfoil DU-00-W-212 is available with an attachable rough airfoil nose to simulate real rough airfoil performance. Additionally, this allows to print a new pure FW or BW introducing LE pattern to test and validate RQ3. Finally, **RSO 5** is to validate real erosion delivered by the parallel running and connected LERcat project to evaluate how ZZT can possibly be applied differently to better simulate different roughness variations.

# 2

## Experimental Setup

This section summarizes the setup of the experimental study that was conducted, aiming to provide transparency of inputs, tools and methodology. The experimental facility at LM Wind Power is introduced, as well as the airfoil choice and tripping methodology - including all design choices along the project development. Finally, the available data acquisition is discussed and the public general data processing approach is introduced to increase understanding of data treatment to allow reproduction of the test data.

### 2.1. The Wind Tunnel Facility

The measurement campaigns were conducted at the LM Wind Power low-speed wind tunnel (LSWT) in Lunderskov, Denmark. This 102m closed circuit wind tunnel has a test section length of 7.00m, a width of 1.35m and a height of 2.70m with a turbulence intensity of 0.10% [17] which approximately relates to an amplification factor  $N_{crit} = 8$  for numerical simulations with the used solvers. Experiments were conducted at three Reynolds Numbers  $Re = [2, 4, 6] \times 10^6$ , at flow velocities of approximately  $U_{inf} = [33.3, 66.7, 100]ms^{-1}$  respectively.

### 2.2. Airfoil Choice

The airfoil choice for experimental studies is crucial, as this will dominate the overall results. Ideally, a well documented and frequently tested airfoil is chosen to allow a good baseline comparison with existing literature and to advance the understanding starting at a baseline level of reference results. Additionally, this increases the relevance of the study as direct comparisons are enabled to add to the ongoing research in the field of roughness. It is however also important to create new data sets to allow a more broad view on the topic, to ensure general understanding of roughness rather than specified airfoil characteristics. The latter motivates the use of several airfoils to validate results.

The airfoil for this project was chosen as DU00-W-212 with a chord length of  $c = 900mm$ . This choice was mainly motivated by the following points:

- the choice for a publicly available airfoil to avoid disclosure of this project,
- the general availability of airfoils in the wind tunnel (especially with good overall quality and discretization of pressure taps),
- the availability of a detachable leading edge version of this airfoil to allow 3D printed erosion patterns to be tested,
- the choice for a thin airfoil with a maximum thickness below 25% to allow 2D assumptions by having an airfoil that is used in the outer board of a wind turbine blade, thus having negligible rotational flow effects in real operations,

- the availability of reference research to increase relevance of the airfoil choice.

The alternative plan was to allow comparisons to the most cited airfoil from state of the art LER studies in Section 1.3 on the NACA 633-418 airfoil by using the same model, which was shifted by the request to use an airfoil that has not been tested as widely and finally the above mentioned facts have motivated the usage of the DU00-W-212 airfoil. The alternative airfoil was targeted as second airfoil to be used, which did not turn out to be feasible with the shift in project sources and wind tunnel availability, thus a more detailed study on the DU00-W-212 was conducted, knowing the best case would have been a spreading of wind tunnel time, which was however not realizable due to internal adjustments.

## 2.3. Roughness Setup

This section aims to introduce an overview of the performed test series within this experimental campaign of tripping the DU00-W-212 airfoil. First priority was to include the standard ZTZ of  $400\mu\text{m}$  thickness and  $12\text{mm}$  width, see Section 1.3. Secondly, to study the effect of a possible critical height as proposed by Bak et al. [3], the thinnest version at  $125\mu\text{m}$  was included, as well as a  $205\mu\text{m}$  version in-between these choices. The Reynolds Number in the wind tunnel is limited to  $Re = 6e^6$  due to incompressible flow limits at  $Ma = 0.3$  and is further studied at  $Re = 4e^6$  and  $Re = 2e^6$  to allow a thicker boundary layer at lower flow velocities. These Re choices are motivated to allow comparison to the sparsely available reference data of Gaudern et al. [7] and LMWP internal data that is excluded from this report. As wind tunnel time is limited, it was aimed to decrease the testing time, which can be achieved by limiting the angle of attack range and ZTZ setups. The angles were chosen in the operational range  $-10^\circ \leq \alpha \leq 12^\circ$  and therefore excluding deep stall. The locations were restricted to studying single tapes focussing on the suction side to keep the setup simple to allow a first understanding, which is the objective of the present study, knowing that the suction side is dominant in the research on LER [9]. Combined effects of suction and pressure side setups are selectively tested as well for few cases. The resulting test matrix can be seen in Table 2.1.

It is important to state that zigzag tape was applied directly to the airfoil surface, while other researchers tend to apply ZTZ on a flat bump tape as base with lower adhesive strength, as this is easier to remove from the airfoil model and results in less cleaning effort. This combined tape option has been tested by setting up  $205\mu\text{m}$  ZTZ on one side, and setting up  $50\mu\text{m}$  bump tape with  $205\mu\text{m}$  ZTZ on top, resulting in approximately same height of the ZTZ elements. This however resulted in a clear increase of drag when combining bump tape and ZTZ as expected in wake rake measurements. This approach has therefore been excluded from this study, accepting more intense cleaning efforts that decreased the available wind tunnel time due to longer individual testing times at the choice of more precise results of purely testing ZTZ impact rather than combined effects. It was decided that a large uncertainty is else introduced to make conclusions on ZTZ applications, when actually doing purely combined setups. Further reasoning has been the required repeating of test series due to large peaks in the wake rake drag when ZTZ was placed too close to the bump tape edge resulting in de-attachment of the ZTZ spikes which increased the local drag heavily. Additionally, testing different widths of ZTZ would have become difficult, as there is no tape available at the required shorter  $6\text{mm}$  width, again increasing complexity and uncertainty. Finally, this would have also excluded the study of the thinnest possible ZTZ of  $125\mu\text{m}$  which was a setup of high priority due to its comparability with Bak et al. [3].

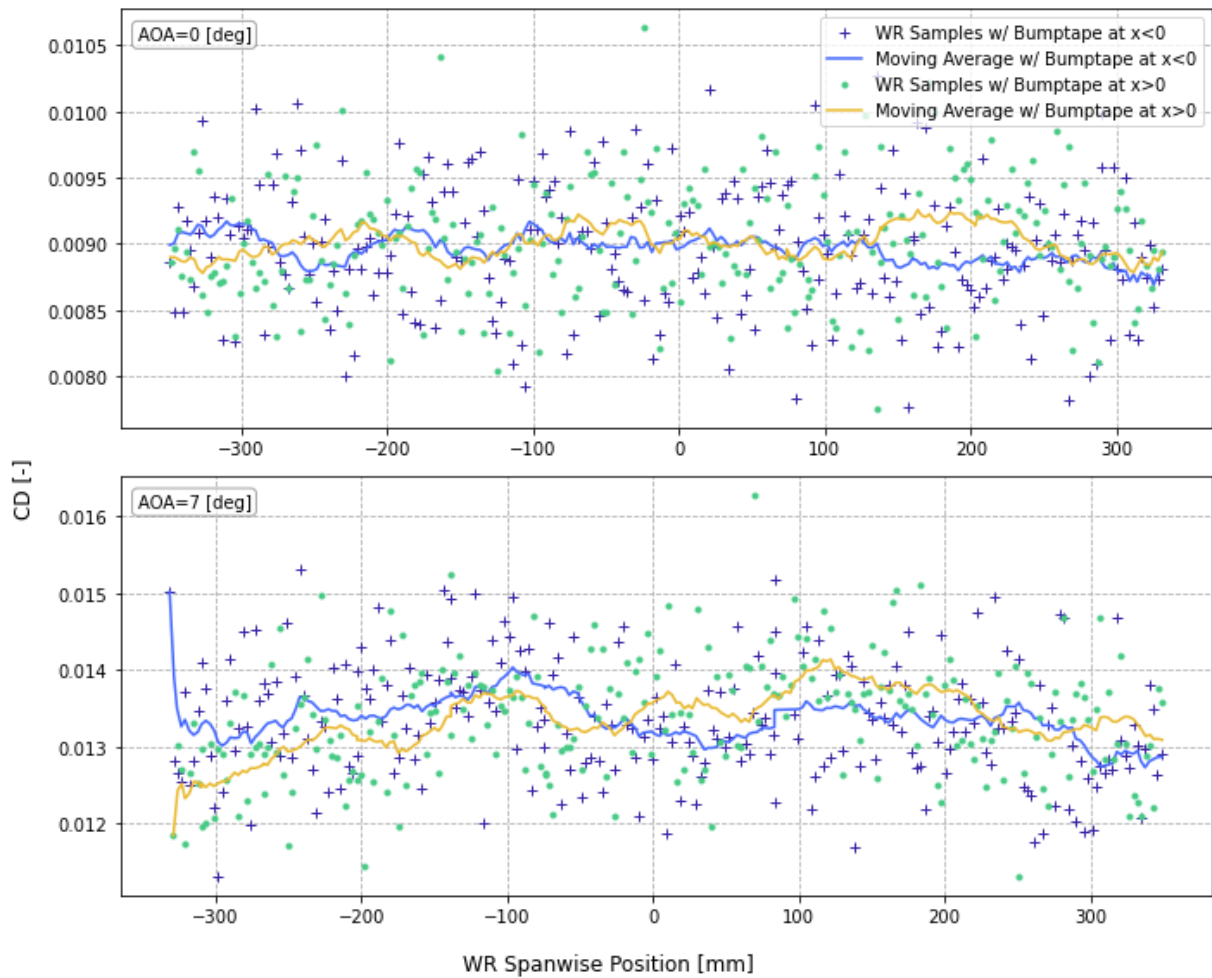


**Figure 2.1:** Moving average wake rake drag for ZZT and combined ZZT plus bumtape

Tripping tapes are overall observed to impact as four distinct points of interest as indicated in Figure 2.2: no relevant impact, critical/initial impact, impact in linear lift and drag bucket, impact in stall. The first two are related to RO1 in Chapter 3, while the latter two are related to RO2 in Chapter 4.

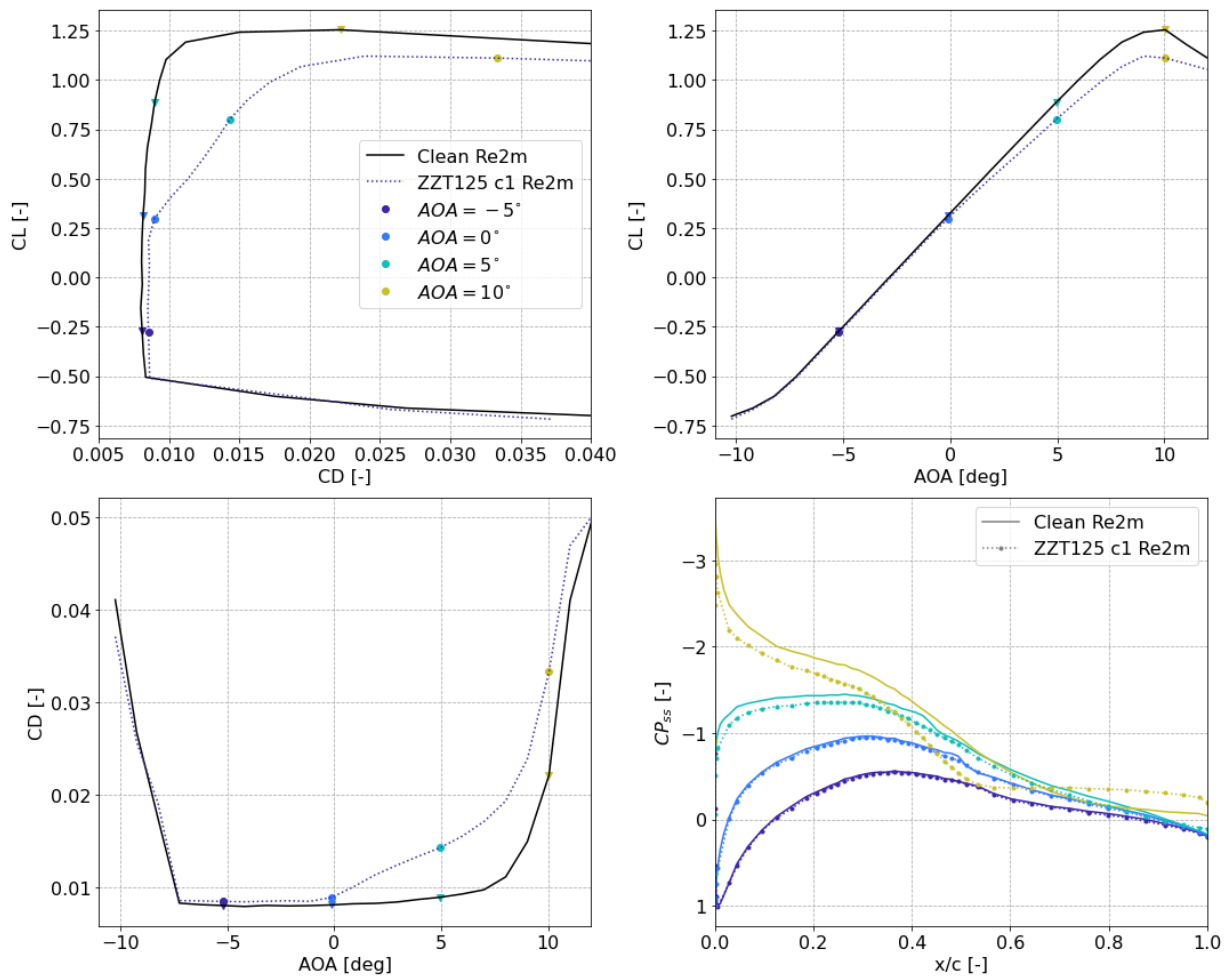


**Figure 2.2:** Polars and pressure distribution: ZTT with  $125\mu m$  height at chord-wise location  $x/c = 1\%$  for  $Re=2e6$  for  $\alpha = [-5, 0, 5, 10]^\circ$

## 2.4. Data Acquisition

The aerodynamic performance was measured using wall pressure, load cells, airfoil pressure taps, a wake rake and additionally by an own design of a boundary layer rake (BLR). The main data is thus composed of pressure readings that can be used to calculate lift, drag and moment polars to evaluate the airfoil performance.

### 2.4.1. Pressure Taps

The airfoil has 88 pressure taps that are distributed on the airfoil model as shown in Figure 2.3. These pressure taps are small holes on the airfoil that are perpendicular to the surface. Static pressure is thus measured on various locations that can be computed to the dynamic pressure distribution by utilizing the difference with respect to the total pressure reference measurements of the pitot tube in the test section inlet. The resulting pressure distribution is furthermore utilized to calculate lift, drag and moment polars to evaluate the airfoil performance at various angles of attack, which has been done by almost all authors stated in Section 1.3, pointing out Timmer et al. [19] and White et al. [14] as representative examples.

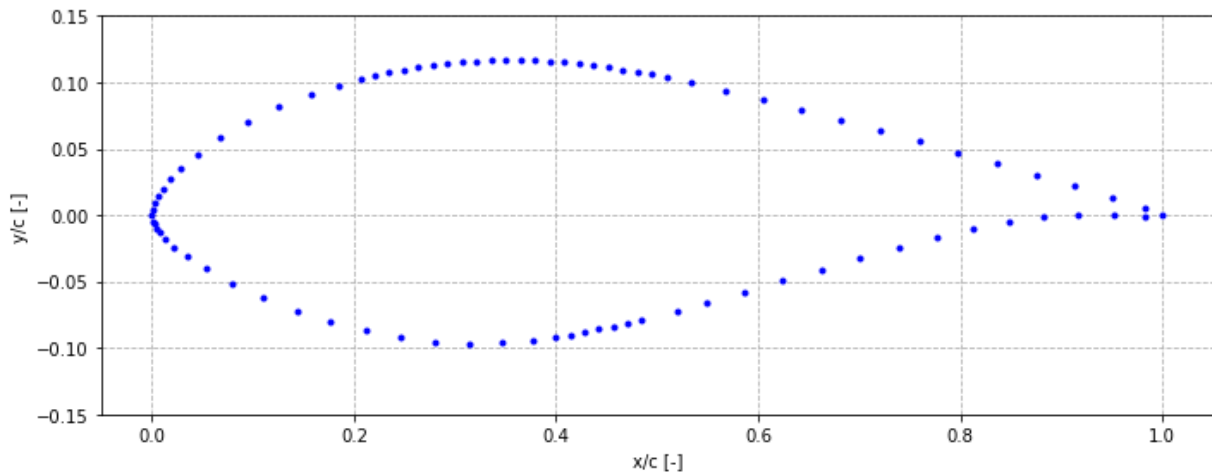


**Figure 2.3:** Pressure tap locations on the DU00-W-212 airfoil model

### 2.4.2. Transition Point Measurements

The pressure distribution of this model is favourable to detect the transition point for the typical operational angles of attack, but further measurements to detect the boundary layer transition point were conducted by utilization of a stethoscope rod that was introduced from the side of the wind tunnel at  $x/c \approx 20\%$ . The experiment leader was equipped with a rod that has a arc shaped end piece that extends towards the measurement tube inlet. The setup is then connected to an audio transducer and the experiment leader is equipped with headphones to detect the flow behavior. Laminar flow resulted in no observable sound, while transition had high frequency sound from Tollmien-Schlichting waves. Turbulent flow causes loud low frequency deep sound, comparable to the sound of old wind turbine hydraulic break systems. Behind ZZT setups, there was either no traceable signal as for laminar flow, or there was turbulence. This confirms the bypass transition behavior, however these measurements had a negligible distance before turbulent flow was observed, such that a quantitative conclusions on bypass distance can not be made without introducing large uncertainties.

### 2.4.3. Wake Rake

Additional pressure measurements are conducted downstream of the airfoil to utilize the momentum deficit approach, again referring to most authors in Section 1.3, pointing out Gaudern et al. [7] and Sareen et al. [6] as representative examples. The wake rake consists of 54 total pressure and 2 static pressure tubes, that are connected to a pressure transducer module. A pressure transducer is a device that exports an electrical signal due to a measured change in pressure. The pressure deficit is computed and integrated according to an algorithm to exclude false measurements when the size of the wake approaches the range of the wake rake. To ensure correct measurements, it is checked whether 3 measurements exist that are indicating free stream conditions in the upper and lower part of the wake rake. If this condition is not met, then the wake is assumed to be too large to be captured by the wake rake, resulting in no drag calculation from the measurements, generally this occurs in stall and drag values are then calculated from the airfoil pressure. The wake rake traverses the wind tunnel in span-wise location, covering the central  $\pm 375$  mm around the  $+20$  mm location, thus yielding span-wise drag information to evaluate the local impacts and to detect possible 3D flow phenomena.

This helps to identify measurement mistakes to repeat series or correct data accordingly if problems occur such as cuts in the tape that will locally result in large peaks in the span-wise

drag readings.

#### 2.4.4. Boundary Layer Rake: Variation, Design and Validation

Additional measurements have been conducted by designing and utilizing a boundary layer rake (BLR). This has been motivated by the the project defining paper of Bak et al. [3] from the project supervisor who initiated this project. There, tripping tape impact is related to the boundary layer thickness from numerical Xfoil simulations. After investigating original xfoil, TUDelft variation Rfoil and company internal Mfoil, it was found that the boundary layer thickness varies a lot depending on the solver, even more when considering 2D CFD as well with different meshing variation and input parameters. The author viewed the approach of deciding on simulated data to compare boundary layer thickness as an arbitrary choice while rather critically and to allow a more qualified guess to choose a representable simulation data source, it was decided to design a measurement instrument that yields data on the actual measured boundary layer thickness of the airfoil in the wind tunnel. This is further discussed in Chapter 5.

## 2.5. Data Correction

This chapter describes the two levels of data corrections, for raw measured data from wind tunnel operations, as well as manually applied filters to processed data by the researcher.

### 2.5.1. Wind Tunnel Corrections

Tests in closed environments such as wind tunnels introduce differences compared to operations in a free stream, such as the standard operational environment for wind turbines. These differences need to be accounted for by data corrections for two-dimensional cases and are called wall corrections [20].

**Horizontal buoyancy** introduces additional drag from horizontal buoyancy as the static pressure varies along the test section when no wind tunnel model is installed and should not be confused with the static pressure impact induced by the model itself.

**Solid blockage** reflects the ratio of the models relative size with respect to the test section due to flow displacement around the airfoil contours, yielding in local velocity increase. These corrections are important for all angles of attack, however rising in importance with higher deviation from  $\alpha = 0^\circ$  and for thick airfoils. Barlow et al. [20] however states that these corrections will not be valid for larger blockage, which can be observed as local speed up over the airfoil for high angles of attack.

**Wake blockage** compares to solid blockage, but refers to the ratio of wake area with respect to the wind tunnel area and is therefore more complicated as the wake itself is a function of the model shape. This is mainly negligible for open test sections as the wake can expand undisturbed, but can significantly increase the drag measurements for closed section wind tunnels as the LSWT and is therefore corrected with higher importance for separated flow with larger wakes as the local blockage behind the airfoil can lead to local speed up of the flow and is considered negligible for attached flow. The wake rake drag is not being corrected.

**Streamline curvature** refers to an alteration of flow streamlines around the airfoil due to the presence of floor and ceiling walls, causing the inflow angle of attack to deviate from the geometric angle of attack that is controlled by the wind tunnel set up. Finally, airfoil force components such as moment and lift are increased for closed test section wind tunnels. The wake rake drag is not affected by this correction.

The **influence of the airfoil model impact on the contraction pressure measurement** causes an error on the free stream dynamic pressure as the static pressure reading is from this

area at the contraction wall and is corrected by identifying the flow speed up due to the airfoil model [21].

Further wall interference is assumed to be present as the **effect of compressibility** is not considered at this point as indicated by Allen et al. [22] to correct dynamic pressures and thus velocity, Reynolds number, Mach number and force coefficients. Also introducing an influence of corrections due to solid blockage and streamline curvature are discussed but not implemented for this project.

### 2.5.2. Drag Filter Correction

Finally, the traversing of the span-wise direction and the resulting wake and thus drag coefficients comply well with the airfoil model quality. Upon inspection of the model quality, various imperfections were tracked and can be visualized in Figure 2.4.

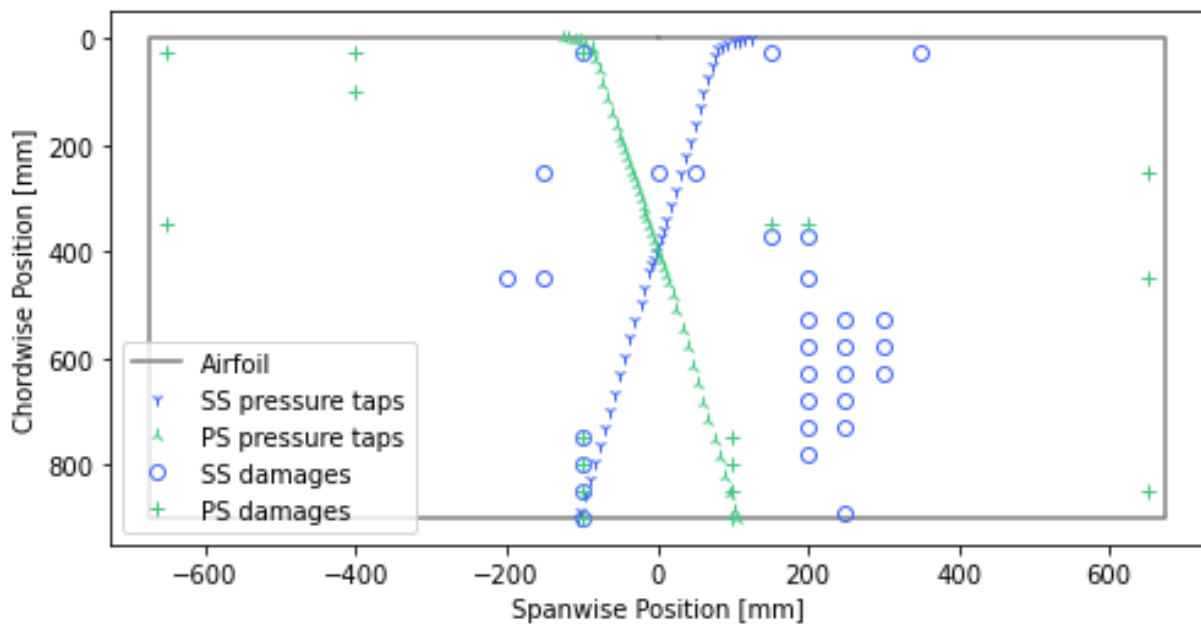


**Figure 2.4:** DU00-W-212 airfoil model imperfections from inspection

It is found that largest imperfections coincide with overall peaks in all span-wise drag measurements and the data has thus been filtered to correct the drag peaks as indicated in Figure 2.5. Similar trends have been found from the previous test campaign "AVATAR" for which this airfoil model has been used. Finally, the end positions of the wake rake have been filtered as to frequently introduce larger deviation in overall span-wise drag measurements, especially at more extreme angles of attack, which is assumed due to wall impacts becoming more dominant. However, a comparison to not filter these end points has been later viewed and is negligible, resulting in this being an unnecessary operation. Drag "valleys" can be observed in Figure 2.5 for suction side imperfections at further aft locations, as further discussed in Section 4.5.

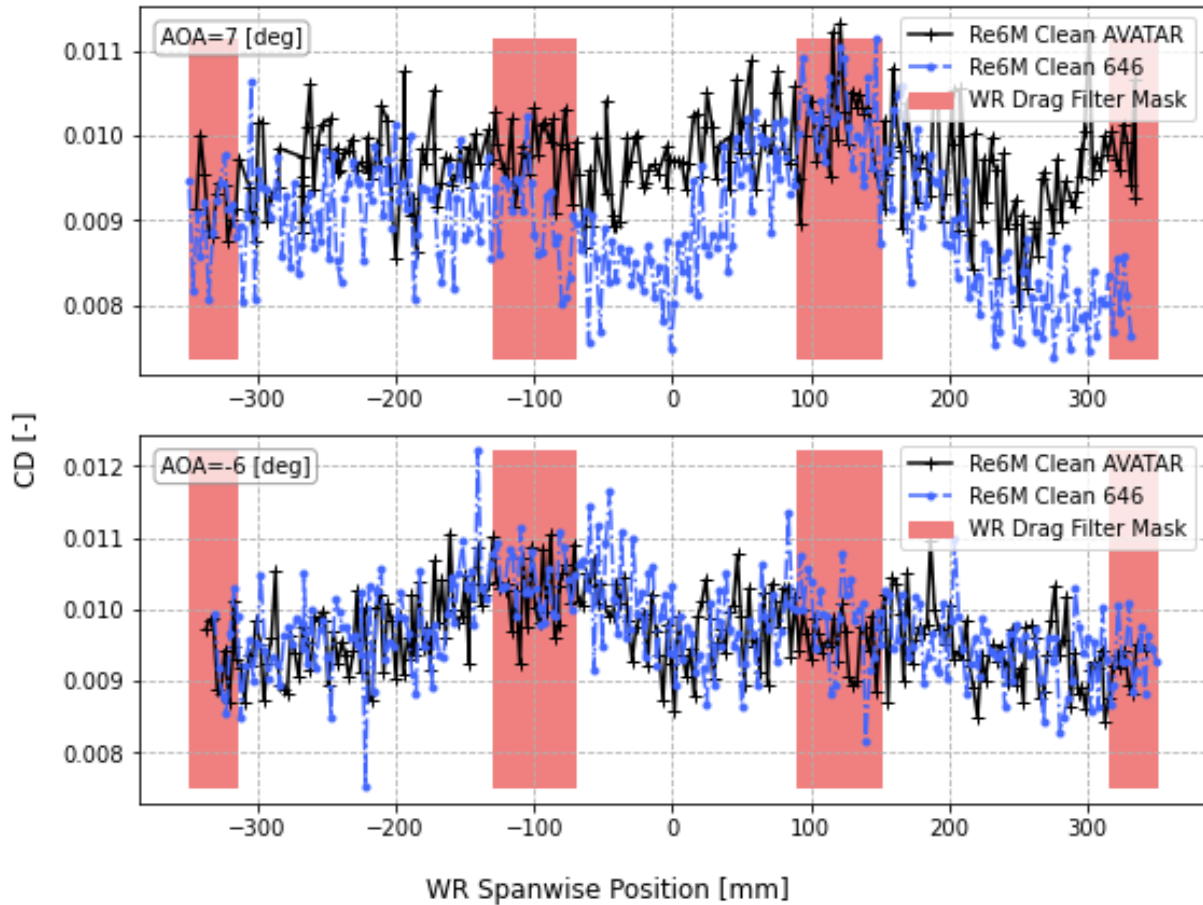


**Figure 2.5:** Wake rake drag filter mask for data correction on DU00-W-212 experiments

## 2.6. Test Matrix

The main test matrix can be seen in Table 2.1 for single ZZT applied to (mainly) the suction side. The research was aimed to yield baseline understanding of ZZT usage, focusing on single tape on the suction side, yet there are selectively applications on the pressure side - the nomenclature for suction side locations are positive  $x/c$  values, while pressure side locations are dedicated as negative  $x/c$  values.

The definition of the location is also important and the author identified a lack of consistency to be communicated in overall research papers. A strip of tripping tape is applied depending on one location being communicated, however the orientation is important as well. As an example, the industry standard is communicated as 5% SS and 10% PS and one would estimate the location to be denoted as forward step with backward step being oriented downstream towards the TE. In this study, all setups have been declared with the suction side notation, meaning the starting point is communicated followed by the tape width spanning towards the suction side trailing edge. This is important as  $-1\%SS \neq 1\%PS$ , due to the former spanning between pressure side locations  $0\% \leq x/c_{ps} \leq 1\%$  while the latter covers  $1\% \leq x/c_{ps} \leq 2\%$ . All following locations are communicated with this notation for consistency and simplicity with the project outline defining a focus on the suction side application. Exceptions are introduced individually where applicable.

| $x/c$ [%] | ZZT 125 $\mu m$<br>width 12mm | ZZT 125 $\mu m$<br>width 6mm | ZZT 205 $\mu m$<br>width 12mm | ZZT 400 $\mu m$<br>width 12mm | ZZT 400 $\mu m$<br>width 6mm |
|-----------|-------------------------------|------------------------------|-------------------------------|-------------------------------|------------------------------|
| -1        | x                             |                              | x                             | x                             |                              |
| 0         | x                             |                              | x                             |                               |                              |
| 1         | x, o                          |                              | x                             | x                             | x                            |
| 1.5       |                               |                              |                               |                               | x                            |
| 2         | x                             |                              | x                             | x                             |                              |
| 3         | x, o                          |                              | x                             | x                             |                              |
| 5         | x, o                          |                              | x                             | x                             | x                            |
| 5.5       |                               |                              |                               |                               | x                            |
| 7         | x                             | x                            | x                             | x                             |                              |
| 8         | x                             |                              | x                             | x                             |                              |
| 9         | x                             | x                            | x                             | x                             |                              |
| 12        | x                             |                              | x                             | x                             | x                            |
| 12.5      |                               |                              |                               |                               | x                            |
| 20        | x                             |                              | x                             | x                             |                              |
| 40        | x                             |                              | x                             | x                             |                              |

**Table 2.1:** Testmatrix for ZZT application on the DU00-W-212 airfoil. 'x' indicates single tape usage on the suction side, while 'o' indicates symmetric application on suction and pressure side.

Different areas to force transition were of interest for the present study. The majority of external conditions will cause erosion close to the leading edge, which resulted in an interest to deviate the standard ZZT setup from  $x/c_{ss} = 5\%$  closer to the leading edge. Additionally investigating the area close to this setup with locations further aft. Finally, wind turbine blade damages are reported and investigated for locations up to  $x/c = 30\%$  [14, 6, 23] to extent in chord-wise direction and when leading edge protections and repair tapes are applied, those will introduce a step in their respective location, motivating to selectively test locations further aft. Locations are separated into the locations around the LE, around the standard setup and selective locations further down the chord.

To research the critical roughness height, low velocities are required. Additionally, reference data from the latest DU00-W-212 tests are available at  $Re=2e6$  as well as for the real roughness reference by Gaudern et al. [7].  $Re=6e6$  is chosen as limiting condition in the LSWT facility and  $Re=4e6$  as third option between the bordering choices, while  $Re=3e6$  would have been a better choice with respect to critical roughness height in Chapter 3.

These 46 setup variations in Table 2.1 have been tested at 3 Reynolds numbers each resulting in 138 test series. Additional tests have been conducted to yield one data set each for the clean airfoil at the *Start* and at the *End* the campaign with a higher resolution in angles of attack, to investigate the impact of these tests and to validate if the airfoil still performs as expected. Another clean data set was gathered prior to the Boundary Layer Rake campaign. From this, clear differences have been identified that will be discussed in Section 4.1.

| Datatype      | Testseries | AOA | x data | y data | z data | Sum       |
|---------------|------------|-----|--------|--------|--------|-----------|
| Pressure Taps | 138        | 22  | 4      | 86     | 1      | 1044384   |
| Wake Rake     | 138        | 22  | 4      | 248    | 55     | 165644160 |
| Sensors       | 138        | 1   | 15     | 1      | 1      | 2070      |

$166.7 \times 10^6$

**Table 2.2:** Resulting amount of data points from the conducted test series in Table 2.1

Each test series presented in Table 2.1 is further divided into the data setup as explained in Table 2.2, which yields a total of  $163 \times 10^6$  data points from the measurement campaign, adding numerous additional values to be computed from this original data set. This large data set is valuable to investigate ZZT impact in detail but also increases complexity of the project, which motivates an initial simple overview of key parameters in Section 4.5.

# Part II

## The Research Objectives

*... the airfoil performance drops ...*

## RO1: Critical Roughness Height

The critical roughness height as objective was motivated by Bak et al. [3] as one of the starting points of the present study. Bumtapes were applied to investigate at which conditions a tripping behavior is observed. In a similar approach, this was investigated for ZZT. Bak et al. applied tapes at  $x/c = 2\%$  on the suction side for different airfoils, where the location was limited, while the present study was limited in airfoil variation. Bak et al. concluded a relation of BL momentum thickness in relation to the roughness height as function of Reynolds number. At equal location and ZZT height, similar trends can be reported, which however shift largely for deviation in tape setups.

### 3.1. Reference Paper Correction

The present study originated from results and future steps recommended by Bak et al. [3] in the research of a critical roughness height relation, where bumtape was investigated. Therefore, similar methodologies are applied in the present study for ZZT with a larger variety of testing matrix, which motivated an analysis of the performed simulation computations in the reference paper. It has been found, that the airfoil geometry was applied and evaluated opposingly, resulting in rating suction side data as pressure side, therefore communicating and utilizing wrong values for the resulting boundary layer momentum thickness (BLMT) relation and polar data from simulations. The identified tape height over BLMT relation (Table 1 in [3]) as result is compared for reference and corrected values in Table 3.1 and the corrected relation as function of lift coefficient for all reference cases can be observed in Figure 3.1 with a confirmation data set (red) by Bak et al. for limited angles of attack for the NACA0015 airfoil, to confirm the findings.

These computations had minor impact on the airfoil choice, as the original BLMT reference values were found similar for the present study airfoil DU00-W-212, therefore initially confirming the selected airfoil to behave similarly in the available reference data content. The discussed errors have only later been discovered and no adaptations on the airfoil choice were taken, as the DU00-W-212 airfoil was still found to be a good choice as discussed in Section 2.2. The corrected values are compared with the present study in Chapter 3.

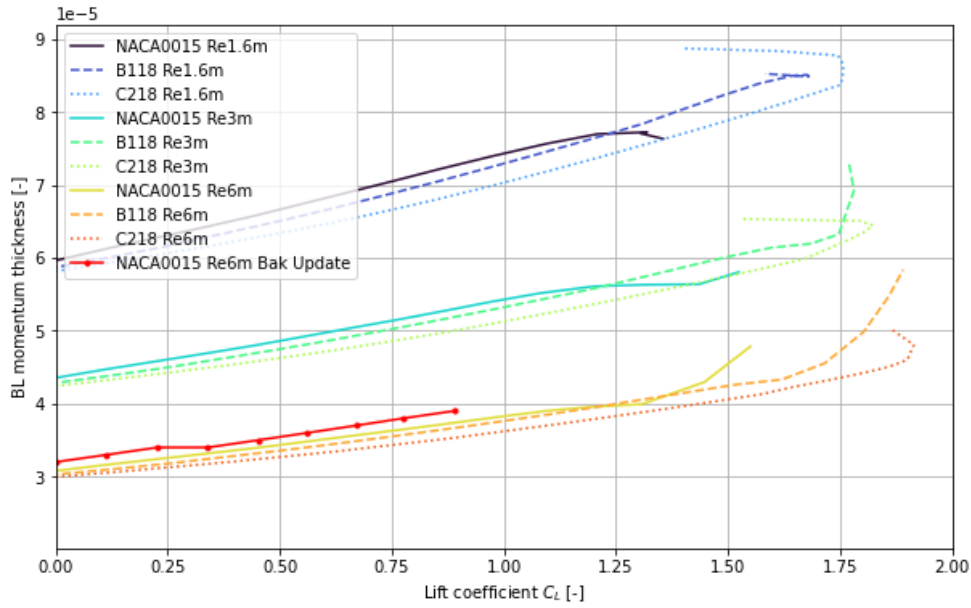


**Figure 3.1:** Boundary layer momentum thickness over lift coefficient: data correction from present study simulations and confirmation data from reference author [3]

| Airfoil    | Re            | AOA | BLMT<br>Bak et al. | TH/BLMT<br>Bak et al. | BLMT<br>corrected | TH/BLMT<br>corrected |
|------------|---------------|-----|--------------------|-----------------------|-------------------|----------------------|
|            | $\times 10^6$ |     | $\times 10^{-5}$   |                       | $\times 10^{-5}$  |                      |
| NACA0015   | 3             | 3   | 4.2                | 2.65                  | 4.7               | 2.37                 |
| NACA0015   | 6             | -5  | 3.6                | 3.09                  | 2.7               | 4.05                 |
| Risø B1-18 | 1.6           | 7   | 5.1                | 2.18                  | 7.8               | 1.42                 |
| Risø B1-18 | 3             | 6   | 3.7                | 3                     | 5.6               | 1.99                 |
| Risø B1-18 | 6             | -3  | 3.3                | 3.37                  | 3.1               | 3.58                 |
| Risø C2-18 | 1.6           | 9   | 4.7                | 2.36                  | 8.4               | 1.33                 |
| Risø C2-18 | 3             | 8   | 3.6                | 3.09                  | 5.9               | 1.86                 |
| Risø C2-18 | 6             | -3  | 3.2                | 3.47                  | 3.2               | 3.47                 |

**Table 3.1:** Reference paper table as relation of TH/BLMT by Bak et al. [3] with original and corrected data

### 3.2. Roughness Reynolds Number Approach

The majority of roughness research states a relation of roughness height based on a roughness Reynolds number  $Re_k$  approach.

$$Re_k = \frac{\rho \times u_k \times k}{\mu} \quad (3.1)$$

Single grit and therefore 3D single particle roughness was found to be related to a critical condition of  $Re_{k,crit} = 600$  by Braslow et al. [24] in Equation 3.3 and confirmed by various authors [25, 18, 26]. Klebanoff et al. [27] investigated mechanisms of 2D distributed roughness and

concluded cylindrical rods related to  $Re_{k,crit} = 100$  while Rooij et al. [12] reports ZTT to force transition at  $Re_{k,crit} = 200$  from experimental investigation on 14 airfoils at different thicknesses. Direct numerical simulations by Balakumar et al. [28] report  $Re_{k,crit} = 300$  for ZTT.

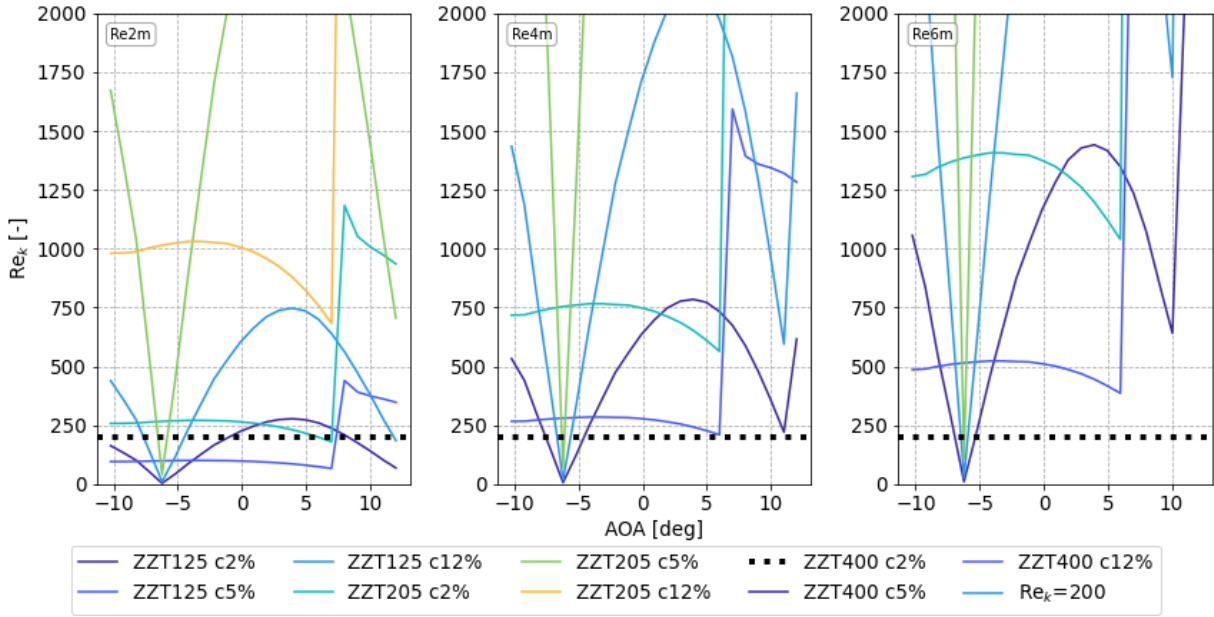


**Figure 3.2:** Roughness Reynolds number estimation based on panel code friction coefficient [7] for selected ZTT setups

$Re_k$  is computed including simulation data as proposed by Ehrmann et al. [15] and confirmed by Gaudern et al. [7]. The friction coefficient  $CF$  was utilized to compute shear stress  $\tau_w$  and the velocity near the wall  $u(k)$  as

$$u(k) = \frac{k\tau_w}{\mu} = \frac{kU_\infty^2 \rho}{2\mu} \quad (3.2)$$

to compute the roughness Reynolds number as

$$Re_k = \frac{\rho\tau_w k^2}{\mu^2} \quad (3.3)$$

The method however is limited to pre-stall behavior, which is the range of interest, as simulation data tends to become less accurate in those conditions. Furthermore, this method is limited by assuming negligible upstream impact as clean conditions are computed and applied for roughness and tripping tape cases, that however influence the flow upstream. And finally, the overall simulation data quality will impact this as computations heavily rely on the shear stress  $\tau_w$ .

Resulting  $Re_k$  values are compared in Figure 3.2 for one selected location in each respective region of interest and for all tape heights as well as an estimation of the critical Roughness number  $Re_{k,crit} = 200$  in comparison. These estimations resulted in the test matrix, raising importance to thin ZTT and to the decision of neglecting the bump tape base in Figure 2.1 to avoid increasing the overall roughness height.

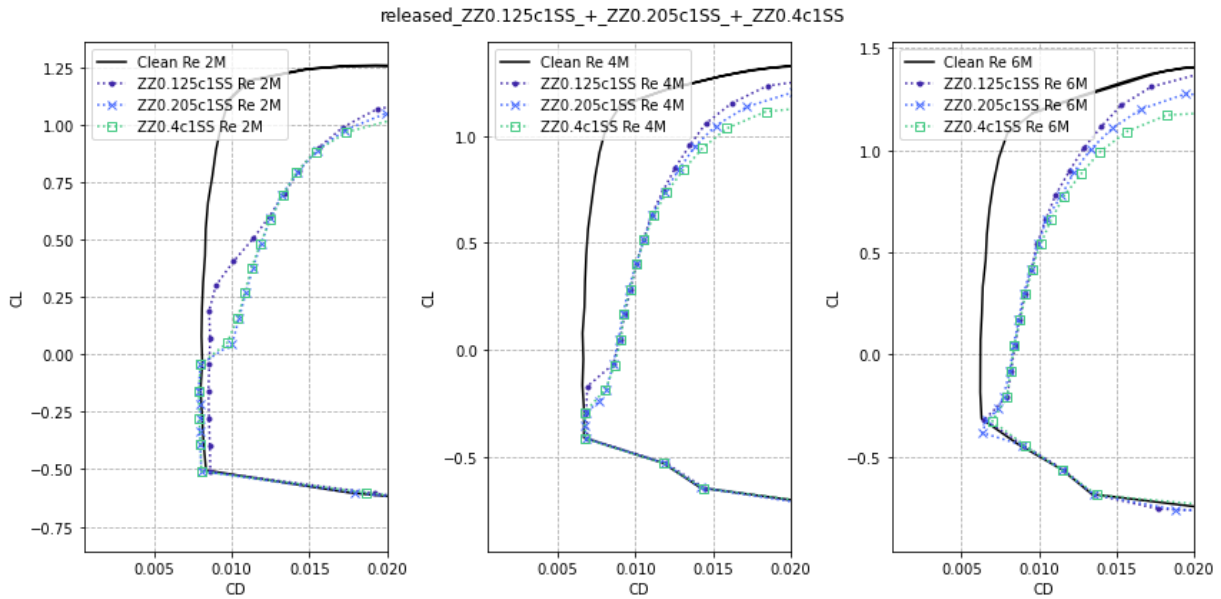


**Figure 3.3:** CL over CD for all tape heights at  $Re = [2, 4, 6] \times 10^6$  at  $x/c = 1\%$

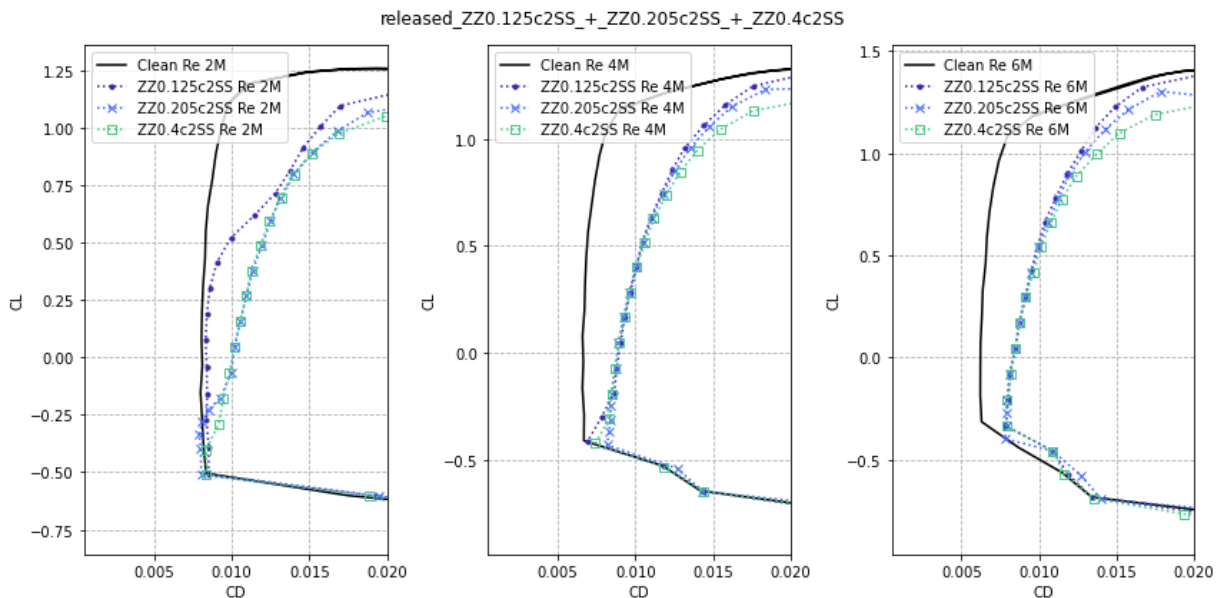


**Figure 3.4:** CL over CD for all tape heights at  $Re = [2, 4, 6] \times 10^6$  at  $x/c = 2\%$

ZZT400 was expected to trip at any operational condition and to not vary over the range of angles to allow detecting the critical trip behavior. ZZT205 and ZZT125 were expected to be relevant for this investigation at  $Re=2e6$  and  $Re=4e6$ . However, only ZZT125 was observed to not instantaneously trip the flow as function of the stagnation point. When pitching the airfoil, the stagnation point passes tape locations in the range of  $-1\% \leq x/c \leq 3\%$  with respect to tested locations. Simple mistakes to expect critical behavior from Figure 3.3 and Figure 3.4 can lead to false conclusions, while these mainly indicate the shifting of the stagnation point.

Results are as expected for ZZT400, however not for ZZT125 and ZZT205. Upon further investigation, it can be concluded that majority of tape setups close to the leading edge, while being almost the only setups to deliver a clear jump response to detect tripping behavior as critical, are due to the shifting of stagnation point over the tape, indicated in Figure 3.5. Locations are taken as backward step location with respect to Chapter 6.

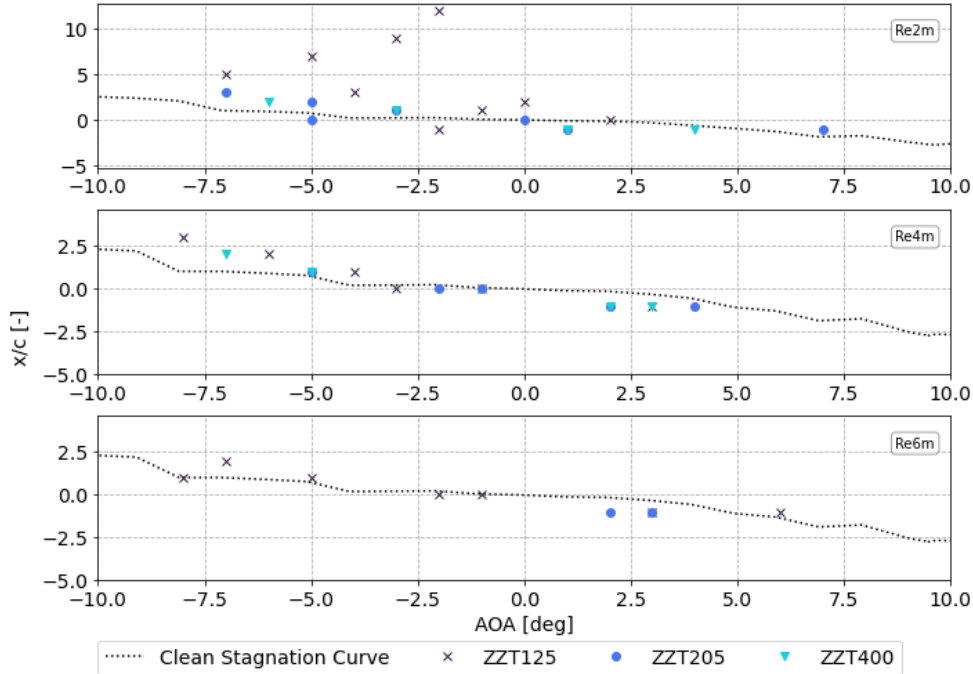


Figure 3.5: Identified critical height setups in relation to clean airfoil stagnation points

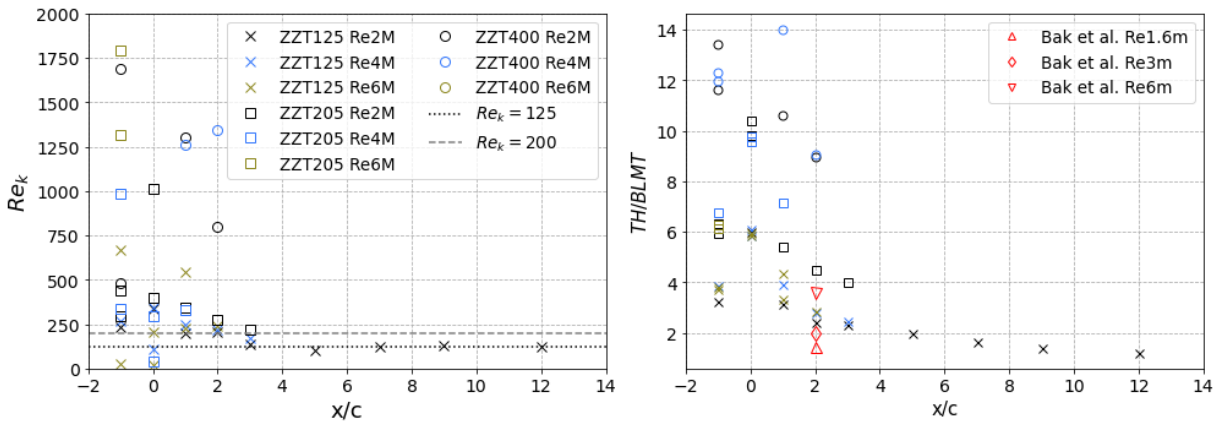


Figure 3.6:  $Re_k$  and  $TH/BLMT$  for observed jump response in ZZT setups

Overall results do not match the expectations of a critical roughness number of  $Re_{k,crit} = 200$  but rather indicate even more effective impact to force flow transition at  $Re_{k,crit} \approx 125$ . This is however also related to the method to compute the  $Re_k$  and might not be a general fact but rather a conclusion based on simulation quality of  $U_f$ , experimental tests and data analysis.

The corrected reference values by Bak et al. [3] are displayed for straight bumtape height  $h = 200\mu m$  at  $x/c = 2\%$  on the Risø B1-18 airfoil, at  $Re = [1.6, 3, 6] \times 10^6$ . Present data agrees approximately with the reference data from other airfoils, confirming the approach. However, the approach to investigate a relation of tape height over BL momentum thickness  $TH/BLMT$  indicates that values further decrease with distance from the leading edge, as expected with boundary layer development.

Basing the expectancy of tripping impact on the critical roughness Reynolds number  $Re_{k,crit} = 125$  is found to be more consistent in this data set. Ideally, this should be investigated and compared with various airfoils to conclude whether this is generally a fact, rather than a parameter of this airfoil and test campaign.

## RO2: Wind Tunnel Measurements

As discussed in Section 1.4 and as categorized by White et al. [14] into roughness studies to yield either overall understanding or researching underlying phenomenon of specific impacts, part of the main objective of the present study is to research gross aerodynamic quantities such as polar performance data to deliver overall better understanding of impacts due to changes in ZZT setups. This chapter will cover general learnings of the wind tunnel campaign and the usage of the DU00-W-212 airfoil model, the resulting overall research output of the detailed test matrix and individual detailed analysis of selected setups.

### 4.1. Clean Airfoil

The clean airfoil has been tested several times throughout the test campaigns at the start and prior to BLR measurements and general performance has been validated and investigated to allow more precise discussion on performance deterioration due to roughness impacts.

#### 4.1.1. Stagnation points

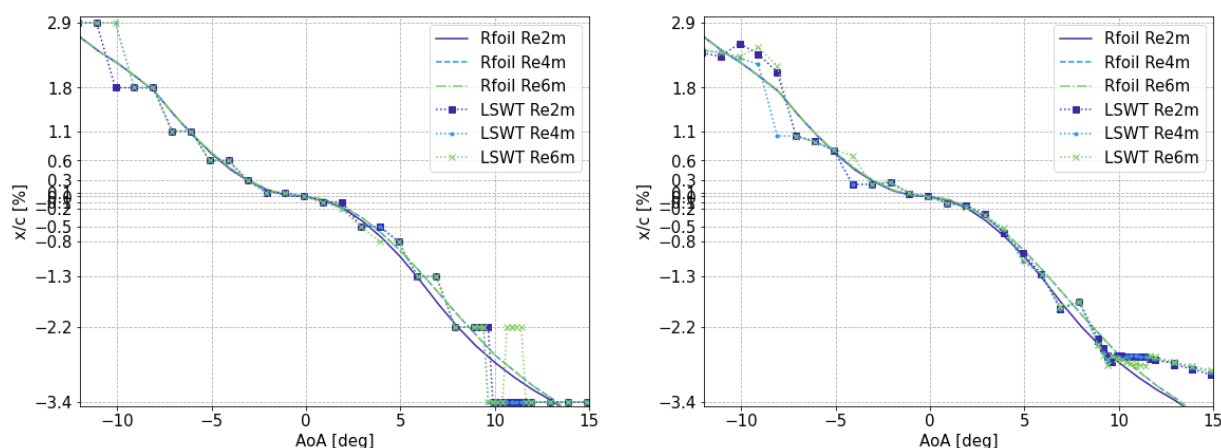


**Figure 4.1:** Stagnation Point for raw pressure taps and interpolated data

The stagnation point is a fundamental point of interest in airfoil aerodynamics as it provides general insights into airflow behavior around the airfoil. The flow encounters the airfoil profile and deceleration due to the shape occurs, resulting in the stagnation point where maximum surface pressure leads to zero velocity, separating the flow into 2 sections around suction and pressure side respectively. The stagnation point is therefore closely related to the boundary layer as it introduces the effective start of BL formation. Tracking its location over a variety of flow

parameters and pitch angles has therefore been of interest and a comparison with simulated stagnation points is shown in Figure 4.1, while the impact of attaching tripping tapes is later discussed in Section 4.5.

The exact location is limited and needs to be carefully treated in further considerations. The stagnation point is heavily impacted by the pressure tap discretization and large gradients as it is generally found as narrow peak in the pressure distribution. When pitching the airfoil, this peak will move between pressure taps, but more importantly, the large gradient of pressure coefficients between  $-3 \leq c_p \leq 1$  shifts at large quantities between few locations. The values are evaluated from raw pressure tap locations and as interpolated values in Figure 4.1. Identifying the closest taps and interpolating around a close fixed distance of pressure taps is found ineffective with nonlinear distances in pressure tap locations as pitching will introduce sudden large increments in interpolation borders due to the large gradients around the stagnation point. A full interpolation over the whole pressure distribution is also found ineffectively as a complex geometry will be required to be interpolated, while only being interested in the most complex point on the curve. Finally, the interpolation scheme was adapted for several orders and methods, e.g. PCHIP interpolation [29], resulting in the current scheme that utilizes a fixed but large section around the stagnation point to only introduce minor interpolation border changes due to pitching, focussing on avoiding peak overshoot. This method results in consistent results for all test series, while however not having perfect accuracy.

The interpolations are limited when pitching in the range  $\alpha = [9, 10, 11]^\circ$ , which was found most troublesome. This describes moving over stall and a small shift is noticeable in the overall interpolation scheme indicating a possible shift in locations. Overall, the values do agree with simulated data outside of stall behavior which is expected. It does however show that improvements towards stagnation point identification are required and need to be considered when evaluating this quantity.

#### 4.1.2. Flow Transition

The transition point is another important parameter when studying the flow over an airfoil. The flow adheres to the surface, thus creating a boundary layer, initially as laminar flow. The flow over the chord-wise extent is pronounced to become unstable due to influences such as airfoil curvature or roughness, causing the flow to transition due to this instability increase at a specific location - the transition point.

Natural transition is often related to adverse pressure gradients, typically found for the point of largest curvature on the airfoil with respect to the flow direction. Flow separation occurs and is followed by transition in the free shear layer shortly behind separation resulting in reattachment, causing sudden increase in the local pressure as explained by boundary layer equation of motion [30]. The transition point location can be identified as point of maximum velocity streamline curvature that corresponds to the second pressure derivative  $\partial^2 p / \partial x^2$  [29].

This method has been confirmed by tracing the transition point on clean airfoils with stethoscope measurements. A rod was introduced into the flow from the side of the wind tunnel with a curved tube on one end to get sound output from the flow and with an audio module on the other end, where the researcher is placed next to the wind tunnel with headphones to receive the signal from the module. The airfoil was marked in steps of 5% to identify locations and manual tracing of the transition location was conducted. This is relevant as the previous method is resulting in less clear results past  $\alpha = 8^\circ$ . The stethoscope tests have confirmed the locations. The resulting transition points and the stethoscope setup example can be viewed in Figure 4.2. The rod is held from outside the wind tunnel through a removable wall piece and the hole is sealed foam. The flexible end piece is held such that it detects the flow on the very surface.

The stethoscope output is audible noise. There is no noise from laminar flow. Turbulent flow is loud deep noise, similar to the noise of mechanical aerodynamic breaking of old wind turbines. The transition is audible slightly before the turbulence as quiet high-frequency pitched noise, which is however difficult to hear with general large noise of the operating wind tunnel. As the area of transitional flow is detected in a very short distance before turbulence, the communicated values for stethoscope measurements are turbulence locations. As the method is not at highest accuracy itself, this was preferred to allow consistency over all tests, as the high-pitched transition noise could not always be detected. Furthermore, holding and remaining the rod at the exact location during flow conditions of  $Re=6e6$  thus  $U_{inf} \approx 100m/s$  was physically difficult to withstand and much larger fluctuations due to suction of the rod are introduced, raising uncertainty towards stethoscope measurements at those conditions. The overall accuracy of stethoscope measurements is estimated to be within  $\pm 2\%x/c$ .

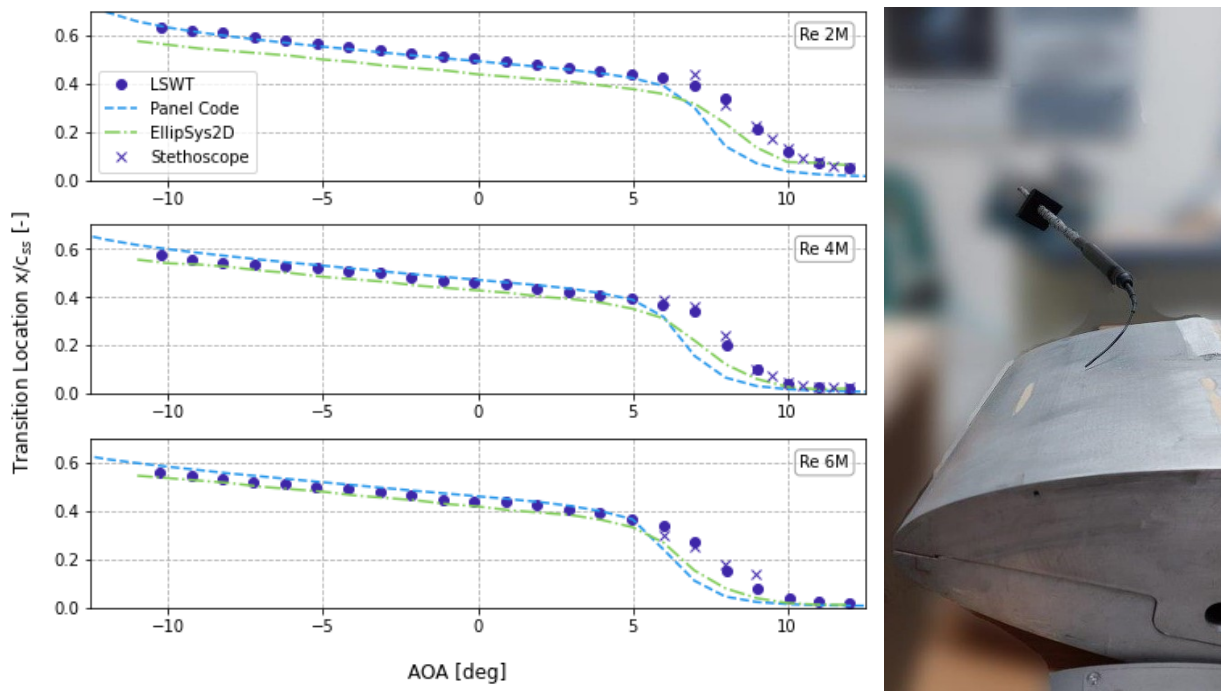


**Figure 4.2:** Natural Transition locations from stethoscope measurements and simulation data

Interesting output from this testing series is the early transition location of the DU00-W-212 that is detected on the airfoil at about  $x/c = 3\%$ , which fully recovers and did not introduce turbulence unless merging with the natural transition locations shifting forward with increasing angle of attack. This leading edge short bubble is expected from the stall behavior of the airfoil [31].

#### 4.1.3. Clean DU00-W-212 Performance

The clean airfoil performance has been cross evaluated with the latest campaign on this model from the AVATAR project. Results between projects are however not included in the public report and findings will only be discussed qualitatively for external purposes.

Test series parameters such as temperature, density and humidity have been tracked and classified into 2 regions where overall larger or lower magnitudes are observed in the total period of test campaigns. For these test series, airfoil pressure distribution and WR data in all dimensions for different pressure tube positions traversing span-wise have been studied detailed to obtain

understanding in testing differences in the setup of the current study.

Performance from testing design differences have been identified and within their limitation allow agreement with previous campaigns on this airfoil. However, the present results might be dependent on these parameters of the test setup design and are potentially not fully repeatable if tested in different setups. This is similar to testing comparison in the AVATAR project [32] between different testing facilities, which are however internal processes not to be focused furthermore in this publication.

## 4.2. Pressure Distribution Analysis

Tripping impacts have been analysed by pressure distribution analysis. Similar to the pressure distribution derivative analysis in Section 4.1.2, it can be identified when the flow trips due to ZZT impact. It was however found that especially close to the leading edge with narrow pressure tap locations, it is difficult to track impacts from the pressure distribution. Pressure taps at the ZZT location will be blocked and are therefore disconnected from the data acquisition system. This can be seen in Figure 4.3, where the  $x/c = 2\%$  data series omits a data point behind the ZZT location as indicated by the vertical dashed line. The general trend is observed as pressure increase prior and pressure decrease post ZZT location, which agrees with the expectation as ZZT causes a step that displaces the flow by the forward step, before introducing a local suction from the backward step as source of instabilities that cause flow transition from laminar to turbulent. Furthermore, the ZZT acts intrusive upstream as function of distance to the leading edge and tape height, causing minor shifts in stagnation points as discussed in Section 4.5. While difficult at the LE, the tape placement has not been done perfectly. Unnecessarily pressure tap blockage was done by applying tape at locations  $x/c = [9, 12]$  due to earlier measurement mistakes, though avoiding additional blockage for all other setups.

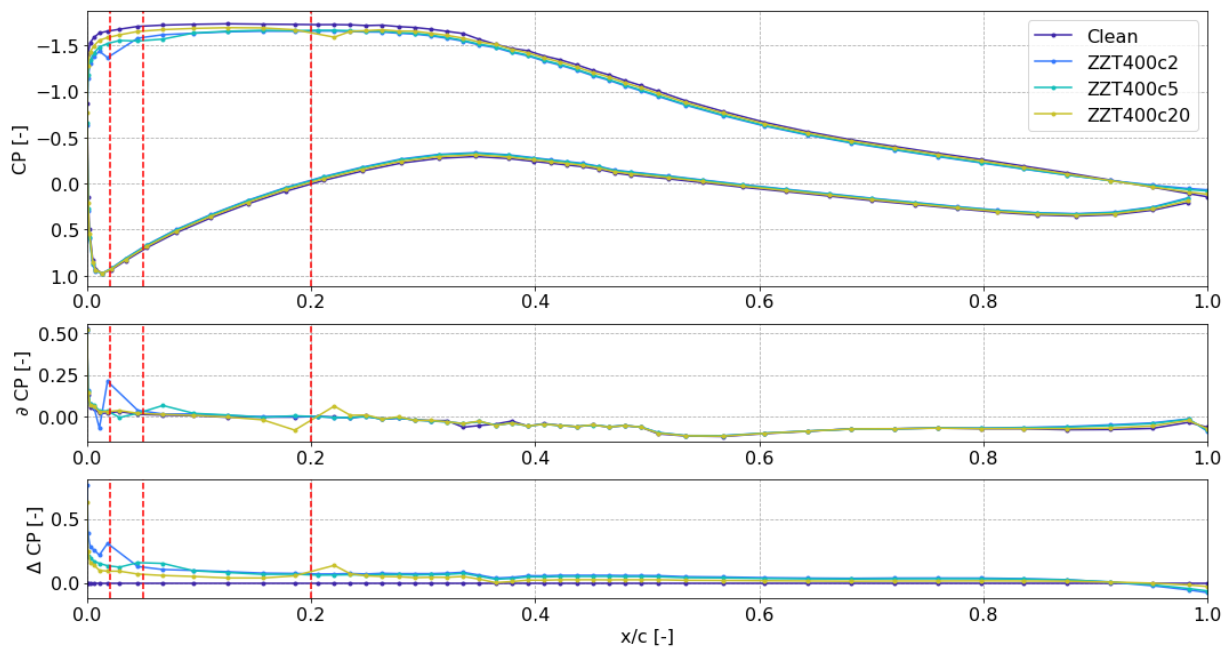


**Figure 4.3:** ZZT impact on the pressure distribution for ZZT400 at  $x/c = [2, 5, 20]\%$  at  $AOA=6^\circ$

### 4.3. Isolated Deviations from Standard ZZT Setup

The industry standard setup of simulating leading edge roughness, with main focus on the suction side, is displayed in Table 4.1. This chapter aims to deliver an introduction to the observed impacts as isolated overview from variations of selected parameters such as height, width, location. A combined overview is discussed as full outcome of the conducted experimental work in Section 4.4 to allow a detailed baseline for combined impacts and mapping of relevant parameters, as well as allowing an improved test matrix for future studies.

| Tripping Tape | Tape Height | Tape Width | Tape Location SS | Tape Location PS* |
|---------------|-------------|------------|------------------|-------------------|
| Zigzag Tape   | 400 $\mu$ m | 12mm       | 5%               | 10%               |

**Table 4.1:** Standard ZZT Setup Parameters with \* indicating frequently used optional combined pressure side application

#### 4.3.1. Standard Variation 1: Tape Height

Isolated tape height impact on performance polars can be observed in Figure 4.4 as the standard ZZT variation 1. Besides the critical height discussion in Chapter 3, tape height is mainly relevant for stall behavior. Roughness height generally moves the transition forward to the BW step location, which is crucial when operating close to critical conditions. At most typical operational conditions such as  $Re=6e6$ , the forced transition will always occur directly behind the tape and the tripping impact changes are negligible between different tape heights.

$$\Delta CD_{3-1} = \frac{\Delta CD_{2-1}}{1 - \frac{h_2}{h_3}} \quad (4.1)$$

In the drag bucket, this change in height can be estimated approximately for unknown height  $h_3$ , if polars based on ZZT height  $h_1$  and  $h_2$  are available as Equation 4.1. Requiring data at two tape heights to estimate

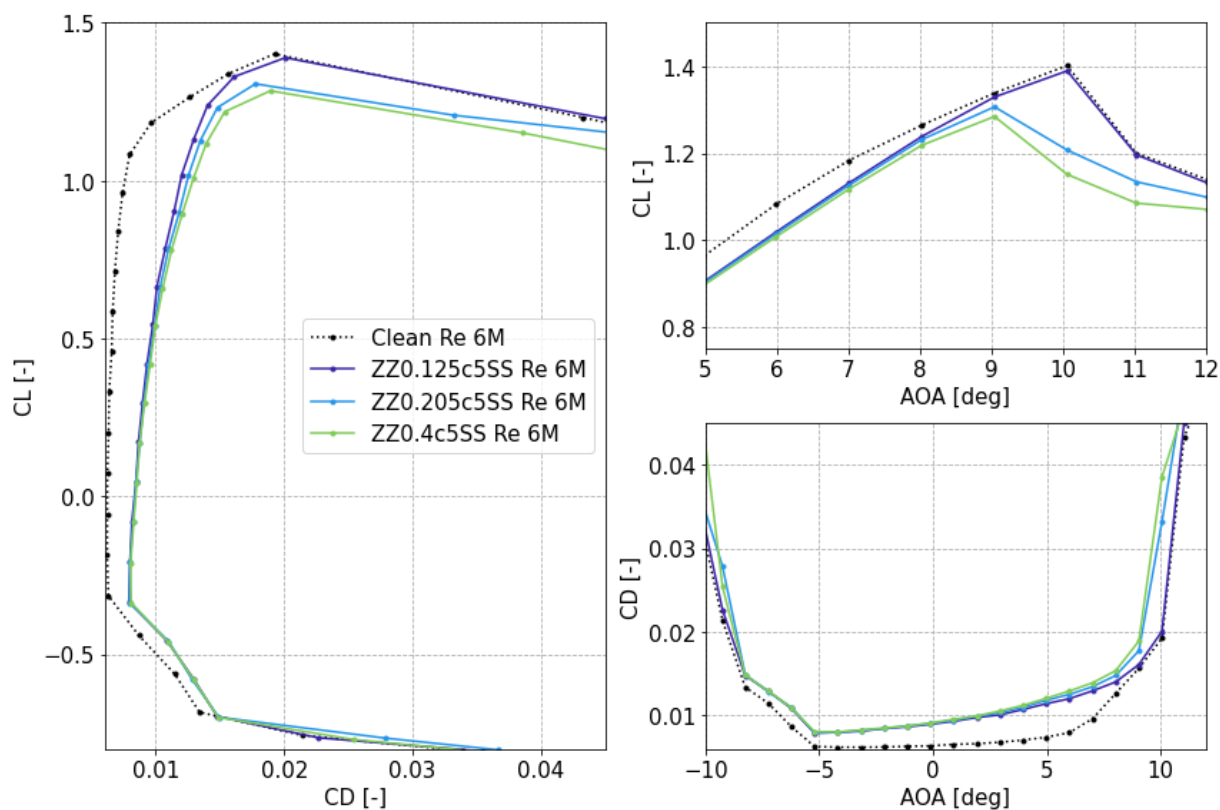


**Figure 4.4:** Polar data for isolated variation type 1: tape height

The general displacement of the boundary layer due to intrusive application of tape height, thus locally increasing the airfoil thickness, can be viewed upstream which proposes the main observed influence on the pressure distribution, when applying thicker tapes pre stall. Past actual tape location, the pressure distribution is equal for all tape heights.

Thicker tapes are pronounced to introduce early stall due to separation resulting in a steep increase in drag due to variation in the wake, as discussed in more detail for combined impact of tape heights and locations in Section 4.5.

#### 4.3.2. Standard Variation 2: Tape Width

Isolated tape width impact on performance polars can be observed in Figure 4.5 as the standard ZZT variation 2. The decreased width was only tested sparsely and it is important to note that the shorter tape also comes with a change in ZZT geometry, as the angle of the pattern changes from  $\beta = 60^\circ$  to  $\beta = 70^\circ$ . The performance was generally found to be similar, introducing a possible alternative to wider tapes, as those become more difficult to apply due to stiffness when placing them at locations of larger curvature.

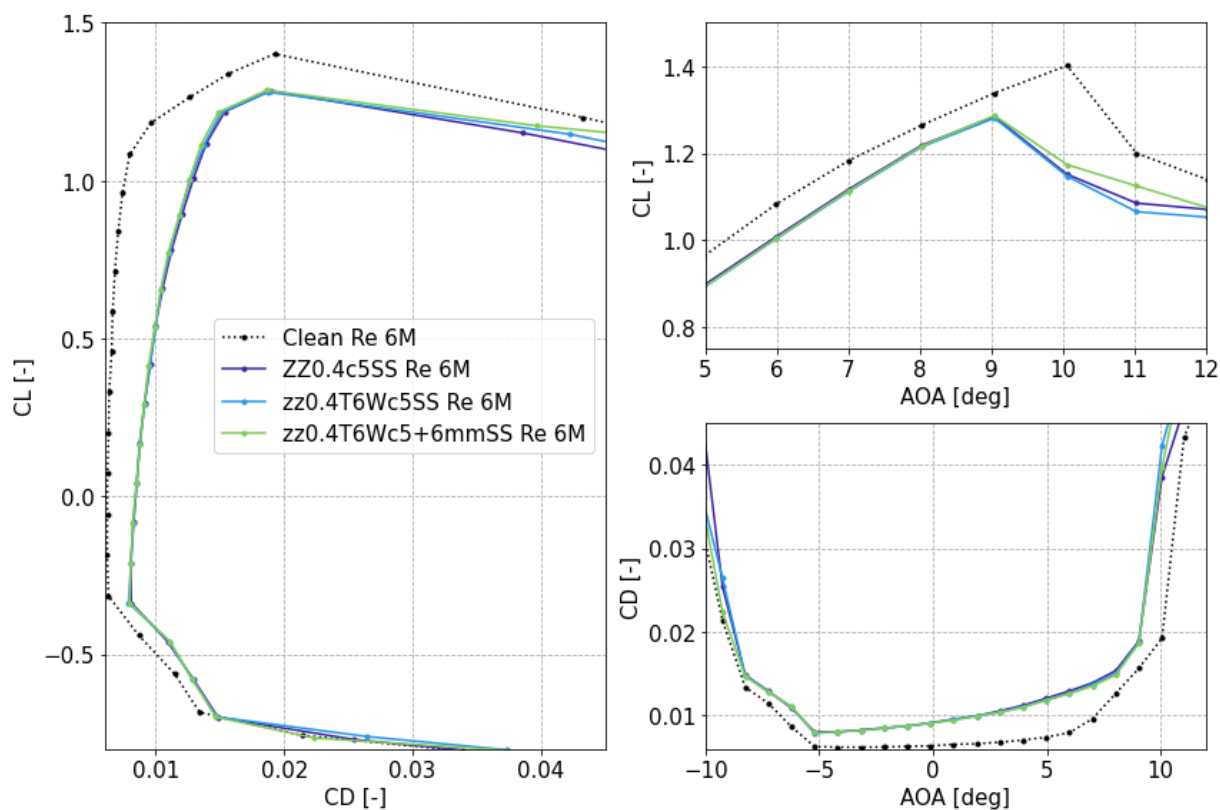


Figure 4.5: POlar data for isolated variation type 2: tape width

### 4.3.3. Standard Variation 3: Tape Location

Isolated tape location impact on performance polars can be observed in Figure 4.6 as the standard ZZT variation 3. This was found to be the most relevant parameter to vary for all operational setups, with respect to angle of attack and flow conditions. This is expected as a larger or smaller part of the flow will be forced to transition by varying the tape location. One example for each region as divided in Section 4.7 is provided in this section, with a more detailed discussion in future sections.

ZZT close to the leading edge will result in early but smooth stall behavior, assumed due to tripping prior to the short bubble. Applying ZZT at the standard setup results in unchanged stall behavior, but at earlier angles. Tripping at locations further aft will introduce turbulence in a similar way as vortex generators, resulting in a smaller wake due to attached flow and therefore also a more smooth trailing edge stall behavior.

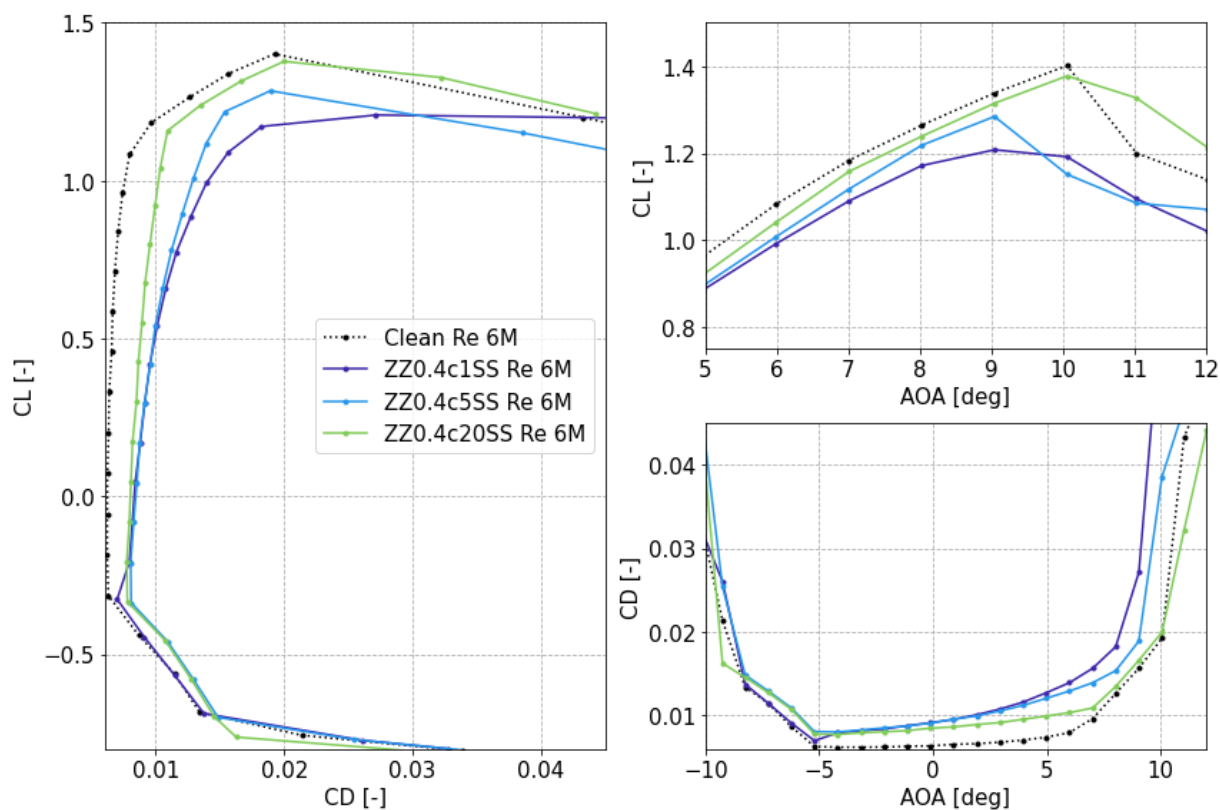


Figure 4.6: POLar data for isolated variation type 3: tape location

### 4.4. Overview of Performance Penalty Polars

The isolated deviations in Section 4.3 indicate possible outcomes, that however shall be mapped in full variety within this chapter, especially stall behavior is a combined function of tape height and location. Approaches to trace a critical relation to cause early stall or stall delay have been conducted as done for the critical roughness height in Chapter 3, but have not resulted in a usable relation.

To introduce the gross research outcome, an overview of all main ZZT setups, flow conditions and angles of attack is provided with respect to  $\Delta CL/CL_{clean}$  and  $\Delta CD/CD_{clean}$  and is displayed in Figure 4.7 and Figure 4.8 respectively. Each field describes the performance penalty for combined ZZT type and flow conditions as depicted in the subtitles as function of tape location and angle of attack. A more detailed discussion of key results is provided in Section 4.5.

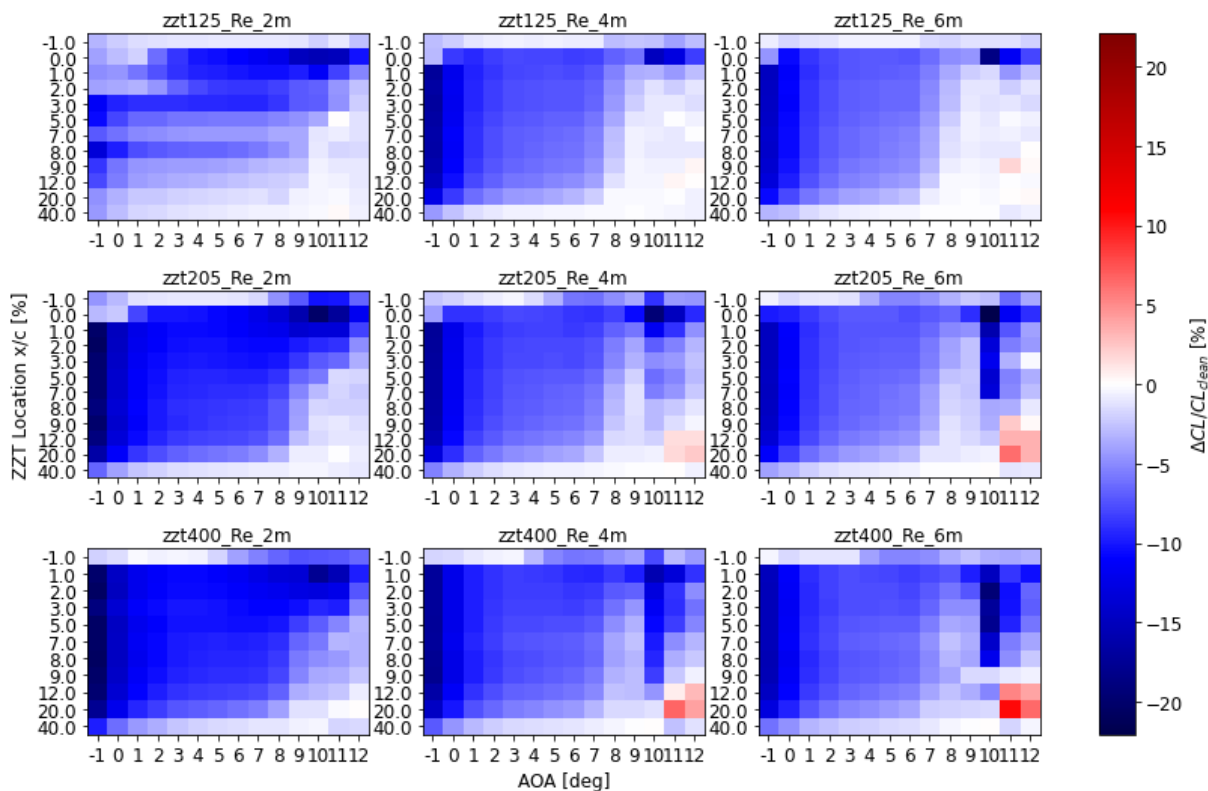


Figure 4.7: Colormap of  $\Delta CL/CL_{clean}$

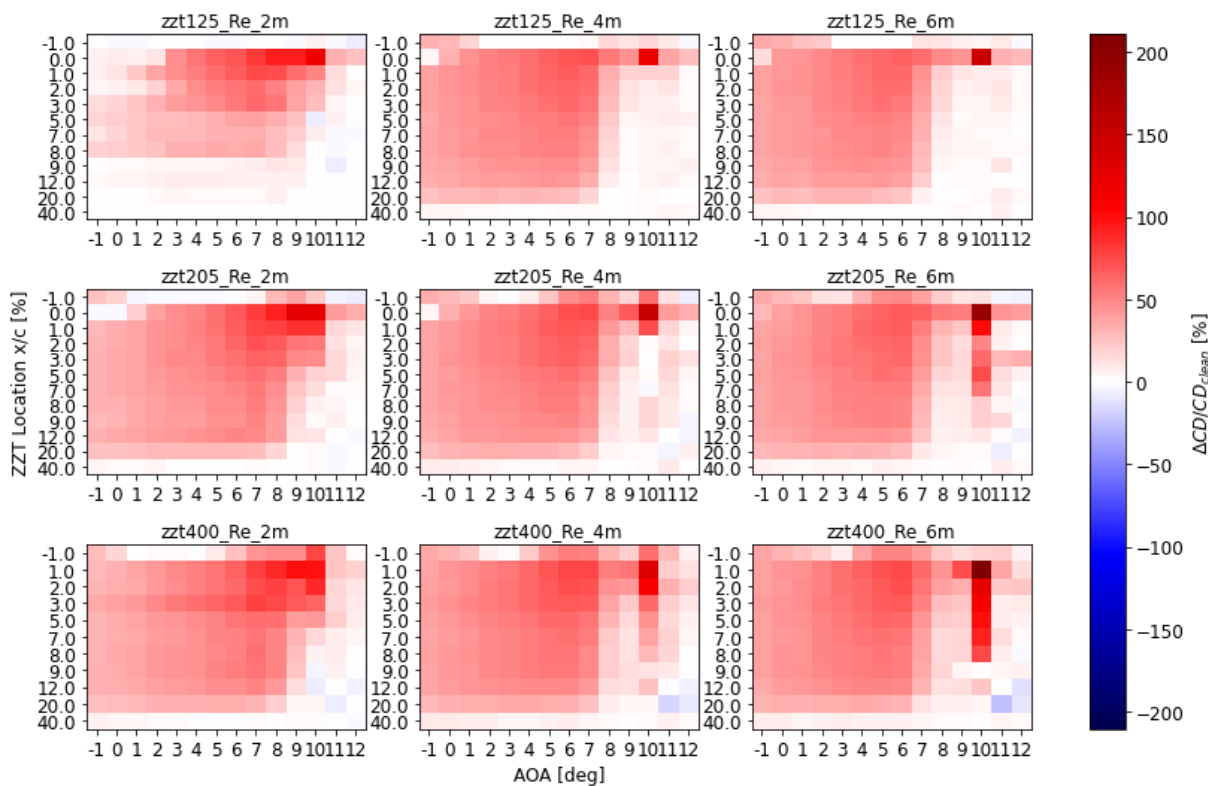


Figure 4.8: Colormap of  $\Delta CD/CD_{clean}$

### 4.5. Statistics

This section aims to deliver an overall overview of gross research output in terms of statistics, meaning that selected relevant parameters are evaluated as function of the selected tape setup parameters. As found in the previous section,  $Re=2e6$  test series are impacted by overall flow conditions, which motivates a more careful evaluation. The overall test campaign results in large importance to tape location application and a detailed investigation on test results for specifically chosen regions is conducted in Section 4.7. The deviating behavior for ZZT125 at  $Re=2e6$  is observed due to operating in the range of the critical roughness height, rather than instantly tripping the flow as for other combinations of tape height and flow conditions, with a more detailed discussion in Section 4.7. It is important to state that ZZT400 was not able to be placed at  $x/c = 0\%$  as its stiffness did not enable attaching it at this location.

#### 4.5.1. Lift Slope

The change of the lift slope in the linear lift region is documented in Figure 4.9. It can directly be concluded that the slope is linearly increasing with the tape location when moving aft, starting at the first suction side position at  $x/c = 1\%$  atleast until  $x/c = 20\%$ . The  $125\mu m$  tape behaves significantly different at  $Re=2e6$  as discussed in Chapter 3 due to not instantly tripping at conditions above the critical Reynolds number. Furthermore it can be concluded that the impact of different tapes is generally equal, but as expected slightly larger in magnitude for thicker tapes.

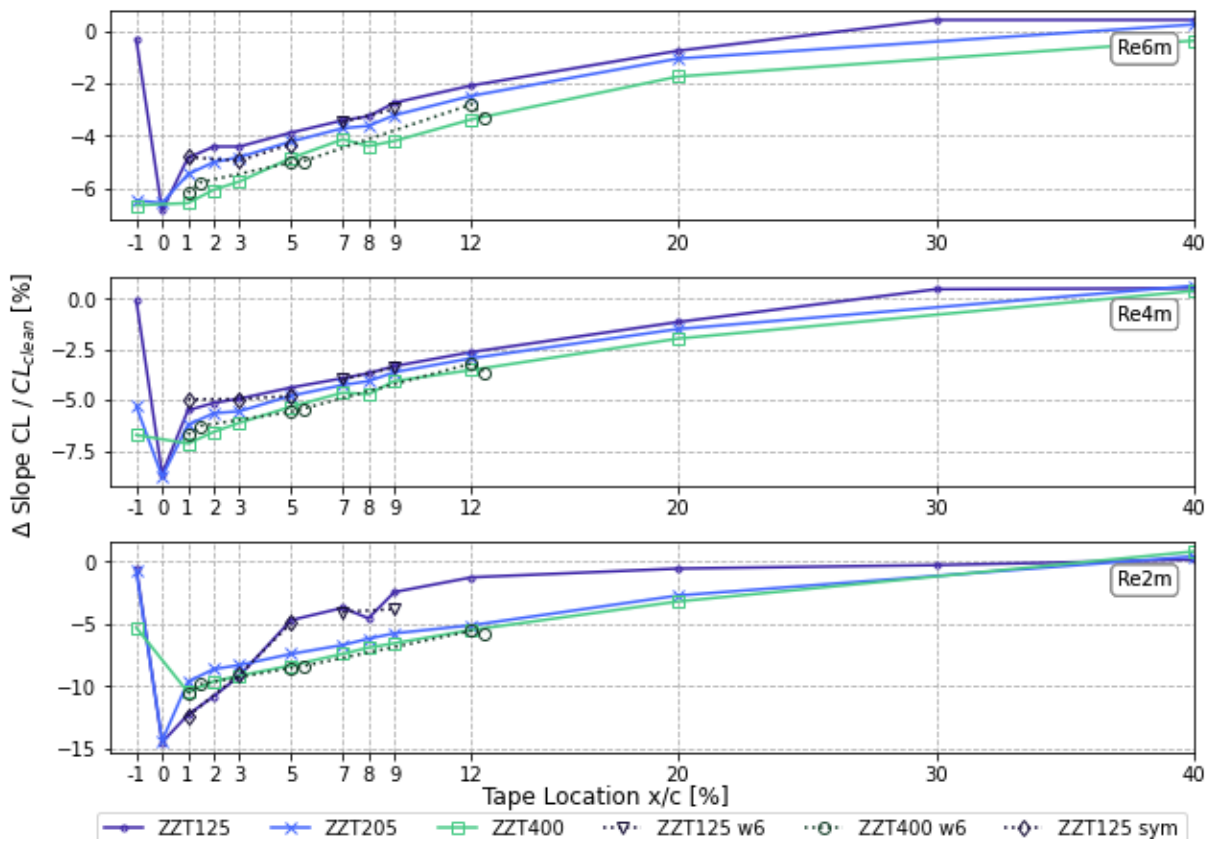


**Figure 4.9:**  $\Delta$  Lift Slope in the linear region of the Lift Coefficient over the angle of attack, typically  $-5^\circ \leq \alpha \leq 8^\circ$

The doubled  $125\mu m$  tapes increase in performance penalty with Reynolds Number, to re-

semble single  $205\mu\text{m}$  tape that is of twice its individual thickness. Though, the impact of the double tape setup becomes more impactful when moving aft, which is due to the stagnation point moving between the tapes, allowing both tapes to affect the flow on suction and pressure side respectively instead having a second strip of tape that is placed in the wake of the previous tape where the flow has already been tripped.

The shorter  $6\text{mm}$  tape of  $400\mu\text{m}$  height shows that less impact can be expected of shorter tapes as expected. The tape that shares the same forward step and thus having an earlier backward step has a higher impact. At the three locations for the shorter tape, the trend flips from larger penalty at early tape at  $x/c = 1\%$ , to lower penalty at early tape at  $x/c = 12\%$ . This trend can be observed for several performance statistics.

### 4.5.2. Stall Behavior

Figure 4.10 compares the deviation in angle of attack for maximum lift coefficient for the various setups, thus giving an idea if early or later stall is achieved. However, the actual angle of attack that was applied to the clean airfoil slightly varies from the actual angle of attack of the ZZT setups, which is due to the more detailed angle of attack resolution of clean airfoil performance and the smallest deviation values actually indicate same angles at maximum lift.

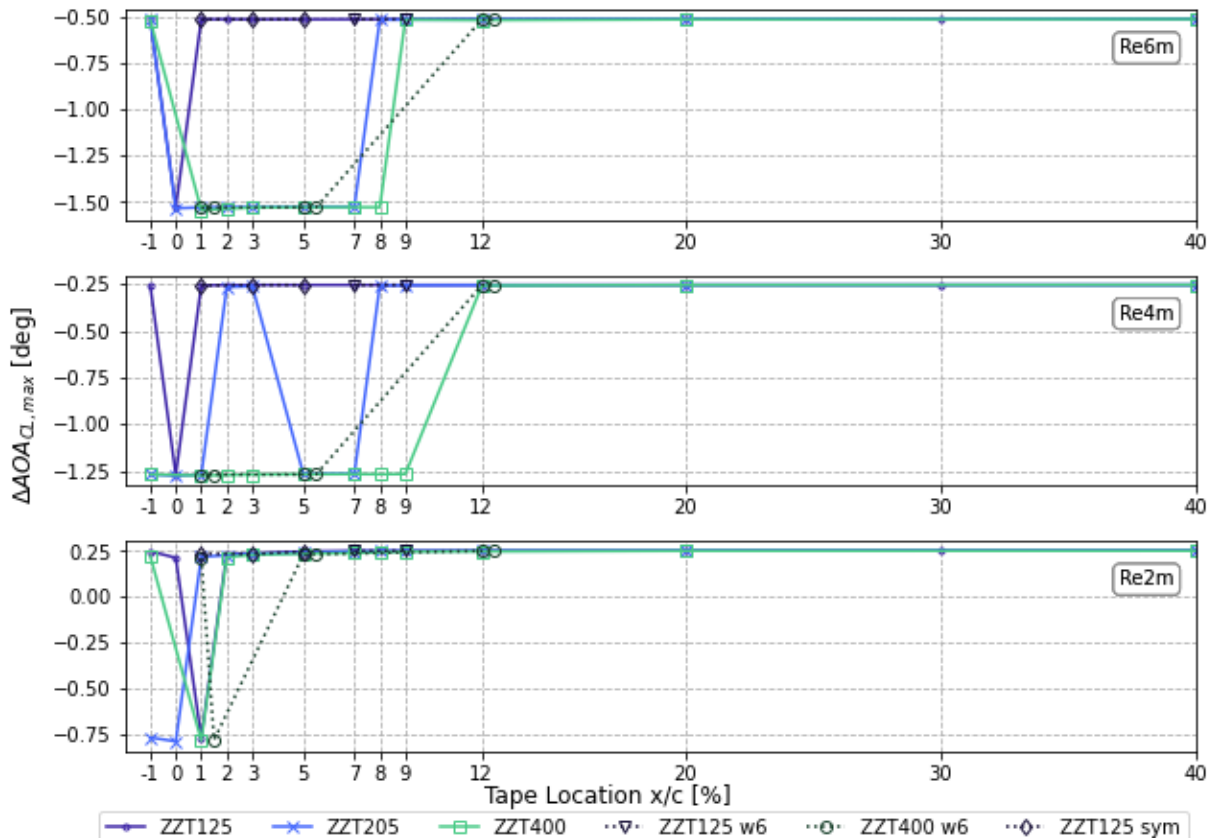


**Figure 4.10:** Angle of Attack for maximum Lift coefficient for the lift polar

For locations close to the leading edge and especially for higher Reynolds Number, an application region can be identified where early stall is achieved. Early stall is mostly observed for the  $205\mu\text{m}$  and  $400\mu\text{m}$  tripping tapes, indicating the requirement of a specific tape height to cause early stall.

Double tape setups were not able to change this behavior for the  $125\mu\text{m}$  tape, that generally does not achieve early stall for most setups. The  $6\text{mm}$  tape however shows an interesting trend, where early stall was only achieved at  $Re = 2 \times 10^6$  for the setup that shared the same backward step as the  $12\text{mm}$  version at  $x/c = 1\%$ .

The ZZT205 at  $Re=4e6$  behavior can be explained from Figure 4.11, the tape setup stalls early at the LE, then normally and then again stall early, before back to the original stall angle of attack. This switching is partially due to angle of attack resolution, where locations  $x/c = [2, 3]\%$  are expected to stall early, but not as early as  $x/c = 1\%$ , yet due to the angle of attack resolution, this exact angle was not obtained.

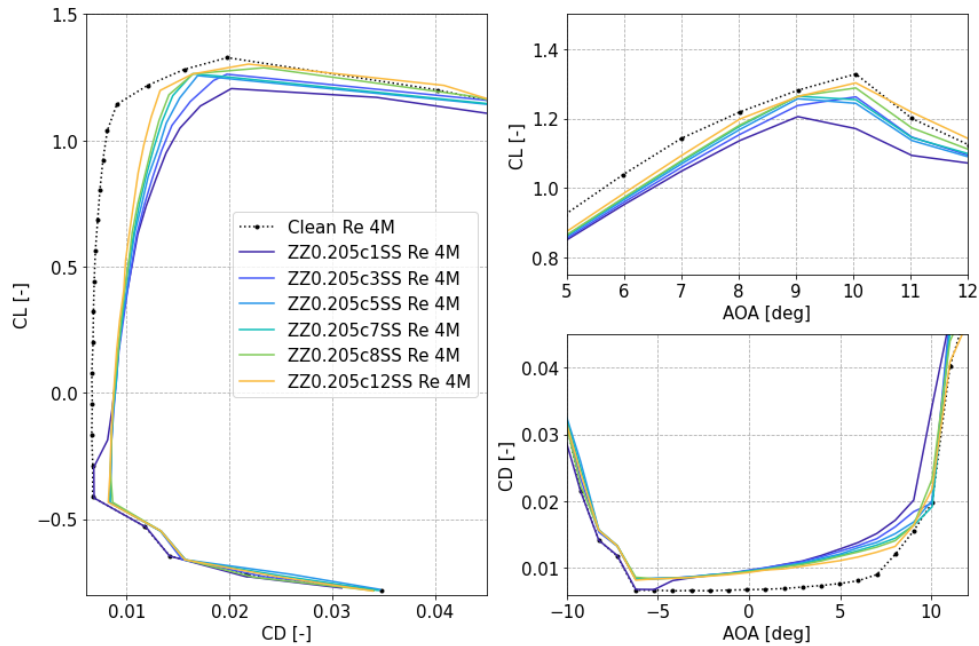


**Figure 4.11:** Angle of Attack for maximum Lift coefficient for the lift polar at  $Re=4e6$  for clean and different zig zag tape setups

In relation to the angle of attack deviation, Figure 4.12 compares the actual deviation in maximum lift coefficient values. Here, three different trends can be observed where a peak impact is observed for tripping tape applications until  $x/c = 3\%$ , a plateau behavior until approx.  $x/c = 8\%$  and an approx. linear decrease with further aft applications. The three regions are observed frequently when investigating tripping tapes and this is further discussed in Section 4.7.

Most interestingly is the  $400\mu\text{m}$  data point at  $x/c = 9\%$  for  $Re = 6 \times 10^6$ . This value can however easily be explained from the polar plot in Figure 4.13. Prior to that location, early stall is achieved as seen in Figure 4.10. The stall behavior is still very sharp as for short-bubble leading edge stall. For further locations, the stall behavior and lift curve become more smooth as with TE stall and enable attached flow for locations more aft.

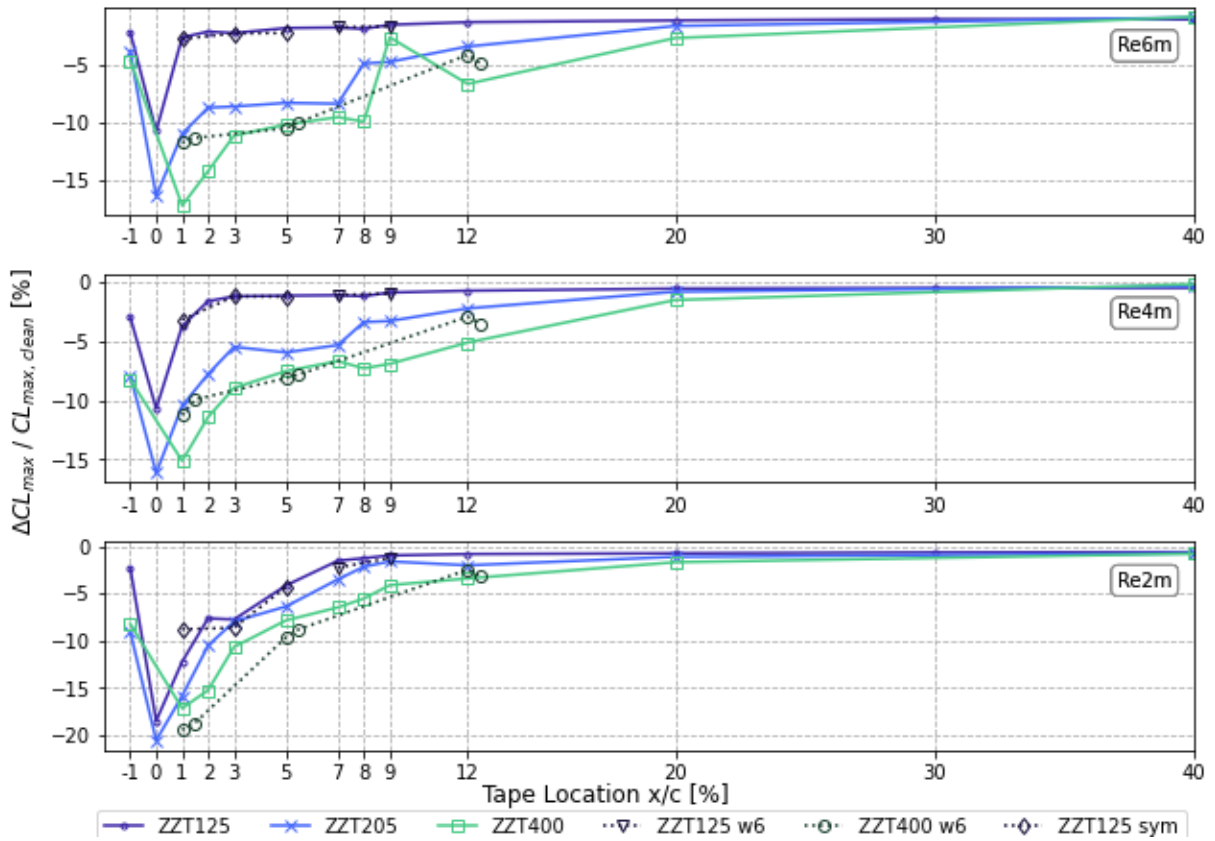


Figure 4.12: Maximum Lift coefficient values for the lift polar

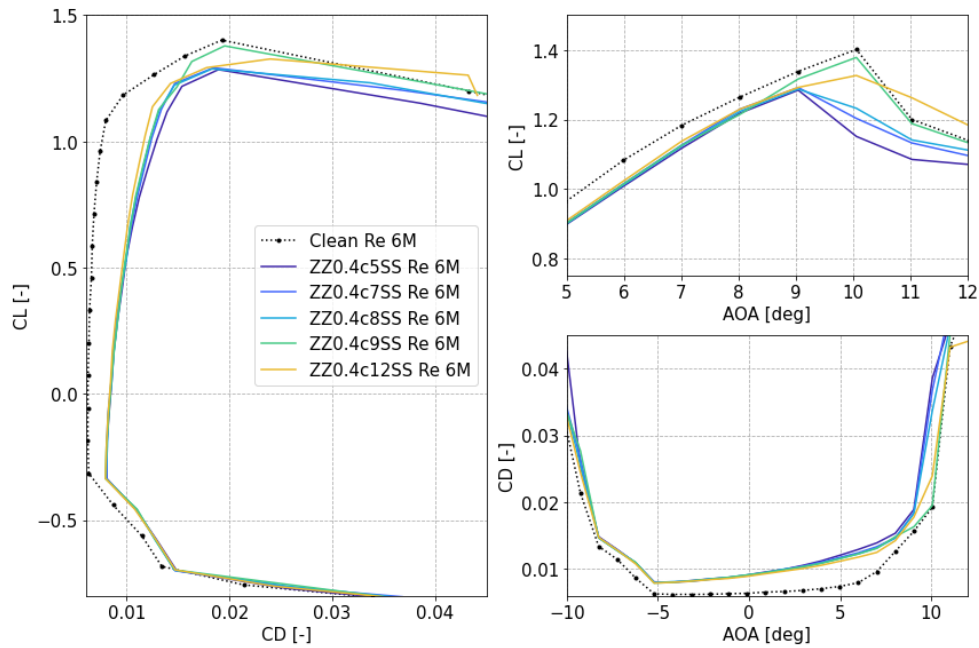


Figure 4.13: Lift coefficient and stall behavior for the lift polar at  $Re=4e6$

### 4.5.3. Lift Coefficient

The following graphs indicate the deviation of actual lift coefficients within specific relevant ranges of angles of attack, opposing the full polar view in Section 4.4. These can identify the contribution of ZTZ impact within different operational ranges.

Starting with the full averaged lift performance penalty in Figure 4.14, indicating that the LE locations are much more effective at reducing the lift force. When considering only angles above the zero lift angle of attack  $\alpha_0 = -3^\circ$  in Figure 4.15, this trend shows to change to a rather linear relation as function of the location, with lift penalty decreasing in aft direction, while indicating a larger penalty for thicker tapes, especially up to  $x/c = 8\%$ .

Limiting the operational range to angles between zero lift and stall in Figure 4.16, it can be understood that the tape height impact becomes much less relevant for the linear lift region. Finally, the stall behavior in Figure 4.17 shows a clear importance to tape height related to the tape location to vary the stall behavior. Again the peak, plateau and flat regions can be identified, discussed in Section 4.7.

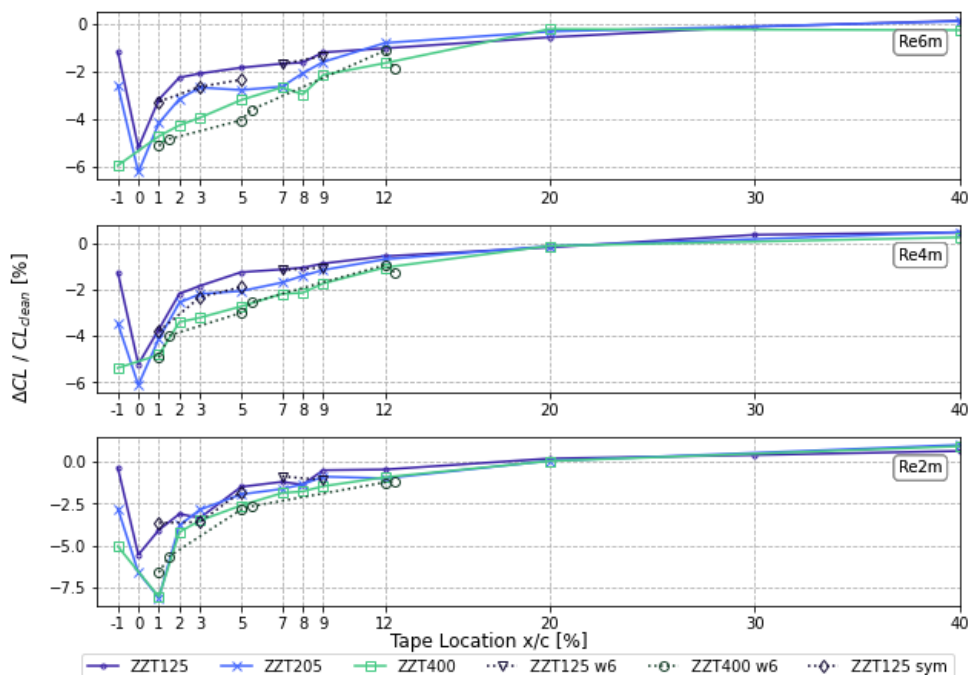


Figure 4.14:  $\Delta CL$  over tape location for full range of  $\alpha$

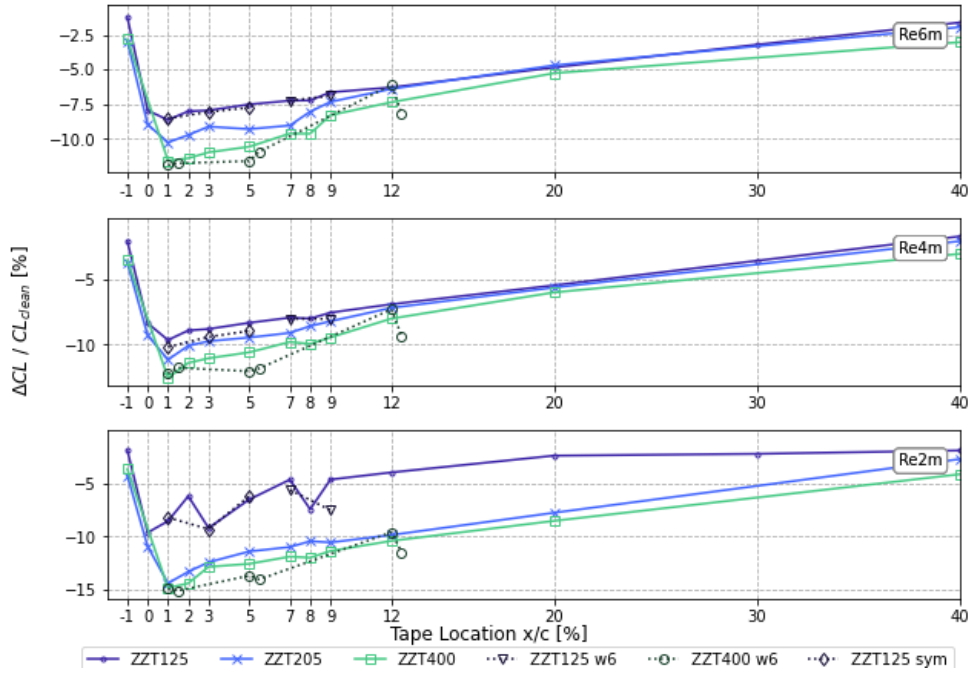


Figure 4.15:  $\Delta CL$  over tape location for positive lift  $\alpha \geq -3^\circ$

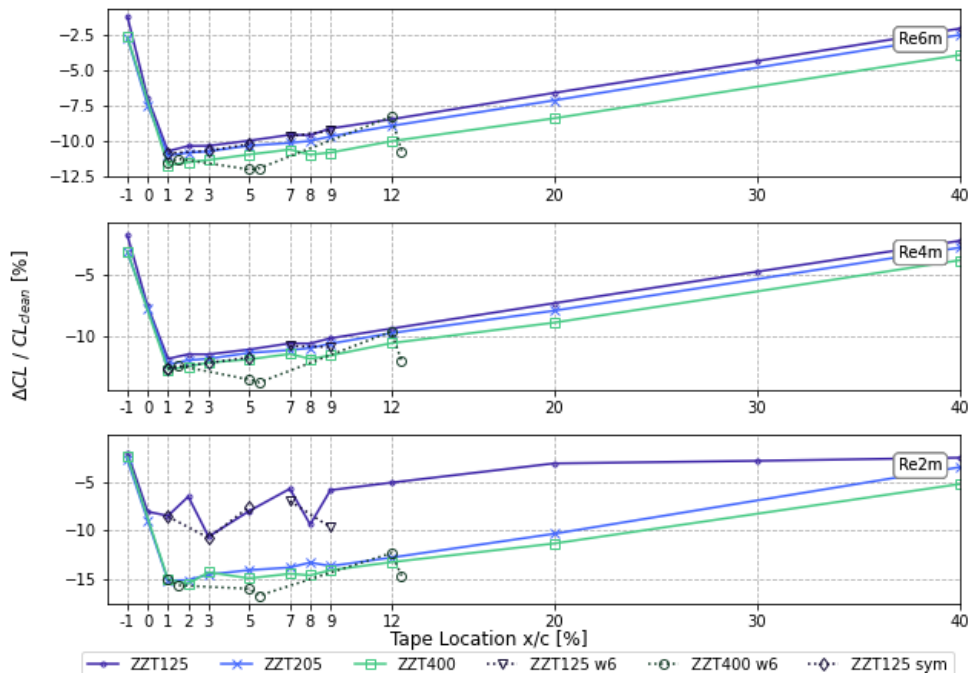


Figure 4.16:  $\Delta CL$  over tape location for positive lift pre stall  $-3^\circ \leq \alpha \leq 9^\circ$

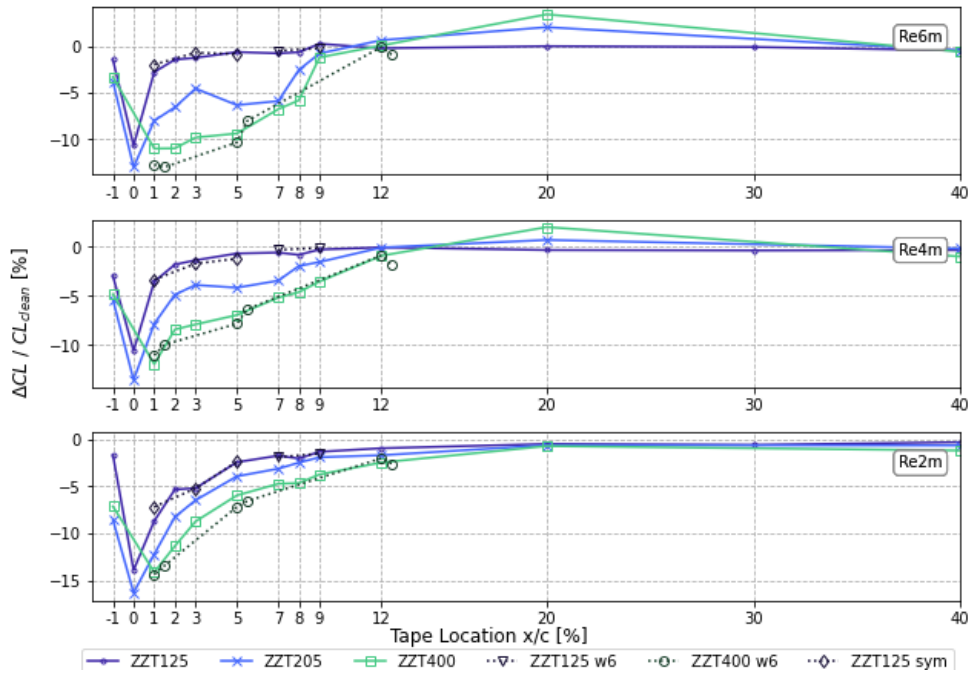


Figure 4.17:  $\Delta CL$  over tape location for positive lift in stall  $\alpha \geq 9^\circ$

#### 4.5.4. Drag Coefficient

The following graphs indicate the deviation of actual drag coefficients within specific ranges of angles of attack. These can identify the contribution of ZZT impact within different operational ranges.

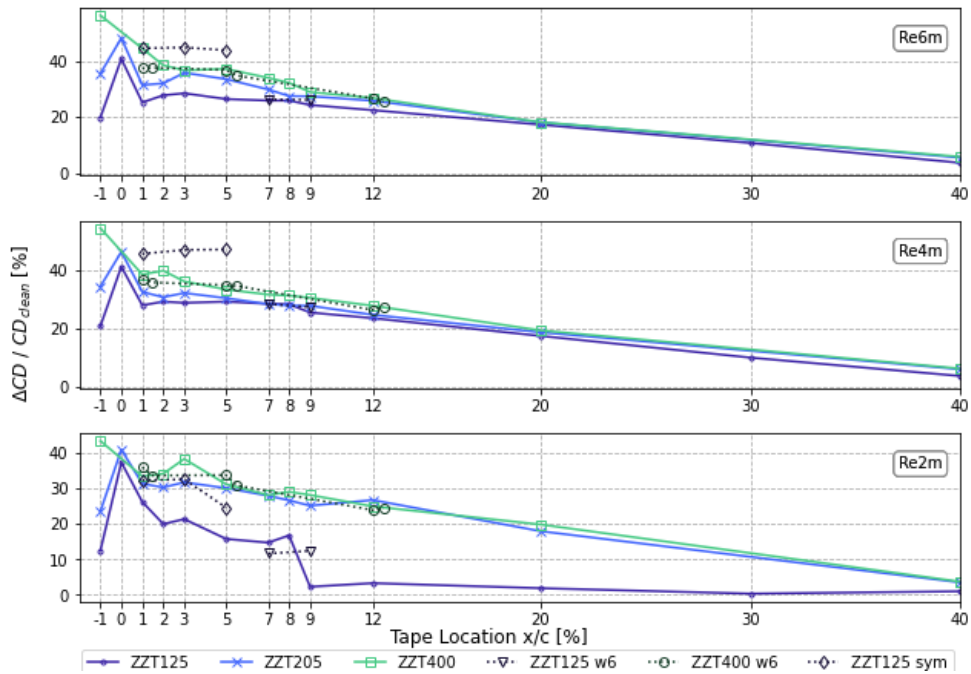


Figure 4.18:  $\Delta CD$  over tape location for full range of  $\alpha$

Starting with the full averaged drag performance penalty in Figure 4.18, indicating that the LE

locations are slightly more effective at increasing the drag. The values again behave more as a linear decrease with location further aft when considering only values above zero lift angle of attack  $\alpha_0 = 3^\circ$  in Figure 4.19. The deviation with respect to tape height again becomes rather negligible when excluding stall operational angles of attack in Figure 4.20. Finally, the importance of tape height can be observed when considering stall in Figure 4.21.

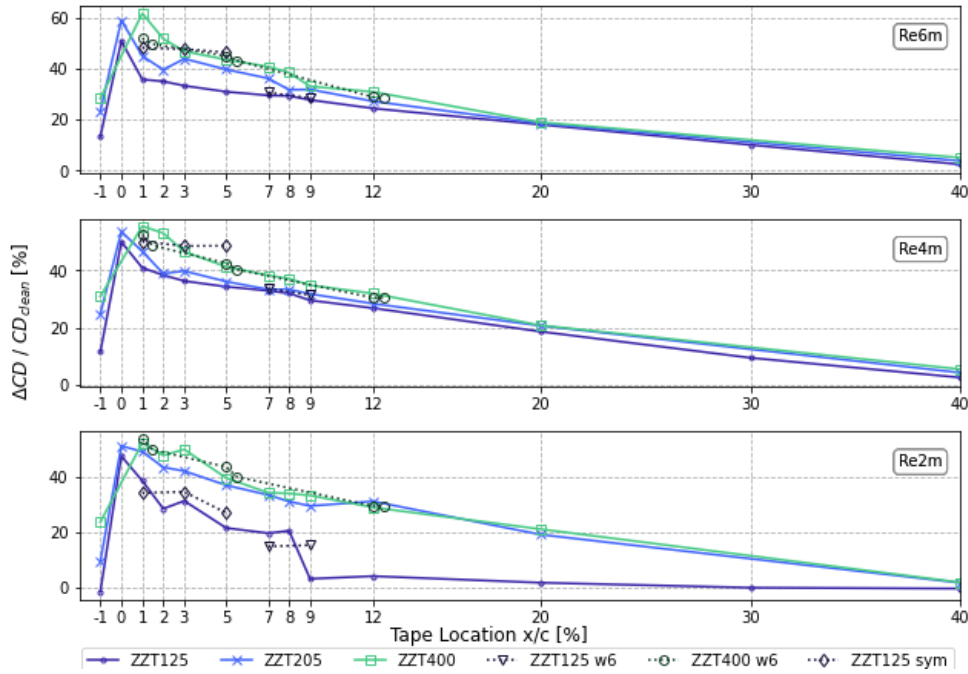


Figure 4.19:  $\Delta CD$  over tape location for positive lift  $\alpha \geq -3^\circ$

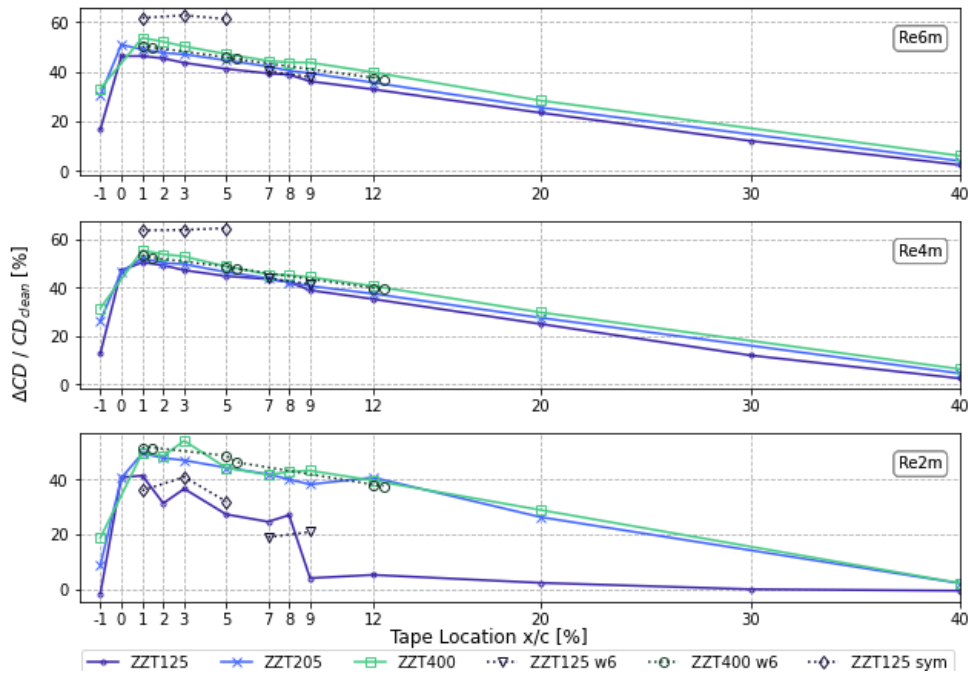
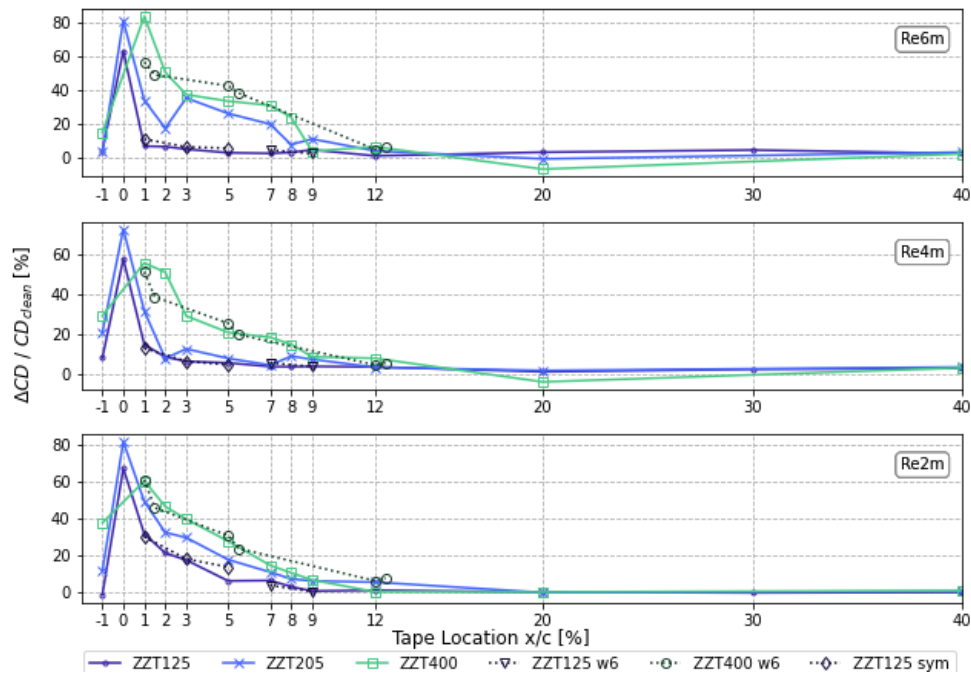


Figure 4.20:  $\Delta CD$  over tape location for positive lift pre stall  $-3^\circ \leq \alpha \leq 9^\circ$



**Figure 4.21:**  $\Delta CD$  over tape location for positive lift in stall  $\alpha \geq 9^\circ$

#### 4.5.5. Tape Width Variation

Tapes at shorter width perform similar to their wider version that is used as standard and are generally a good alternative to trip the flow.

At lowest tape height, the  $6mm$  version is not recommended by the author. The ZYT125w6 tape was found to be generally very sensitive to damages, as it has low material strength and small cuts easily occurred that were clearly detectable as drag peaks in the span-wise WR drag. Additionally, the adhesive glue on these tapes was frequently observed to introduce small collections of glue in the zigzag patterns that again locally increased the WR drag.

The rigidity of tripping tape at height  $h = 400\mu m$  restricted its use at the very leading edge for the wider version of  $12mm$ , which has been found to be the most severe setup with respect to performance penalties as observed in Section 4.5. Thicker tapes at a width of  $12mm$  are found to be impractical at the high curvature of the leading edge and have been observed to even fly off during testing due to not completely remaining attached to the surface at high curvature. At shorter width, these applications can be achieved, raising motivation to apply shorter tapes close to the leading edge, which was identified to be the setup to cause heaviest impact if intense roughness is required to be simulated.

#### 4.5.6. Symmetric Setup Variation

While the project scope was designed to focus suction side impacts, a limited amount of symmetric setups have been conducted where ZYT125 has been placed on suction and pressure side. Over the range of selected angle of attack ranges, it can be confirmed that pressure side tripping impact on the lift force is negligible. The drag is heavily impacted due to overall wake increase, except for in high angle of attack range in stall operations as observed from Figure 4.20 and Figure 4.21.

### 4.6. Additional Impact of Tape Application

While erosion usually erodes material away and creates distributed roughness elements and a negative area from de-lamination at highest states, ZYT rather continuously adds material over

the span wise direction. This fundamentally changes the flow parameters and the boundary layer thickness will increase to pass this local thickness increase.

Besides performance parameters such as lift and drag, other flow quantities will vary such as the aerodynamic center location with maximum shifting compared in Figure 4.22 with respect to the actual aerodynamic center. The aerodynamic center is generally shifted aft when applying ZZT and tripping the flow on the suction side, with larger shifting being generally related to thicker tapes as the Reynolds number increases and related to applying ZZT in the region  $1\% \leq x/c \leq 9\%$  having the maximum impact. The largest difference is obtained when pitching around zero-lift angle of attack  $\alpha_0 = -2.75^\circ$ , where lower Reynolds number flow is impacted for lower angles at  $\alpha = -3^\circ$  with lower zero-lift angle of attack and the stagnation point closer to the leading edge towards pressure side with pitching towards higher angles, while higher Reynolds number flow has a higher impact at higher pitch values of  $\alpha = -2^\circ$  when the stagnation point also moves closer to the leading edge. It can be seen that the  $125\mu\text{m}$  tape behaves differently at low Reynolds numbers, which indicates that the flow regime with this tape height causes a different impact on the flow field.

This behavior does however settle for all tapes, locations and Reynolds numbers for higher pitch angles  $\alpha \geq 2^\circ$ , indicating only a change when pitching around the zero-lift angle of attack  $\alpha_0$  and having negligible impact on other operational points.

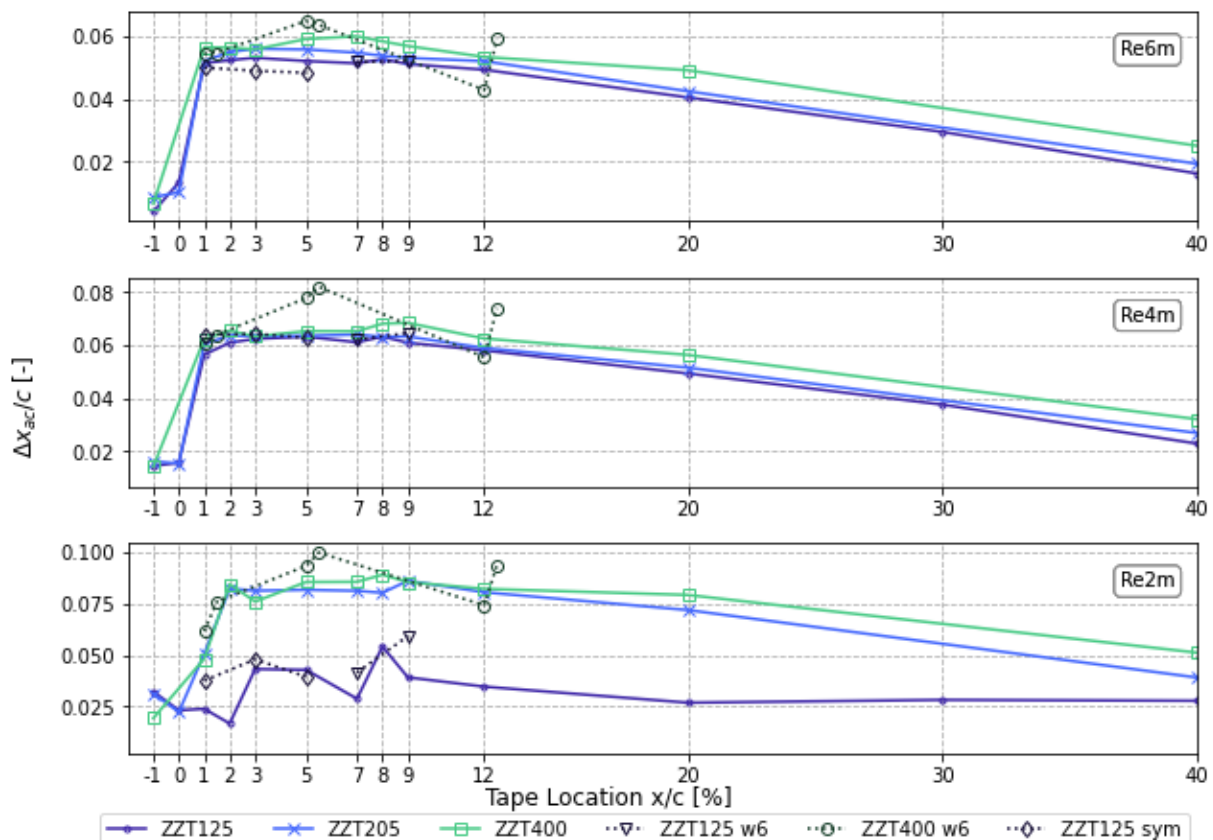


**Figure 4.22:** Mean Shifting of the aerodynamic center location due to zigzag tape application normalized by the chord length.

Furthermore, the stagnation point will shift as in Figure 4.23. However, this data is limited to the resolution of pressure taps on the airfoil and the required interpolation to yield actual values.

Therefore, the analysis lacks quality and certainty due to failed universal interpolation scheme. The overall shifting has however been selectively compared by manually viewing the pressure distributions and the overall conclusion of the stagnation point shift was found to be correct. The actual values however need to be considered carefully and the author recommends purely viewing results as indication that the stagnation point shifts aft.

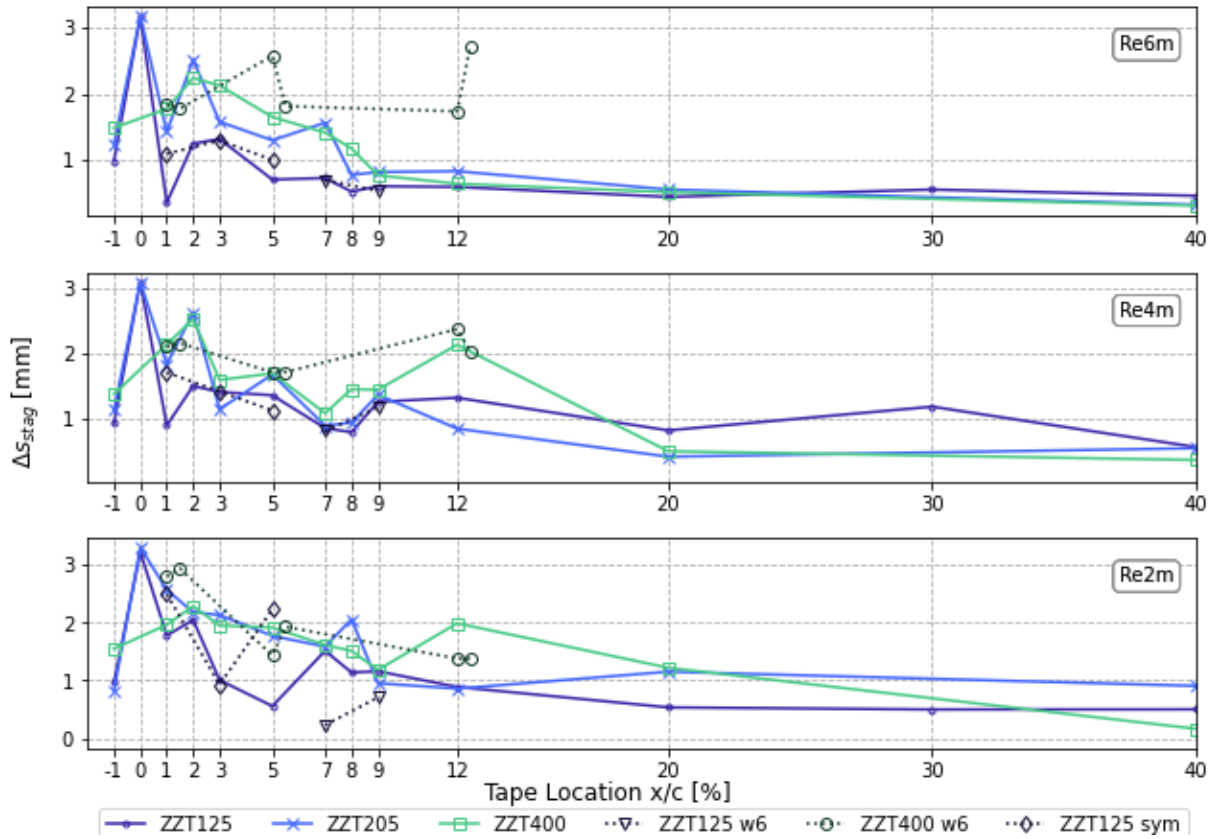


**Figure 4.23:** Mean Shifting of the Stagnation point in arch length for  $\alpha \geq -3$ . Positive values indicate aft shifting over the suction side.

### 4.7. Pressure Distribution

The previous plots in Section 4.5 have indicated 3 general trends where performance parameters tend to perform differently when varying tape setups with their location. A peak with large gradients until  $x/c = 3\%$ , a plateau behavior until  $x/c = 9\%$  and a linear relation further aft. Upon detailed investigation of the pressure distributions of all test series individually for various angle of attack, it was found that there are clear differences in how the ZTZ application impacts the pressure distribution over the airfoil. In this behavior, the tape height, width and flow conditions from Reynolds Number seem negligible and only influence the magnitude of the behavior while the trends seem to be purely dominated by tape location within the tested setups. The identified regions are listed in Table 4.2. Most recognizable is region 2, that behaves drastically different from the others and "cuts" through regions 1 and 3.

| Region | Start x/c [%] | End x/c [%] |
|--------|---------------|-------------|
| 1      | -1*           | 2           |
| 2      | 3             | 8           |
| 3      | 9             | 50*         |

**Table 4.2:** Three identified regions to vary clearly in pressure impact due to ZTT application within these regions. Starred values indicate the boundaries of tested conditions.

A visualization was generated as pressure coefficient distribution vector plot at their respective pressure tap location, due to the fact that the pressure deviation is small between cases compared to the overall pressure values. The chosen plotting method allows a visualization of vectors to be scaled differently between actual pressure coefficient distribution and the deviation  $\Delta CP$ , using vector scaling factors  $f_{vec,0} = 15$  and  $f_{vec,\Delta} = 0.5$  respectively, to emphasize on the small magnitude trends of  $\Delta CP$ , that behave drastically different. Each  $\Delta CP$  plot is scaled equally. Figure 4.25 is an example of this visualization, indicating the clear trend changes when moving over the border of the regions simply by shifting  $\Delta x/c = 1\%$  as it is done from row 1 to row 2 and from row 3 to row 4. Columns indicate clean pressure distribution (repeated per row) and the 3 different ZTT heights.

Interestingly, the trends remains equal within each respective region for all Reynolds numbers and tape heights. The trends vary for different angles of attack, but at same angles, each setup within its region again behaves equally. Only tiny changes in magnitude can be identified, apart from fundamentally different stall behavior differences that have been identified previously in Section 4.5. Proof of these statements (equal trends within regions) is documented in Section A.3 for different conditions, as well as a more traditional pressure distribution plot over chord-wise location.

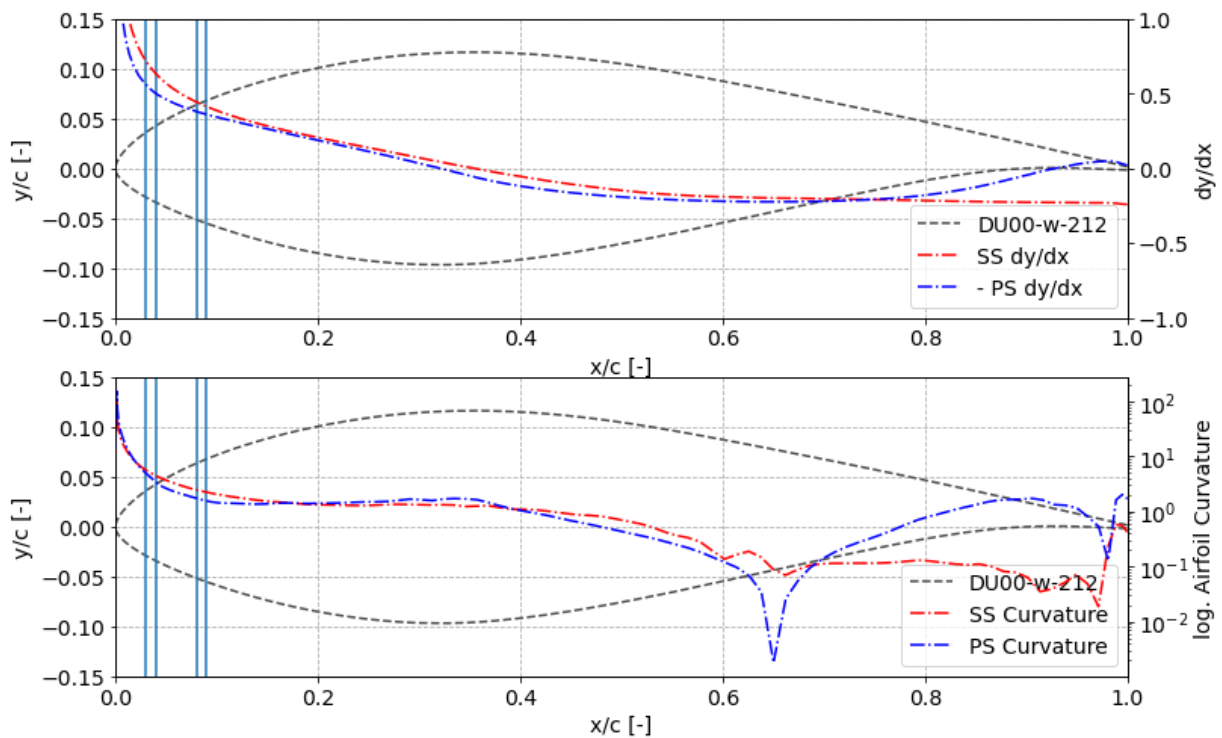


**Figure 4.24:** DU00-W-212 airfoil shape, derivative and curvature

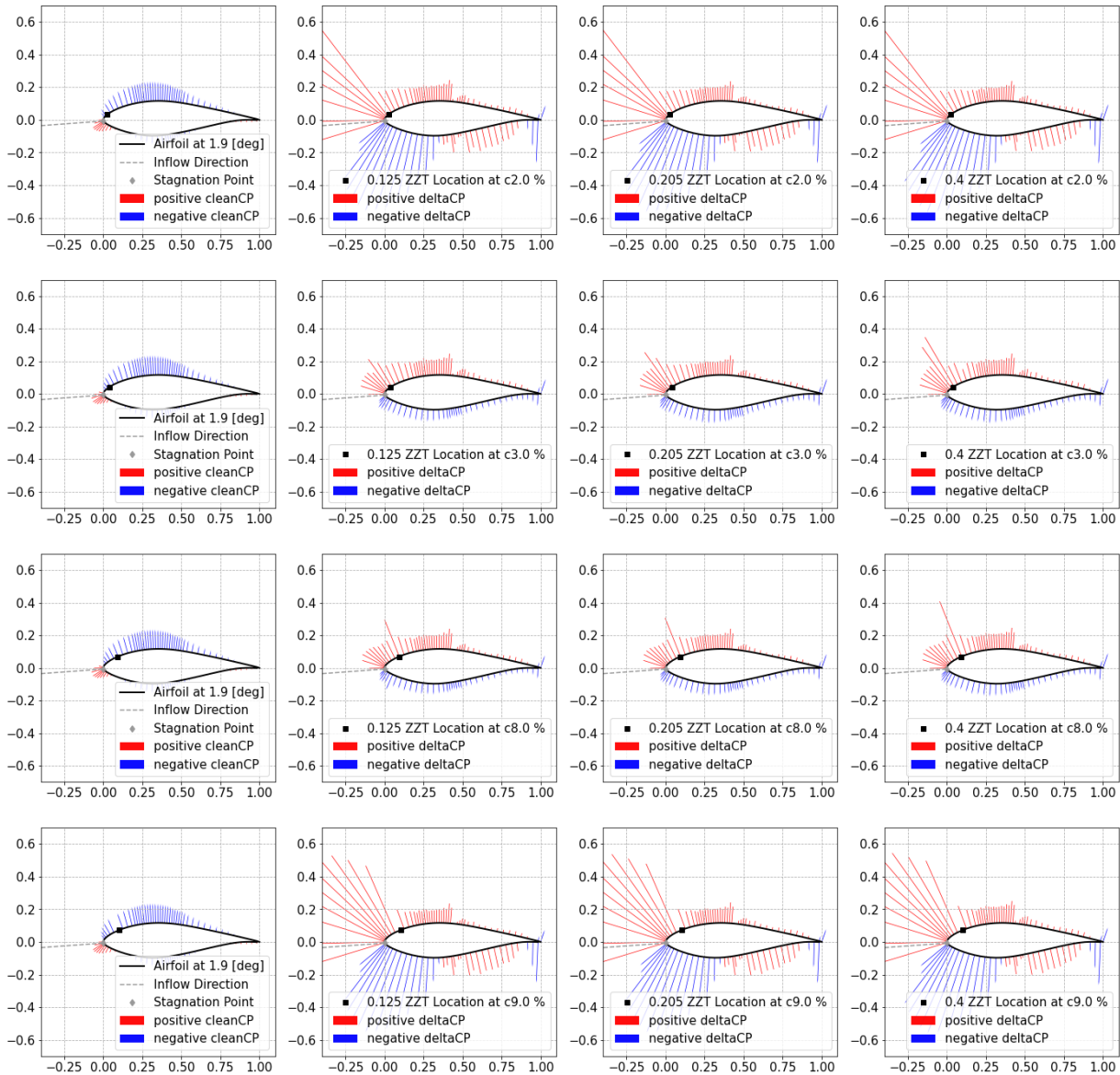


**Figure 4.25:** Three identified regions from analysis of  $\Delta CP$  force vectors

The main shared behavior is the direct impact behind the tripping, where for typical operational angles of attack, an increase in pressure is observed, until the natural transition location on the clean airfoil. Region 2 causes an overall pressure drop on the pressure side, thus causing a speed up over the pressure side. It is estimated that this behavior is related to the airfoil design and its shape as viewed in Figure 4.24. Vertical lines indicate bordering end and start ZZZT locations when moving into and out of region 2.

## RO3: Boundary Layer Rake

Previous studies of a boundary layer rake by Veraart et al. [33] have shown a disagreement between the design choice based on simulated boundary layer thickness and actual measurements with the manufactured instrument, which raises questions whether the boundary layer simulations are a key potential source of the error in the comparison between simulation data and wind tunnel measurements. Additionally, the existing design was tested on an airfoil that resulted in a rather slim boundary layer thickness, which is not recommended. The current airfoil choice allows for a thicker BLT and thus enables to perform this study at an expected improvement when taking into account, that simulation data could indicate wrong trends, as a generally thick BLT will still be able to be captured if designing with these expectations.

The improvement of the previous straight vertical BLR was adapted by an arc-shaped version as successfully done by Bui et al. [8]. The general concept with simulated BLR from panel code *RFoil* can be seen in Figure 5.1.

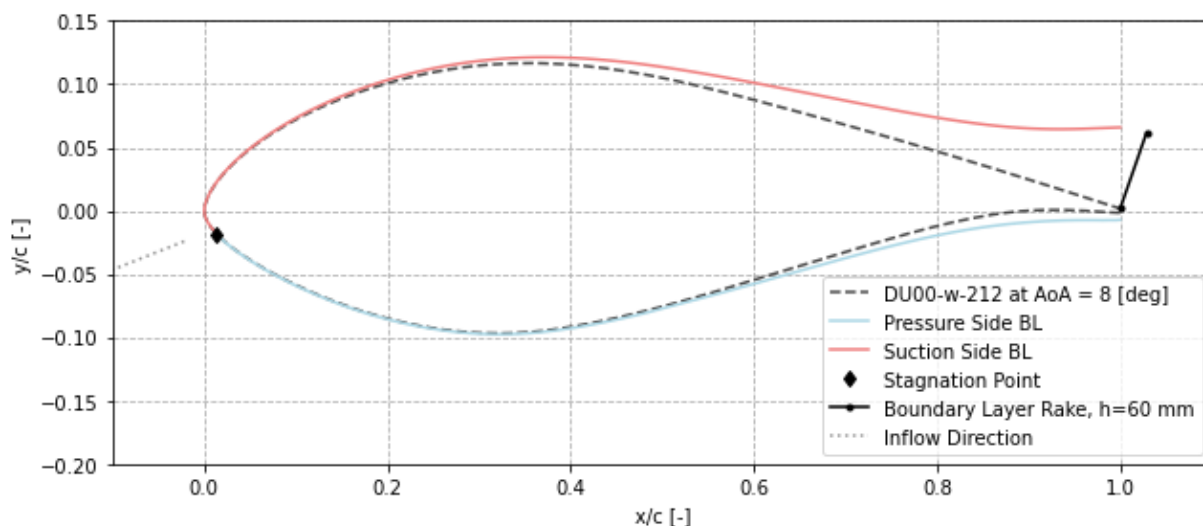


**Figure 5.1:** Conceptual idea of the BLR measurement plane on the DU00-W-212 at  $\alpha = 8^\circ$

### 5.1. The BLR Design

The existing BLR was tested by Veraart et al. [33] for an airfoil resulting in a BLT of  $\delta_{99} \approx 10\text{mm}$ , while the simulations based on panel code indicated a BLT of  $\delta_{99} \approx 20\text{mm}$ . Thus the results suffered due to relying the design on insufficient accurate initial panel code simulations and the BLR measurements resulted in poor resolution with only 2 pressure tubes in the height

$\delta_{99} = 10\text{mm}$  as the panel code overestimated the BLT.

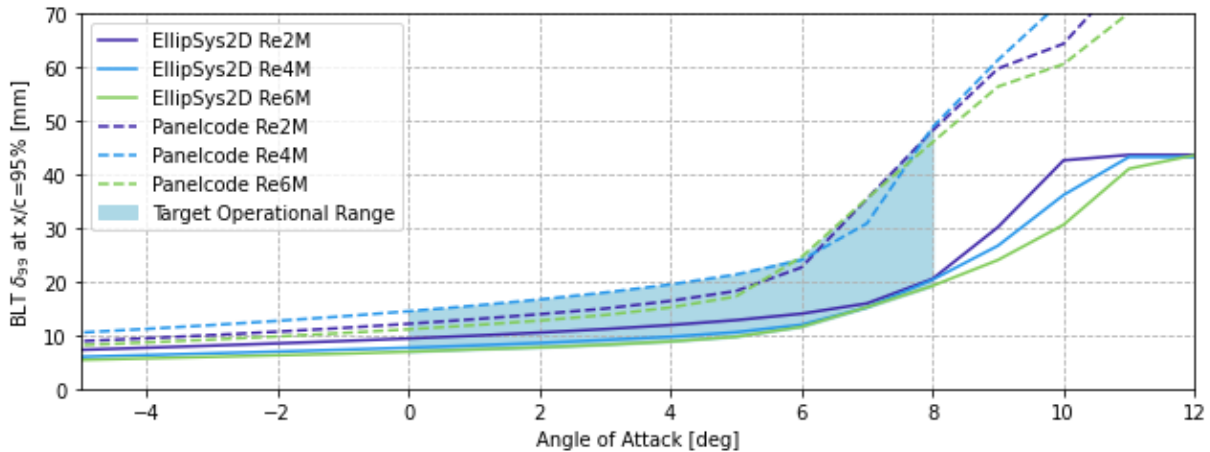


**Figure 5.2:** Simulated BLT at  $x/c = 0.95$  for 2D-CFD EllipSys and panel code RFOil over angle of attack

Similar simulations have been conducted for the DU00-W-212, adding 2D-CFD with EllipSys into the considered design parameters. The target operational range was chosen as  $0^\circ \leq \alpha \leq 8^\circ$  as typical operational range of wind turbines [7] and as safe option to avoid stall for this first design. Additionally, as the BLT varies largely during pitching of the airfoil, it should be avoided to have the BLR designed for too large heights as the intrusiveness will also increase. However, for this first prototype, safety of yielding data was chosen as main design objective over design optimization and priority was given to actually capturing and identifying the required BLT, thus including pressure tubes that could capture large heights. Reasoning for this is to be resourceful with testing time, as a too large BLR results in insights to optimize in the future, while a too small BLR introduces a risk of failed measurements due to not measuring the points of interest that would then require a redesign and repeated measurements even just for the prototype.

As the BLT increases with chord-wise extent, first measurements are aimed at the trailing edge and to utilize the static pressure measurement from the airfoil pressure taps, it is to be installed such, that the BLR total pressure tubes align with the trailing edge suction side pressure tap at  $x/c = 95\%$ . The attachment system is discussed in Section 5.1.2.

Assuming adiabatic walls to utilize BL theory [8] and a constant static pressure within the boundary layer [30] such that  $\delta P_{stat}/\delta y = 0$  allows to utilize the total pressure measurements of the BLR and static pressure measurement of the last pressure tap to compute the dynamic pressure and respectively the velocity for each pressure tube location.

### 5.1.1. U-Shape

With the experience of shifting schedules and required flexibility, it was chosen to design a boundary layer rake (BLR) with design focus on safety. Safety in minimum required distances, safety in aquired data by doubling the initial plan to have a redundance in data, safety in overall geometry to avoid missing the measurements of interest by trying to optimize this first prototype, safety in quick reproduction in case of an incident and safety of utilizing available material. It is thus expected that the first prototype is not an optimized version that indicates final possibilities with such an instrument. Finally, while potentially suffering in measurement quality, this approach has been proven to be correct as there was no availability for further experiments on an improved design and the first prototype had to be working in one run in the required field of interest for this study, that is the boundary layer thickness.

The design was decided to be arc-shaped in the lowest section of the BLR up to a height of  $h_{BLR,arc} = 20mm$ , matching both the majority of panel code estimated BLT values as well as the final BLT at the highest pitching angle of  $\alpha = 8^\circ$  for the 2D-CFD BLT values in Figure 5.2. The arc-shaped section is extended by a straight and vertical section to further improve measurement resolution.

With those insights and the design choice of prioritizing safety of results for all angles (and opportunity to go for even higher angles), the overall height for pressure tubes was selected as  $h_{BLR,vert} = 60mm$ . With the possibility to improve the static and dynamic reference values by including a pitot tube into the top of the BLR, an additional location is included in the design, at a larger distance due to increased diameter of the pitot tube and the requirement to have undisturbed flow at the pitot tube to get valuable reference values. This resulted in a final design height of  $h_{BLR,des} = 75mm$  plus wall thickness thus effectively yielding a height of  $h_{BLR,tot} = 78mm$ .

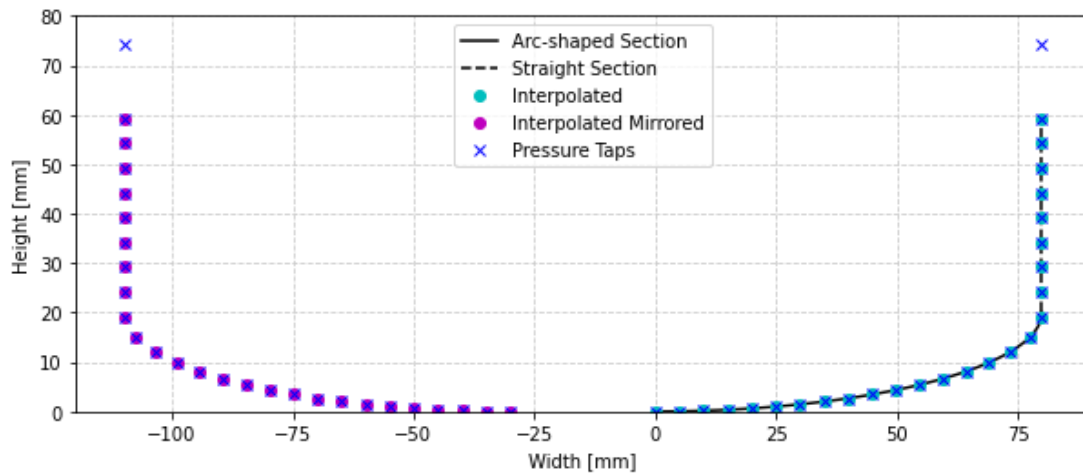


**Figure 5.3:** U-shaped BLR Pressure Tube Layout with effective 2.5 Diameter distances

The arc-shape was designed such, that simple and quick adjustments can be made in future designs and the design is therefore taken as quarter arc of a circle with previously selected radius  $h_{BLR,arc} = 20mm$  and then manipulating the x-coordinates by applying a stretching factor of  $f_{stretch} = 4$ . This results in a width of  $w_{BLR,side} = 80mm$ . However, this possibly introduces one of the largest problems of the design, as the BLT will not be evaluated at the same span-wise location for the height range of  $h \leq 20mm$ . The airfoil model inspection in Figure 2.4 has indicated that the span-wise extent varies with respect to airfoil surface quality and to avoid measurement mistakes due to local phenomena such as increased BLT due to surface imperfections, it is chosen to duplicate the measurement points by mirroring the design - resulting in the U-shape. This final design yields two sets of boundary layer data, that can indicate measurement quality when comparing data to validate the instrument and the reliability of measurement data. While this again increases intrusiveness, it still complies with the design choice of data safety with respect to validating whether this instrument is valid and delivers repeatable data by having a full redundancy for each measurement point. Additionally, for improved rigidity, this design allows connecting both sides to avoid bending of the individual sides to avoid measurement mistakes, which was assumed to be unnecessary after 3D printing the model.

As first step improvement with respect to the current design, it is chosen to utilize similar pressure tubes, which additionally has the advantage of not requiring specific tubes to be ordered to not increase the project budget. Recommended better choices are discussed in Section 5.4. The existing pressure tubes have a length of  $l = 120mm$  and a diameter of  $d = 2mm$ , with a wall

thickness of  $t = 0.67mm$ . As square cut pressure tubes, the directional sensitivity is  $\theta = 11^\circ$ . Bui et al. [8] used a spacing of 2 diameters between measurement points, which has been increased to 2.5 for this design, resulting in a total of 26 pressure tubes per BLR side, with 14 measurement points in the first  $h \leq 10mm$  of the BLR height, another 4 measurement points between  $10mm \leq h \leq 20mm$  and finally another 8 measurement points for  $h \geq 20mm$ . The final geometry of the design can be seen in Figure 5.3. The depth of the design was selected as  $d_{BLR} = 50mm$  and the design was drawn and 3D printed utilizing in-house CAD and 3D-printing soft- and hardware. The design parameter overview can be seen in Table 5.1.

| Parameter                     | Units | BLR U-Shape Prototype |
|-------------------------------|-------|-----------------------|
| Width per Side                | mm    | 80                    |
| Width Center Piece            | mm    | 30                    |
| Width in Total BLR            | mm    | 190                   |
| Height of Arc-Shape           | mm    | 20                    |
| Height of Pressure Tubes      | mm    | 60                    |
| Height of Total BLR           | mm    | 78                    |
| Nr of Pressure Tubes per Side | -     | 26                    |
| Nr of Pressure Tubes in Total | -     | 52                    |
| Spacing between Tubes         | mm    | 5                     |
| Depth of BLR                  | mm    | 50                    |

**Table 5.1:** Boundary Layer Rake Design Parameters

### 5.1.2. Attachment Design and Installation

The BLR is designed to measure at  $x/c = 95\%$  at a distance of  $x = 20mm$  away from the trailing edge and the pressure tube length of  $l = 120mm$  indicates that the instrument needs to be installed and attached behind the airfoil. A dynamic attachment to the airfoil was favored over a static attachment on the ground or wall due to fixing the frame of reference with the airfoil being superior as it enables a single installation to be applicable for a various range in operational angles of attack, while a static installation in the frame of reference of the wind tunnel would require manual adjustments. It is estimated that this saves wind tunnel testing time by having lowest installation efforts. This is however at the costs of having to introduce an additional attachment system to the airfoil, further intruding the flow. This solution however has the advantage that it utilizes the general intrusion on the airfoil mode, as the pressure plastic tubing needs to be exported from the test section via a small hole on the side of the wind tunnel to be connected with the pressure transducer module. These plastic tubes will be attached to the pressure side trailing edge.

The attachment system is designed such that it does not interfere with the suction side, where the measurements are conducted, thus only intruding the flow on the pressure side, similarly to the existing plastic tubes. With an angular difference between suction and pressure side of  $\beta = 12^\circ$  and a distance of additional  $l = 100mm$  to be covered, this resulted in the attachment adapter as seen in Figure 5.4 that was again 3D printed in-house. To ensure the attachment, the BLR is glued to the attachment adapter with pressure sensitive tape "Nastro Adesivo" by 3M, by applying pressure over night with a clamp. Similarly, the combined system of BLR and adapter is then attached to the airfoil pressure side the day before the testing campaign over night utilizing similar clamps. To avoid damages on the airfoil, it was chosen to use foam on the contact surfaces and a wooden block was placed to increase the range of the clamps. The installation was successful

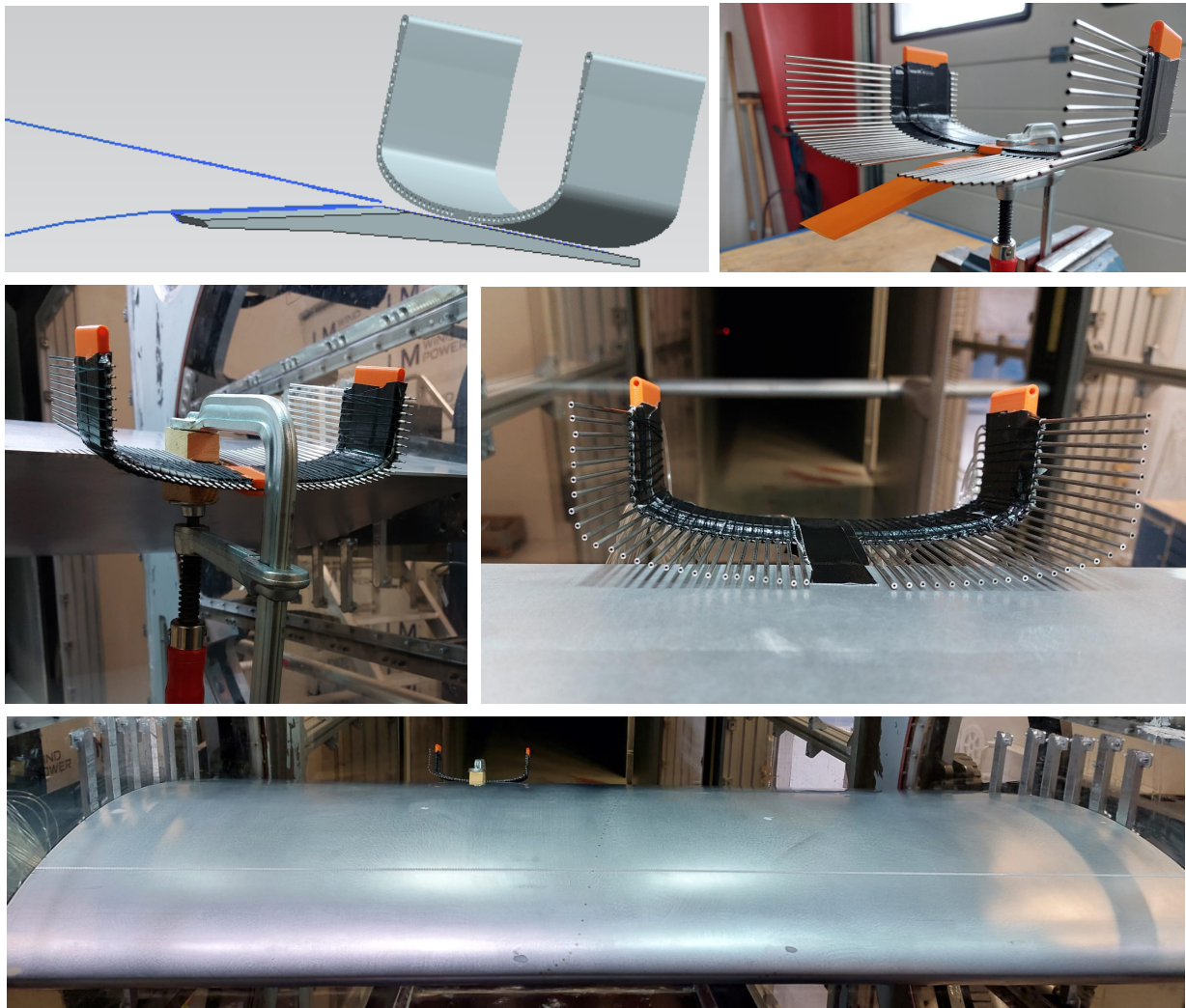


**Figure 5.4:** Visualization of the CAD design, final BLR instrument with attachment adapter and installation on the DU00-W-212 airfoil

and very rigid as it later even withstood maximum operational conditions of  $U_{inf} = 100m/s$ .

However, this introduced an installation error where the BLR was slightly tilted in span-wise direction, resulting in a deviation of actual installed height with respect to theoretical height of pressure tubes that needs to be corrected for and the deviation was documented by measuring the actual height of 10 reference pressure tubes. The chord-wise alignment was successful and parallel to the trailing edge at the planned location. The actual installation of the printed BLR in the wind tunnel can be seen in Figure 5.4, indicating the installation method using clamps, the installation error and an estimate of span-wise comparison with the DU00-W-212 airfoil model (the visualization though includes the wooden block and clamps in the center). The heights of the installation error were re-evaluated post testing and were confirmed to motivate a height correction in Section 5.2.1 and also validates that the attachment system withstood the testing cases.

## 5.2. Boundary Layer Rake Testing

The BLR has been tested according to the test matrix in Table 5.2. The main points of interest were clean performance and tripping at the very leading edge, to allow a comparison on simulation

data. With respect to the project scope and timeline, the discussion is focused on the actual boundary layer thickness  $\delta_{99}$ , while further research could investigate the velocity profiles more detailed as well.

A working method at the wind tunnel control bridge has been established by utilizing first measurements on the pre-installed and therefore additional case of ZZT with height  $400\mu m$  and width of  $6mm$ . The BLR campaign measurements were conducted manually, by setting up wind tunnel parameters individually instead of relying on pre-defined standard processes for regular wind tunnel operations. These measurements were conducted at a angle of attack range of  $\alpha_{BLR,1} = [0, 2, 3, 4, 5, 6, 7, 8]^\circ$ , which was later increased by adding  $\alpha_{BLR,2} = [-6, -4, -2]^\circ$  as estimated time of the experiments allowed for a higher resolution in angles of attack. Each test series was measured for  $t = 30s$  and the WR was only traversed for selected angles  $\alpha_{BLR,WR} = [0, 8]$  to allow insights at the borders of the pre-defined range of interest. The final test series was conducted at  $Re=6M$  to view if the BLR and attachment system can withstand the wind tunnel operations and maximum capacity, which is the reason that only the clean performance has been tested at those conditions. This test succeeded and the instrument system is rated sufficiently strong at tested conditions, the series was however interrupted after  $\alpha = 7^\circ$  as manual observation on the side of the wind tunnel indicated possible first deflection of the BLR. These observations have been made by the author, while it remains unsure if the small magnitude in observed deflection were indeed detected on the model or were rather observed due to the vibration on the plexy glass walls of the wind tunnel itself. The BLR was not pushed to possible failure to avoid any incidents at the initial testing series.

| Case       | Re=2e6 | Re=4e6 | Re=6e6 |
|------------|--------|--------|--------|
| Clean      | x      | x      | x      |
| ZZT 125    | 1%c    | 1%c    | -      |
| ZZT 400    | 1%c    | 1%c    | -      |
| ZZT 400 w6 | 12%c   | 12%c   | -      |

**Table 5.2:** Test Matrix of the BLR applied on the DU00-W-212 trailing edge at  $x/c = 95\%$

### 5.2.1. Height Correction

The installation error is corrected as the height precision is crucial when studying the boundary layer. While the velocity profile was not the main objective of this testing campaign with respect to the point in time of the project, an indication has been computed, especially to validate the previous statements to rate the left and right side of the measurements with respect to the installation error. The measured displacement and resulting height adjustment to the left side coordinates can be seen in Figure 5.5 as well as a comparison of both sides of the measurement instrument with and without the corrected coordinates. The values for both sides agree well for all test series and angles.

### 5.2.2. Intrusiveness

Introducing an external device as the BLR is expected to disrupt the flow locally and both WR span-wise drag as well as airfoil pressure distribution have been evaluated to rate the intrusiveness of the instrument as can be seen in Figure 5.6. First of all, the BLR seems to be applicable for general wind tunnel operations, as the most relevant data sources can be utilized, possibly allowing BLR measurements even for general wind tunnel test campaigns, as the overall airfoil pressure tap impact is assumed negligible and the WR drag can be utilized as drag source when adjusting the WR filtering.

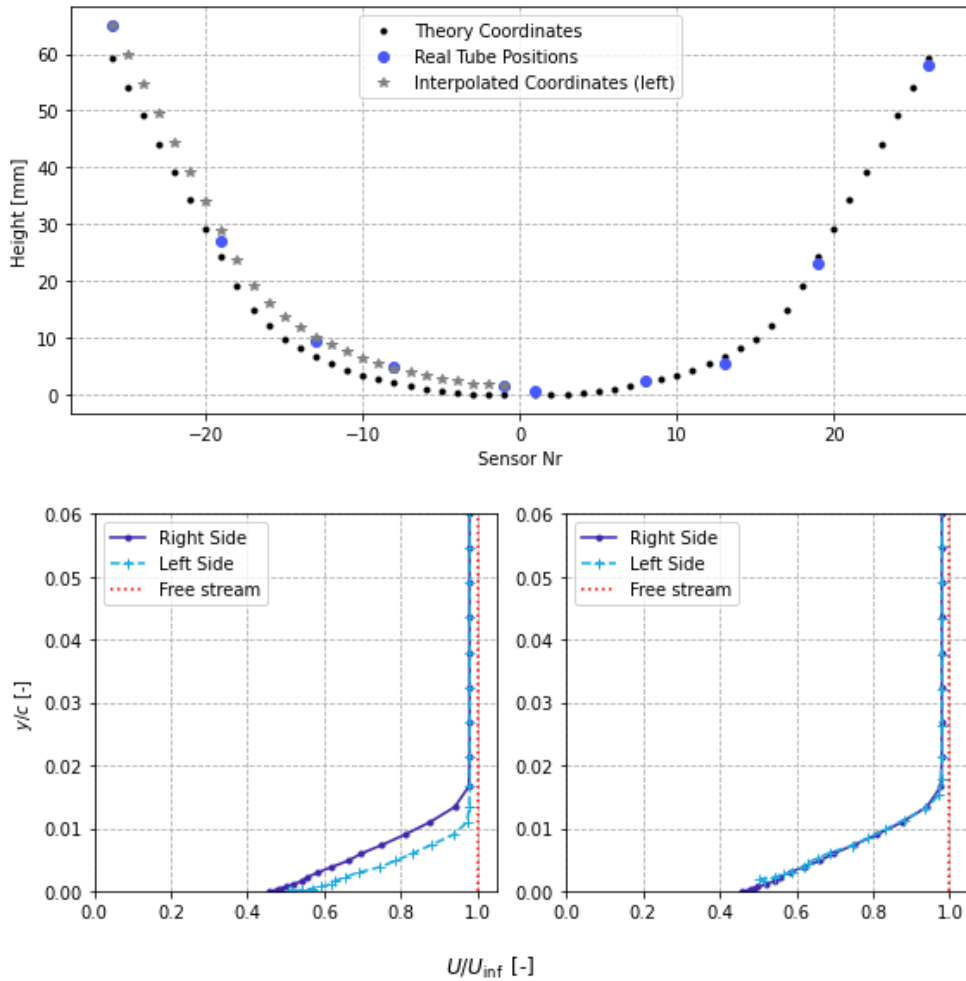


**Figure 5.5:** Uncorrected and corrected velocity profile for  $Re=6e6$  at  $\alpha = 2^\circ$

This does however not solve the local intrusiveness and this part thus remains questionable and would have required testing according to schedule to allow for those additional experiments.

### 5.3. Results

The resulting boundary layer thickness measurements are compared to simulated data in Figure 5.7.

Panel code simulations generally overestimate the boundary layer thickness. This holds for various input variations with respect to  $N_{crit}$  and Mach number. The clean computations however agree better for higher  $Re$  number, which can be seen from the trend when comparing  $Re=2e6$  and  $Re=4e6$ . While the  $Re=6e6$  series should be considered as more uncertain due to previously mentioned observations in that test series, it does show a similar trend and the author is confident that the test series is trustworthy at its limited data point range. A general deviation as function of angle of attack for panel code simulations is observed for  $\alpha \leq 5 \pm 1^\circ$  for different  $Re$  numbers. This can directly be related to the transition point prediction of panel code simulations, which predict earlier natural transition than observed from actual measurements based on pressure distribution and stethoscope tests. With an earlier natural transition, the boundary layer becomes transitional and likely also turbulent at an earlier chord-wise location, thus increasing in thickness as turbulent boundary layer for a longer chord-wise distance. With therefore larger boundary layer

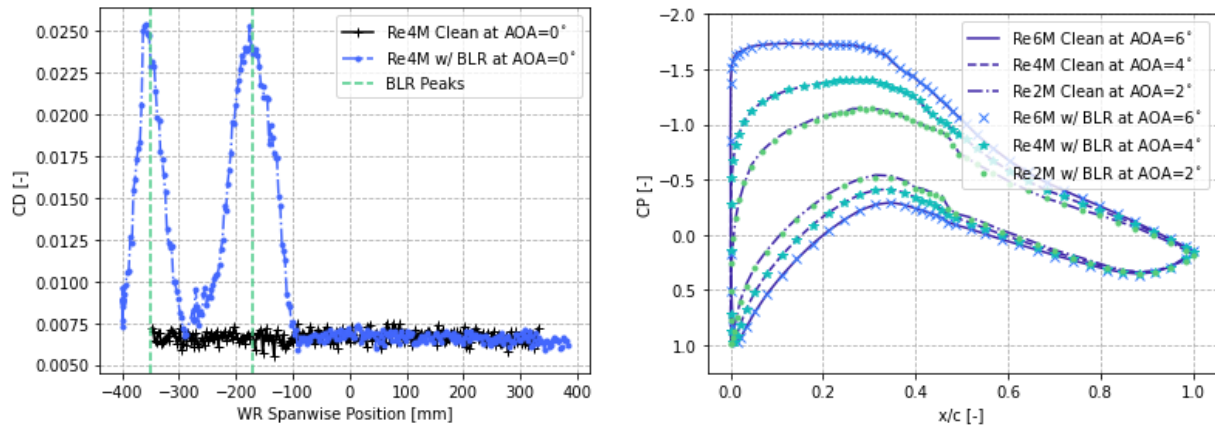


**Figure 5.6:** BLR Intrusiveness of WR Drag and CP Distribution

growth, the thicker boundary layer is expected for panel code simulations for earlier transitioned flow.

When tripping the panel code simulations, a similar trend of a generally overestimated boundary layer thickness can be seen. However, the shape matches fairly better as the mentioned mismatch of natural transition is bypassed. When tripping close to the leading edge and within the range of stagnation point shifting due to changes in angle of attack, it can be observed that the change from clean flow to tripped flow, effectively the jump at  $\alpha = -6^\circ$  occurs too early. When considering a too early jump, one could consider comparing to a more aft trip location, which does though result in an even earlier jump as it will be passed earlier by the stagnation point, which is when this jump occurs. When comparing it to the opposite, thus a location closer to the leading edge and thus being passed later by the stagnation point, it was not found to be sufficient to match the jump response of the measurement data even if tripping at the earliest suction side location at the very leading edge.

Finally, the panel code values have been evaluated isolated from their respective angle of attack by manipulating that array. This different jump can then generally be adjusted for clean and tripped case when evaluating the simulated data at  $\alpha_{fix, clean} = \alpha_{sim, clean} + 1.5$  and  $\alpha_{fix, trip} = \alpha_{sim, trip} + 3$  respectively as can be seen in Figure 5.7. This proposes a possible improvement for panel code *RFoil* and it would be required to be investigated on different airfoils to draw general conclusions.

When comparing the adjusted BLT from panel codes with the different tape height applications at  $x/c = 1\%$ , the closest BLT as function of angle of attack is found for the thin tripping tape in the  $Re=4e6$  case, which is expected. In this flow regime, the ZZT causes instant tripping of the flow and as the panel code purely introduces a trip behavior to the flow at a selected location, it is expected to be similar to thin tape setups, as these introduce less of a general boundary layer displacement due to their tape height as it is found for thick tapes. Furthermore, it has been identified that towards stall, the tape height is directly related to phenomenon such as early stall.

Clean simulations in EllipSys2D underestimate the boundary layer thickness and the expected low drag is confirmed in Figure 5.8.

## 5.4. Limitations and Improvements

Tests were limited to one testing series and different chord-wise positions should be tested for the BLR to get BLT comparisons at different locations to allow creating a general relation as with the adjustment of AOA values in Figure 5.7 and to then propose an improvement to current panel

codes. Panel code computations seem to be accurate, but the points of interest such as natural transition location and trip behavior jump effect with respect to wind tunnel operations are off and expected to be a major source of errors.

Furthermore, the velocity profile, while not a research objective at this point should be tested with PIV or HWA array to validate and potentially create correction functions as the tool is assumed to be rather intrusive even if it allows applicability such that undisturbed polars are possible as observed in Figure 5.6. Especially the measurement points closest to the surface are expected to be highly influenced by the small spacing to the wall as no 2 diameter spacing can be utilized there and blockage effects are expected to be dominating.

The momentum and displacement thickness should be investigated as originally planned, which was not realizable due to the 8 week delay in these final tests.

Thinner pressure tubes with improved directional sensitivity as utilized by Bui et al. [8] are recommended as well as a instrument shape design to be more aerodynamic. Furthermore, after validating the methodology, the redundant mirrored side should be removed to further decrease intrusiveness. Finally, the planned top location should be utilized with pitot tubes for further input on static pressure and second reference of dynamic pressure in free stream, which again failed due to wind tunnel delay.

The interested reader is recommended to view the currently running LERcat project, that aims to design and utilize a similar BLR with proposed improvements.

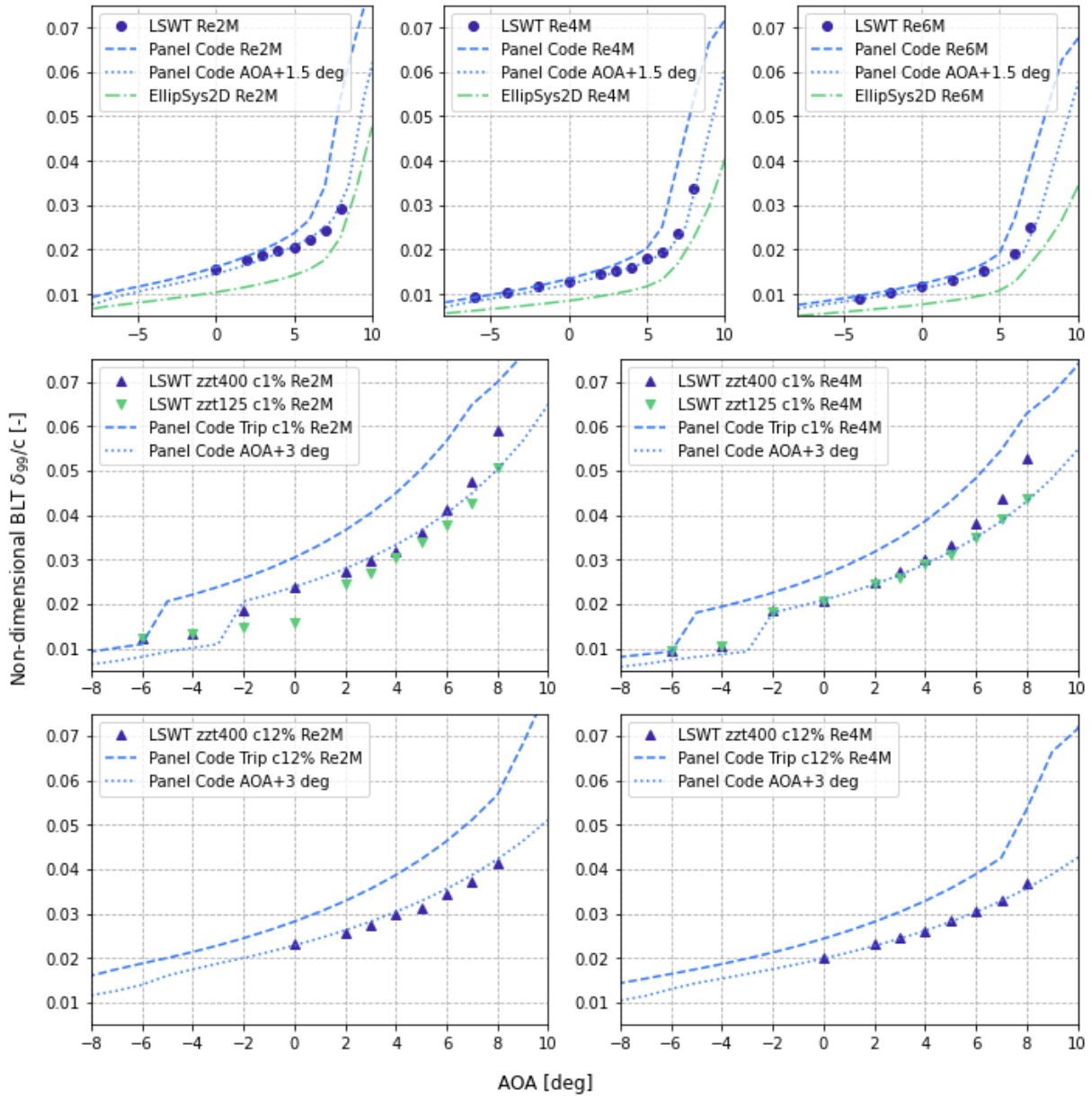


**Figure 5.7:** Comparison of BLT measurements and simulation cases including proposed Panel Code modification

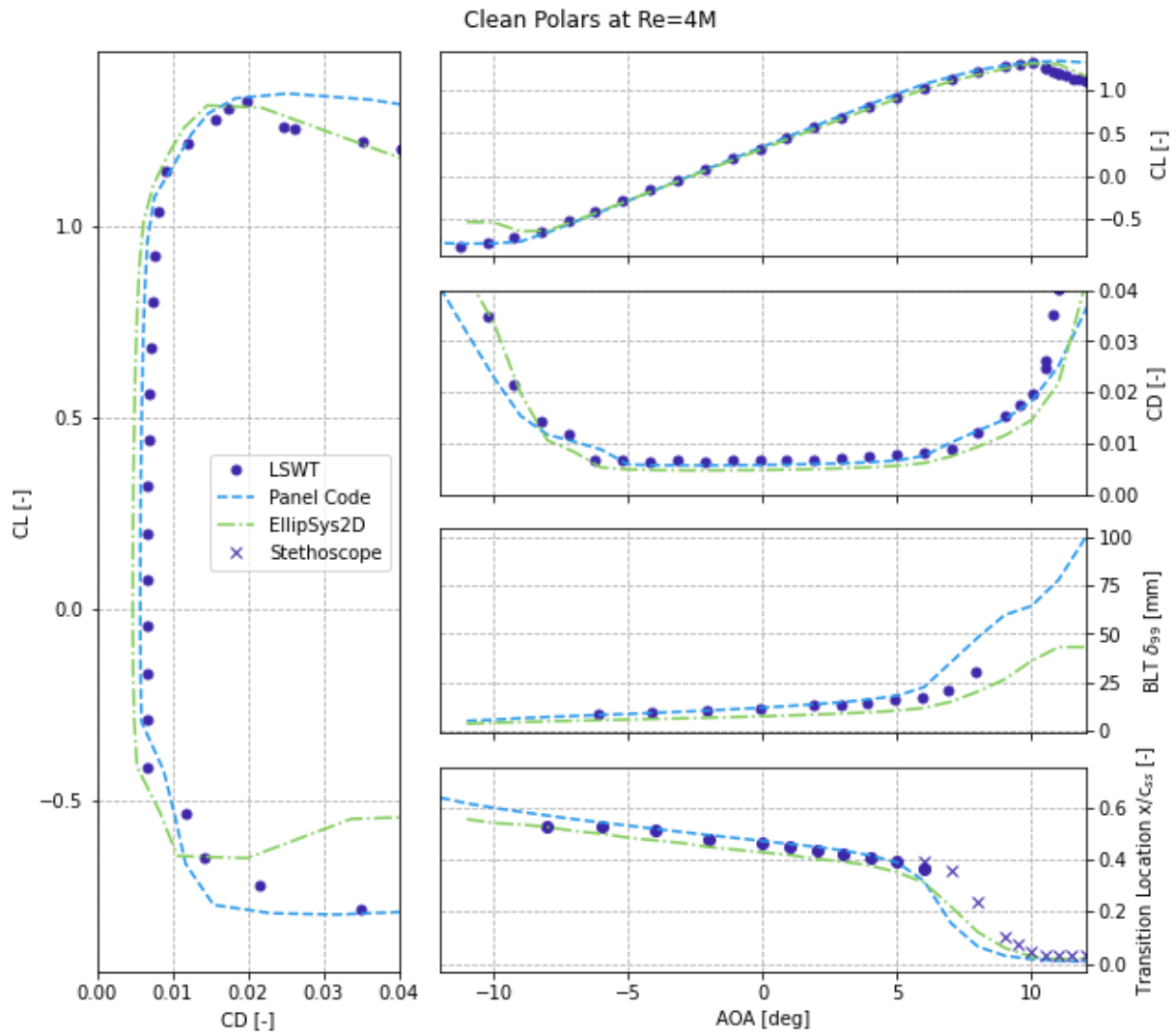


**Figure 5.8:** Wind Tunnel Tests compared to Simulation Data for polars, BLT and transition location

## RO4: Step Orientation

The study of reference literature indicated a disagreement whether the forward (FW) or the backward (BW) step is more critical for roughness impact. Forsting et al. [9] conducted a detailed CFD study with various geometries for frequently observed airfoil imperfections, including a FW and BW step, for which the pure FW step has been identified to have a more crucial impact. However, Bragg et al. [10] states that transition for roughness has been observed only at the trailing edge of the roughness element, agreeing with the tripping methodology of inducing instabilities as a function of the BW step.

To study the difference, a changing setup was planned with the detachable leading edge model (DLE), where either a pure FW or BW step was introduced. However, due to the DLE model at times of the project being unexpectedly of poorer quality than expected, this approach was not doable to get wind tunnel capacity and alternative experiments have been conducted. Overall, this research objective is not expected to be fully solved and only an indication from the alternative approach is discussed.

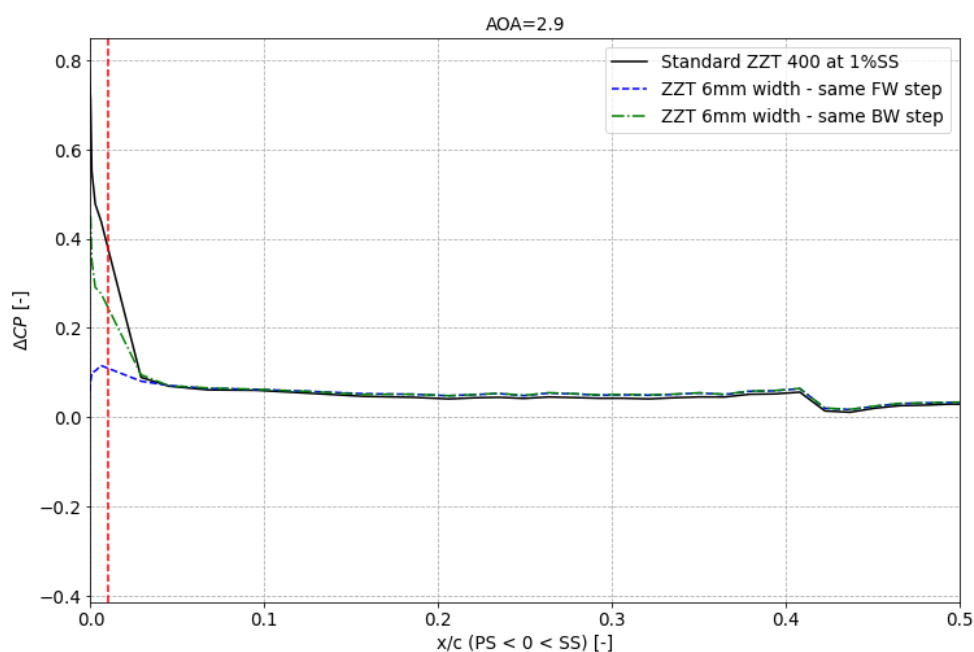


**Figure 6.1:** Forward vs Backward step of 6mm ZTT wrt. shared reference of 12mm ZTT

Therefore, 3 setups of ZTT were tested:

- (a) 12mm ZZT,
- (b) 6mm ZZT with same FW step location as (a),
- (c) 6mm ZZT with same BW step location as (a).

This setup does have the weakness, that no exact same ZZT in 12mm and 6mm is available and there is a small change in geometry as well, where (a) has a  $60^\circ$  angle and a  $70^\circ$  angle for (b) and (c). This minor change in angle is assumed to be negligible with respect to the geometry change of reducing the width by 50%.

Additionally, this setup has been tested for different AOA, Re and locations to identify a clear trend in the pressure distribution impact  $\Delta CP$ . Figure 6.1 shows these trends for  $400\mu m$  ZZT at  $x/c = 1\%$  and for more locations in the appendix in Section A.4.

It was chosen to not view the polar data to rate impacts with respect to a FW and BW step comparison, as the shared FW step setup (b) will have higher performance penalties than setup (c) due to an earlier trip, resulting in a larger region of the flow to be impacted by the ZZT.

This raises awareness that notation should potentially be changed to BW steps, or to raise awareness that when tripping tapes are used, it is crucial to state geometry clearly to allow identifying the actual BW step locations, e.g. combining FW step location and tape width.

## RO5: Reference Roughness Data

This chapter discusses the comparison of various tripping tape setups with respect to the limited reference data on real erosion utilizing the detachable leading edge with 3D printed leading edge modules for clean, incubation, erosion and heavy erosion cases by Veraart et al. [33] in Section 7.1 that is based on the same airfoil model. Data can be compared for this reference at matching conditions  $Re=6e6$ . Lastly, with granted permission by and great thanks to T.Vronsky, N.Gaudern and Vestas A/S, the Risø 18% thickness airfoil data as investigated by Gaudern et al. [7] is compared for the different stages of erosion in Section 7.2. Data can be compared for the available data at  $Re=2e6$ . While small comments are made on how it is expected to better perceive the profiles, both sections assume a realistic and successful recreation of real roughness as reported in the respective papers.

### 7.1. Detachable Leading Edge

The detachable leading edge model is a DU00-W-212 airfoil model with a modified leading edge that allows the attachment of various profiles, including 3D printed erosion patterns at different erosion stages based on rain erosion test samples. As light to heavy patterns did not vary largely and an overall overestimation with tripping tapes is reported, this section will also relate to the heavy erosion profile. The existing gap in span-wise direction on the DLE is required to be as smooth as possible and filled with minimum deviation with respect to the overall airfoil geometry. The aerodynamic performance of this model was analyzed and the aerodynamic performance of the clean DU00-W-212 is not recreated for any pattern of a clean detachable leading edge, neither aluminium nor 3D printed. With an improved filling method, the DLE model was expected to be successful for future test runs but the initial tests on the clean leading edge patterns disproved expectations and at the current state the model was not sufficiently convincing to be tested for the present study. This section considers mainly the heavy erosion patterns and the "breakthrough" DLE profiles at a higher erosion stage are neglected as those propose no further performance penalty and are expected to not be a realistic representation of "breakthrough" effects to the main laminate of a wind turbine blade, similar to the stage 5 delamination case by Gaudern et al. [7] as can be seen in Section 7.2. Finally, it needs to be stated that these DLE profiles are designed based on one operational setup of rain erosion tests and real erosion can result in various erosion patterns.

Nonetheless, the existing data allows interesting insights when compared to the present research with a variety of tripping tape setups. The overall performance penalty on the leading edge profiles are best resembled with tripping tapes around the very leading edge, thus raising importance to match the actual tripping location. This can be connected to the *DLE* data point that drops to clean performance in the CL over CD subplot. At this angle of attack, the stagnation point covers the leading edge and the erosion pattern, thus disabling any penalizing impacts, as

| Reference Name | Severity | Author         | $\Delta CL$ | $\Delta CD$ |
|----------------|----------|----------------|-------------|-------------|
| A2             | 2/9      | Sareen et al.  | -5 %        | + 80%       |
| 1              | 1/5      | Gaudern et al. | -4 %        | + 50%       |
| Heavy Erosion  | 3/4      | Veraart et al. | -5 %        | + 45%       |

**Table 7.1:** Ranking the DLE heavy erosion with roughness stages by Sareen et al. [6] and Gaudern et al. [7]

it can be found for ZTT applications discussed in Chapter 4. The ZTT however covers a smaller range on the surface and therefore that range of angles of attack is observed to be larger for which tripping effects are disabled. For real erosion, the chord-wise extent of eroded regions is expected to be further than design range of the DLE profiles in the range of  $-2\% \leq x/c \leq 2\%$ . The flow will trip for the earliest location that depicts the start of the suction side flow aft of the stagnation point for which the critical conditions are met. With a larger coverage on the chord-wise direction, this range of disabled tripping effect will therefore disappear.

Generally rating the patterns by Veraart et al. [33] and their performance penalties, even the heavy erosion cases, are over-predicted by most ZTT cases. This is unexpected as reference studies rather rate ZTT to be under-predicting roughness impacts. The author therefore proposes an adjustment in how to evaluate the DLE profiles. Related studies that rated different roughness stages disagree to rate the DLE performance as heavy erosion, but rather as low erosion in the lower 10-20% with respect to severity of roughness stages, 100% being classified as delamination cases. The DLE erosion performance is therefore compared with roughness classifications of different stages by Sareen et al. [6] and Gaudern et al. [7] in Table 7.1. The DLE model is therefore estimated as good representation to evaluate light erosion cases that are generally found to be over estimated when simulated with ZTT.

The aerodynamic performance for lift and drag polars are compared in Figure 7.1. The 3D printed eroded DLE data can be compared to 2 states of clean airfoil performance, the actual aluminium clean profile or its 3D printed clean profile counterpart. The deviation of the aluminium clean DLE profile with respect to the clean DU airfoil depicts the same trend of tripping tape applications at the very leading edge, but at much lower intensity than for ZTT. The point of the traversing stagnation point can be detected to match with the DLE model gaps and DLE data will therefore be impacted by this additional impact besides the erosion patterns. An even larger and overall drag increase can be observed in lightgrey for the  $\Delta CD$  in the lower subplot as well as in the left subplot, raising doubts over the material usage of 3D printed profiles. The peaks in the  $\Delta CL$  plot indicate a slight shift in zero angle of attack, which behaves different for ZTT applied on the suction side.

The pure erosion pattern impact should thus be compared to the 3D printed clean DLE profile. Assuming the  $\Delta CD$  and  $\Delta CL$  due to the 3D printed version can be isolated, comparisons to the aluminium clean DLE profiles are possible.

Lift and drag are impacted at similar magnitude as for the selected ZTT 125 0%*c* comparison setup, while ZTT cases all present a larger performance penalty. This ZTT choice most closely represents the erosion patterns of the DLE model, by testing thinnest tapes and at a different location than the standard ZTT. The performance penalties can be increased by utilizing thicker tapes or decreased by moving the tape further aft, which will have several impacts as discussed in Chapter 4, such as stall impact. The polar data penalty is however not met with DLE data for any case. The best alternative comparison setups with their application reasoning are listed in Table 7.2. Their respective results can be seen in Section A.5.

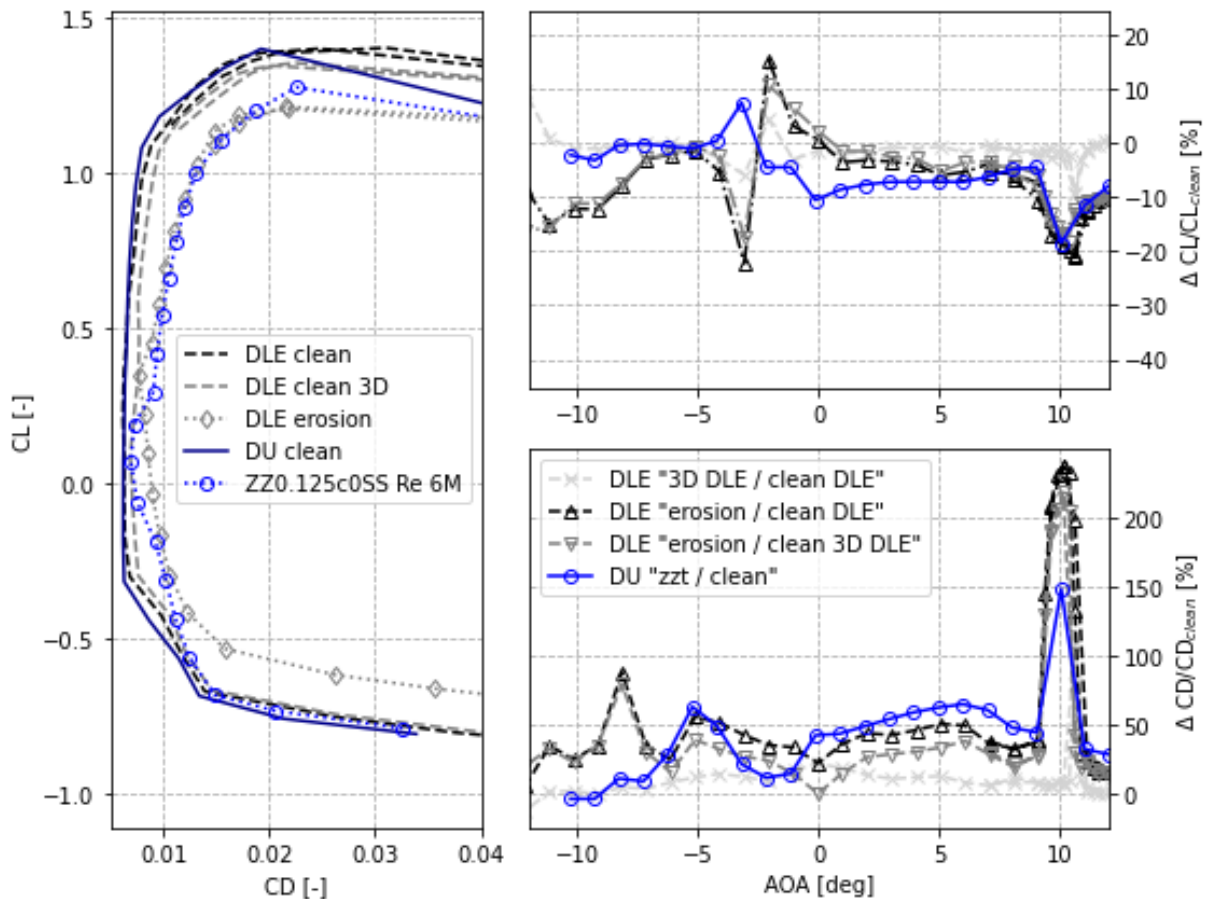


Figure 7.1: CL,CD comparison with the detachable leading edge model [33] at  $Re=6e6$

## 7.2. Roughness Profiles by Gaudern et al.

The second reference data set on real roughness is based on airfoil modifications on a Risø airfoil that has been tested in the Stuttgart Wind Tunnel by Gaudern et al. [7]. It is important to state that the reference data is therefore based on a different airfoil with different thickness of  $t = 18\%$  rather than the  $t = 21.2\%$  of the DU airfoil in the present study. The main objective of this section is to make qualitative additional comments to overall generalizations that are often found in current literature when evaluating tripping tape usage [14, 7, 19]. The available data is relative performance penalty of lift and drag in the typical operation range of wind turbine blades stated as  $0^\circ \leq \alpha \leq 8^\circ$  for created leading edge roughness patterns with heights 0.23mm, 0.36mm, 0.60mm and 1.50mm thus exceeding the tripping tape heights of 0.125mm, 0.205mm and 0.40mm tested in the current study. As different airfoils are being used additionally at different thicknesses, roughness impacts are expected to vary and the limited data availability does not allow a general comparison for the different airfoils at high confidence.

While Section 7.1 covered a comparison with estimated real erosion of minor severity, this section allows a comparison how roughness data can better be resembled for more severe roughness, which is observed to be underpredicted by ZZT applications, as similarly found by Sareen et al. [6]. This data set however allows to further investigate this general statement.

The drag performance penalty can be seen in Figure 7.2 for the original data set of the Risø roughness stages and tripped setup, as well as for DU00-W-212 data of the present study. Tripped conditions indicates for both studies the standard setup of ZZT with a height of  $400\mu m$  and width

| Case        | Application   |
|-------------|---|
| ZZT 125 0%c | Best overall trend for full range in operational angles but overall overestimated performance penalties         |
| ZZT 205 0%c | Similar as its thinner counterpart, better stall resemblance at even larger overestimated performance penalties |
| ZZT 400 8%c | Similar as ZZT125c0 but with lower stall impact and no resemblance below $\alpha = 2^\circ$                     |
| ZZT 125 8%c | Performance penalties match in operational range of $2^\circ \leq \alpha \leq 7^\circ$                          |

**Table 7.2:** Alternative ZZT setups to resemble DLE erosion patterns

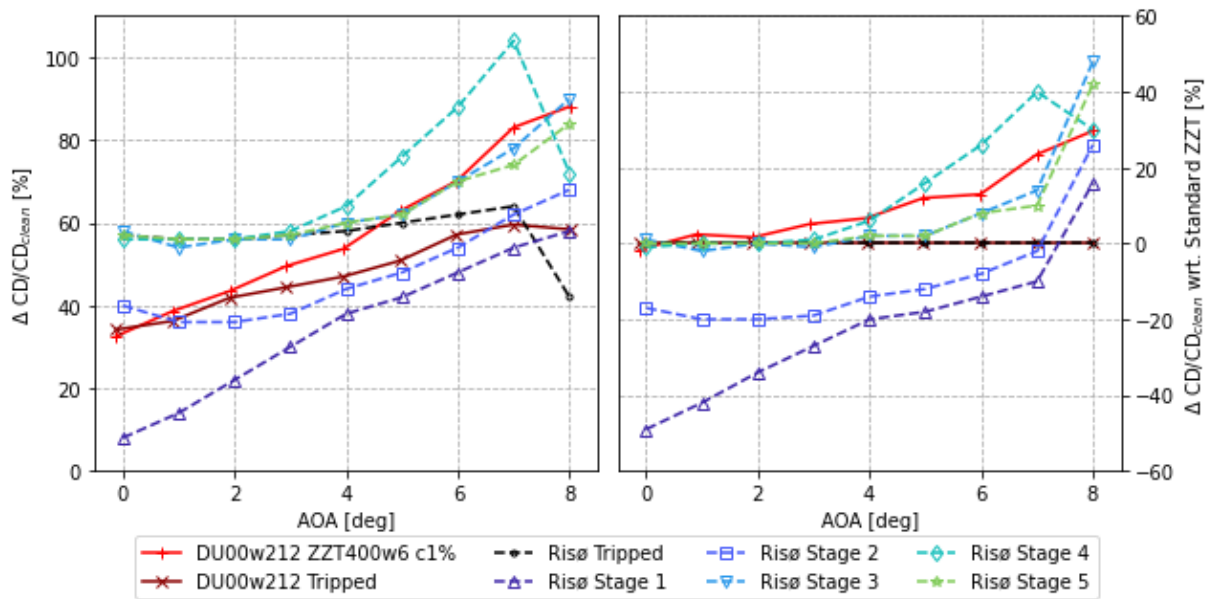


**Figure 7.2:** CD comparison with Gaudern et al. [7] at  $Re=2e6$

of  $12mm$  at  $x/c = 5\%$  on the suction side. Finally, a proposed improved ZZT setup of same tape height with width of  $6mm$  at the  $x/c = 1\%$  location is introduced for the DU00-W-212 airfoil, to indicate improved possibilities to simulate more severe roughness. Highest performance penalties are observed for earliest tripping location, resulting in the advised  $6mm$  width ZZT over its  $12mm$  counterpart, different variations are available in Section A.5 to validate the choice. The tripped case at the  $x/c = 5\%$  location shows similar trends on both airfoils, with a decreasing curvature towards higher angles of attack while leading edge roughness further increases, similarly to ZZT at the leading edge.

Assuming equal behavior changes on different airfoils when varying ZZT setups, the data is then transformed as a respective data set with respect to the standard tripped setup of its respective airfoil choice in the second subplot. Hereby, a prediction can be made, how the proposed setup can improve roughness simulations for more severe stages of leading edge roughness. The new setup agrees well with all performance penalties besides stage 4 up to  $\alpha = 7^\circ$  and is therefore expected to be a better choice to simulate roughness, indicating that ZZT can be used to simulate more severe leading edge roughness stages when investigating other setups than the standard tripping setups.

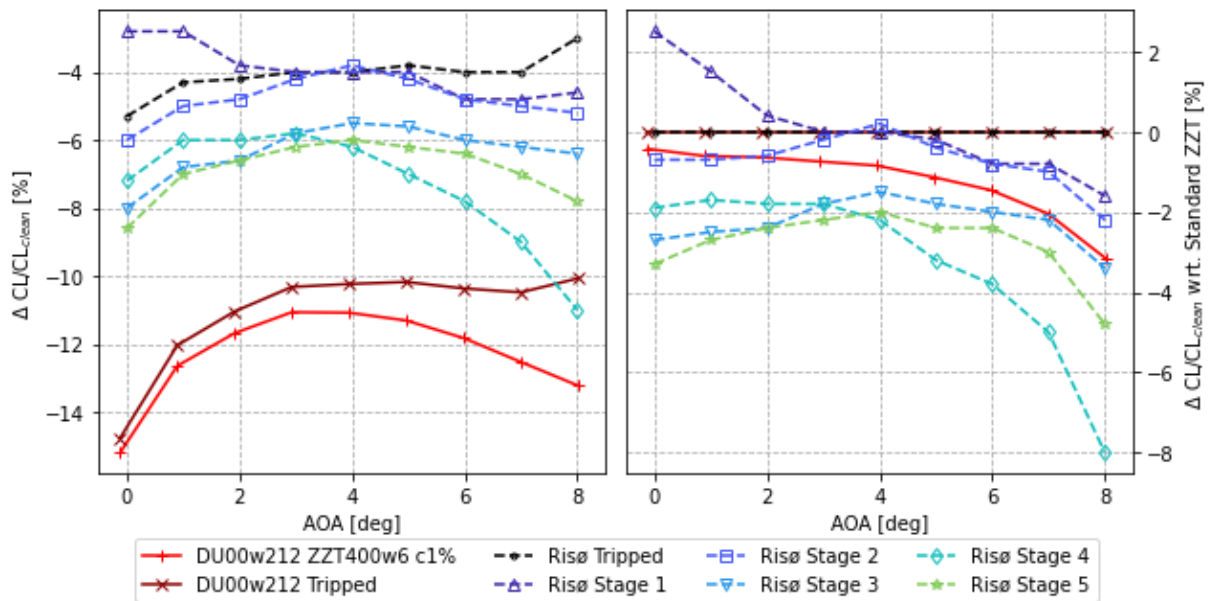


**Figure 7.3:** CL comparison with Gaudern et al. [7] at  $Re=2e6$

These trends are confirmed when comparing the  $\Delta CL$  data in Figure 7.3. A clear improvement on the lift penalty trend can be observed that matches more closely for the new setup when compared to more severe roughness stages. The DU00-W-212 airfoil however suffers from a much higher magnitude of lift decrease, which can be expected from thick airfoil sections having an increase in suction side pressure gradients in the aft part [12]. The roughness stages however also introduce a  $\Delta CL$  over the whole range of angles, which can be achieved with setups closer to the leading edge, for example ZTT400w6 at  $x/c = 1\%$  rather than ZTT400 due to shorter width tripping at an earlier location or by applying ZTT205 at  $x/c = 0\%$ , rather than at  $x/c = 1\%$ .

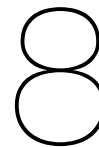
These insights have been taken as sufficient for the main objective and there were no wind tunnel series to optimize recreating the data by Gaudern et al. [7], as it seemed to be an unnecessary use of resources and a better potential for this is expected in the parallel running project of LERcat.

In the original report by Gaudern et al. [7] it was thus concluded that ZTT generally underpredict leading edge roughness, while the author advises to broaden the view of tripping tape applications. Even at limited considered height of  $400\mu m$ , a good representation was observed, allowing to investigate further improvements, as ZTT seems to have the possibility to simulate real roughness if applied more accurately than the standard setup.

# Part III

## The Conclusions

*... crucial 'LER' impact.*



# Post Project Reflection

## 8.1. Challenges

During the project, several challenges have influenced the project and it should be stated to know limitations and allow improvements for further research, as well as to define future work.

The tape was not placed by the author directly and it was not emphasize how important it is to try a consistent placement with respect to same ZZT peak and valley locations to allow exact tracking of same impact close to pressure taps at different tape heights. While this detail was not an original objective, it could have allowed potential further insights. Tape location choice was focused rather than application, meaning it was selected by location of interest to take specific locations, rather than making the locations somewhat more arbitrary to ensure that ZZT does not cover pressure taps. While this is not possible due to the tape thickness at all locations close to the LE, it was possible for some locations that have been covered as  $x/c = [8, 12]\%$ .

A big delay in the project was created and time was lost due to misaligning results when comparing to the reference paper due to the later identified mistakes in that paper as discussed in Chapter 3 and the project plan was never fixed for it. BLR tests were delayed by 8 weeks due to wind tunnel schedule and having to drop a large part of the analysis generated uncertainties of the big part of the work before actual testing.

## 8.2. Lessons Learned

The general difficulty of experimental work is that it opens many paths besides the main plan. One has to individually assess whether taking a look into another aspect of the project is worth it or not, as it can yield promising improvements at risk of wasting time or generating a way too large work load as observed in this project.

With a pessimistic view on the project planning, milestones and disruptions, it can be stated that Murhpy's law applied perfectly and everything that could have gone wrong, did go wrong. Starting that the project was planned to further investigate an existing study, for which it has been found to also due to errors in the paper that have been discovered. Followed by unexpected change in the new environment at the testing facility, where experiments have been conducted at full individual responsibility instead supervised as expected. Finally, the testing schedule was not as planned and additionally, no second airfoil was able to be tested, as well as a failure in utilizing the detachable leading edge model, which upon further investigation did not seem to have the required quality to reason its usage at this stage and a final large delay due to wind tunnel schedule shifting. While the large amount of objectives was a risk, it was the reason to get the project feasible regarding wind tunnel access and industry partner and while not perfect, can still be viewed as majorly successful, as objectives have been (partially) solved or limitations have been identified.

# Results

## 9.1. Conclusions

**Research Objective 1: Critical Roughness Height** was mostly successful. The project starting point with a boundary layer momentum thickness relation defined by Bak et al. [3] was not confirmed as general relation at different locations, which is expected. Instead, for varying setups including locations, the critical height was traceable with the Roughness Reynolds number for ZZT usage as  $Re_{k,crit} = 125$ , opposing the expected reference values from literature for  $Re_{k,crit} = 200$ . This is however limited to the thinnest tape at  $Re = 2e6$ , as this condition below  $Re_k = 200$  was not met for other setups.

**Research Objective 2: Wind Tunnel Measurements** was successful. A detailed investigation of tripping tape applications on the suction side was conducted to study parameter variations of ZZT with a focus on tape location and height. Shorter width tapes are observed as competitive alternatives, that can allow applications at larger tape height and high airfoil curvature. In the linear lift region, tape height is somewhat negligible if critical conditions are met and performance penalties are decreasing linearly with distance from the LE. Close to stall and actual stalling is more complex and height as well as location need to be evaluated combined. Highest performance penalties and early stall are observed for locations close to the LE and tape height has a major impact on the magnitude of performance penalties. At locations further aft, tripping impact can introduce smooth stall behavior by introducing turbulence similarly to vortex generators, even increasing performance polars, which raises interest to topics such as protection tape placement.

**Research Objective 3: Boundary Layer Rake** was partially successful. The BLR was designed and constructed successfully as first prototype. Within the further LER research in LERcat, this allows initial insights while enabling different sources of comparisons with the simulation data. The prototype is however oversized and not optimized regarding intrusiveness by having a more aerodynamic shape. Furthermore, the used tubes could be chosen smaller and with different inlet shape to allow better directional sensitivity versus the current choice with  $\pm 11^\circ$ . Simulation data is observed to have similar misaligned trends in BLT, as for natural transition, indicating that BL development is rather accurate in clean case but the moment to start BL development is off, as equally found for tripping tape applications, with deltas of  $1.5^\circ$  and  $3^\circ$ . This introduces additional insights on error sources of current panel code Simulation to allow investigation and possible improvements in future. Finally, more tests should be conducted at different chordwise and spanwise locations to confirm data from currently only 1 location in the test section. Especially tests closer to the pressure taps could allow more insights on intrusiveness, present study was focused on the clean airfoil surface area to first get measurement quality before getting insights on intrusiveness. The latter being removed from tasks due to external wind tunnel shifting.

**Research Objective 4: Step Orientation** was mostly unsuccessful. The project plan was early found to be not realizable and the alternative approach is lacking in delivering clearly isolated results as always both the forward and backward step are introduced. Nonetheless, an indication is given that the backward step is more critical, which aligns generally well with the tripping tape mechanism as studied by Klebanoff et al. [27].

**Research Objective 5: Real Erosion** was partially successful. Interesting comparisons were conducted, but those are limited to the small amount of available reference data. Reference roughness data was supposed to be delivered from 2 sources: DLE and LERcat. Partnering LERcat project did not deliver within the project and could therefore not be used. The DLE was found to be not usable as intended. The existing DLE data is therefore to be treated carefully but was found to be rather light than the given "heavy" case describing name. This real erosion comparison therefore comes with some uncertainty and heavily relies on how realistic the reference "real roughness" actually is. Nonetheless, these cases were resembled best at the very leading edge by applying thinnest tape for light erosion and thick tape at the LE for heavy erosion. Future real roughness data can be tracked and compared with the existing testing matrix to deliver higher certainty to give advice on best setup for real roughness. Finally it can be stated that ZZT is capable of more than the industry standard setup and changing application drastically changes impact, therefore rating generalizations based on one setup variation as invalid.

## 9.2. Future Work

Not all plans were realizable within this project due to several external factors and while alternative approaches and additional efforts have allowed to yield acceptable results, returning to the original plan would be ideal and several options should be tested in future.

- a more detailed research on different airfoils should be conducted to validate current findings,
- test facility and setup should be chosen such that critical roughness height can be studied in more detail with more tape variations and with new insights on  $Re_k$ ,
- the BLR will be tested with proposed improvements and needs to be validated with possibly HWA and PIV to generate correction functions,
- The velocity profile and boundary layer momentum and displacement thickness should be investigated in detail and compared to theory and simulations,
- the FW vs BW step setup should be tested as originally planned with a pure FW or BW step to allow actual conclusions,
- the ZZT matrix should be evaluated against a larger test matrix of real reference roughness from LERcat to deliver more certain conclusions on an improved setup in future to simulate LER in wind tunnel operations for WT purposes.



# Appendix

## A.1. CL over CD

### A.1.1. Region 1: Leading Edge

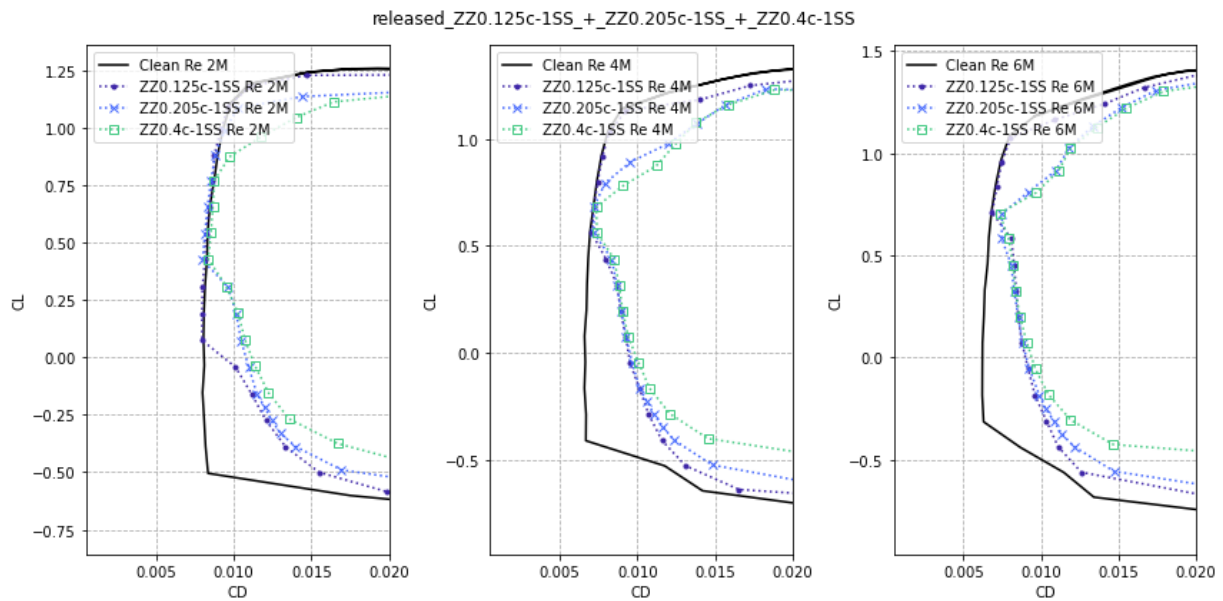


Figure A.1: CL over CD at  $x/c = -1\%$

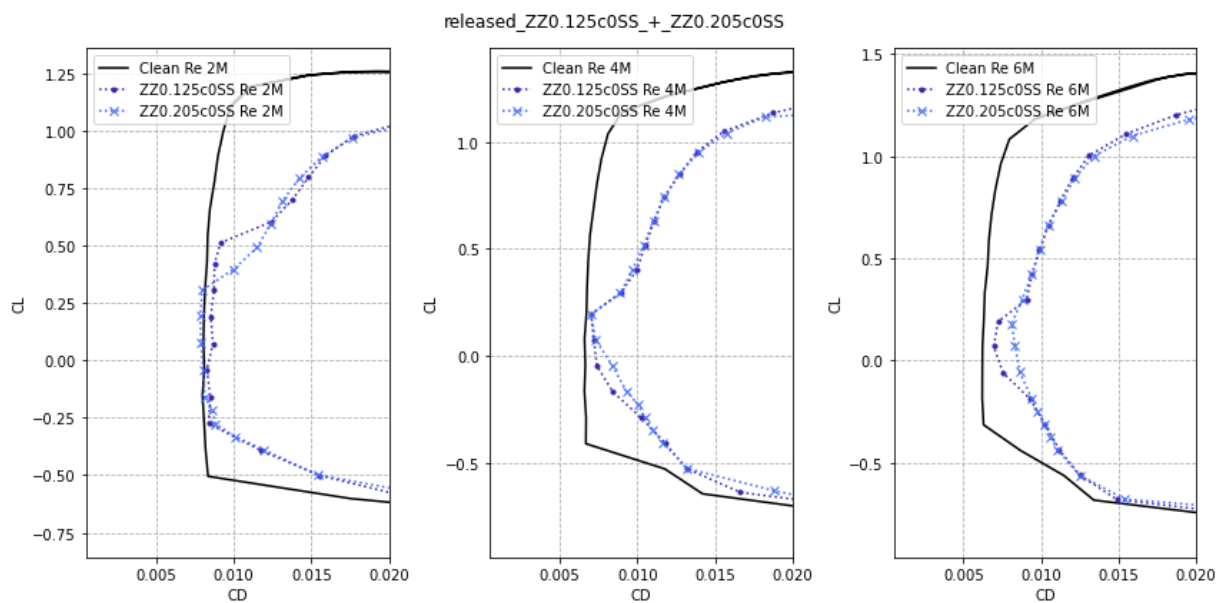


Figure A.2: CL over CD at  $x/c = 0\%$

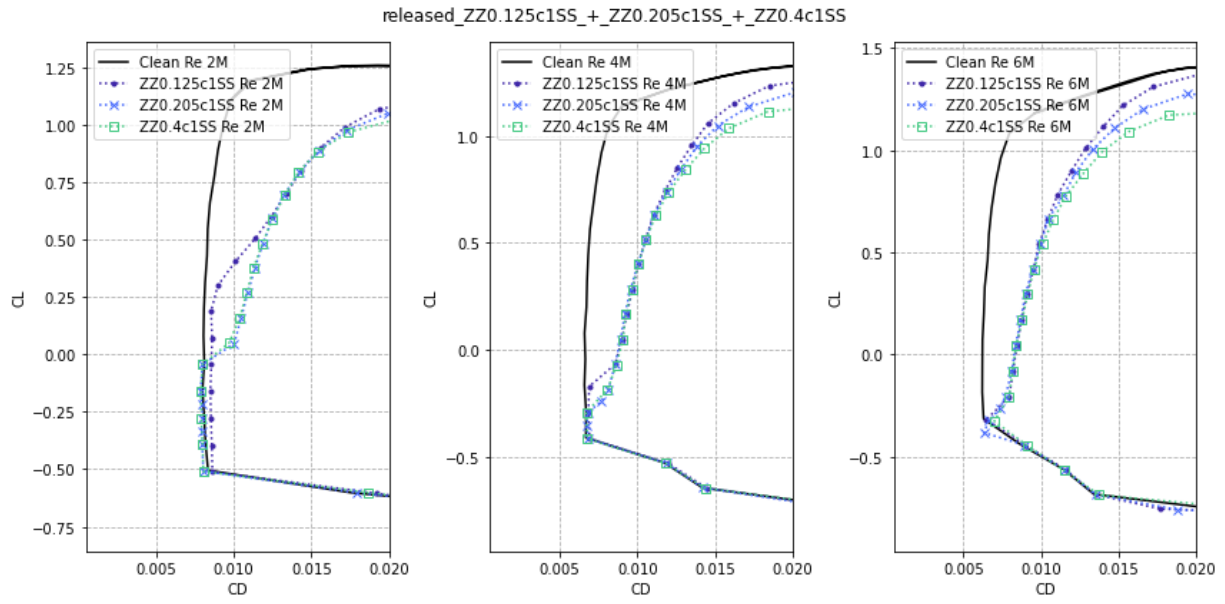


Figure A.3: CL over CD at  $x/c = 1\%$

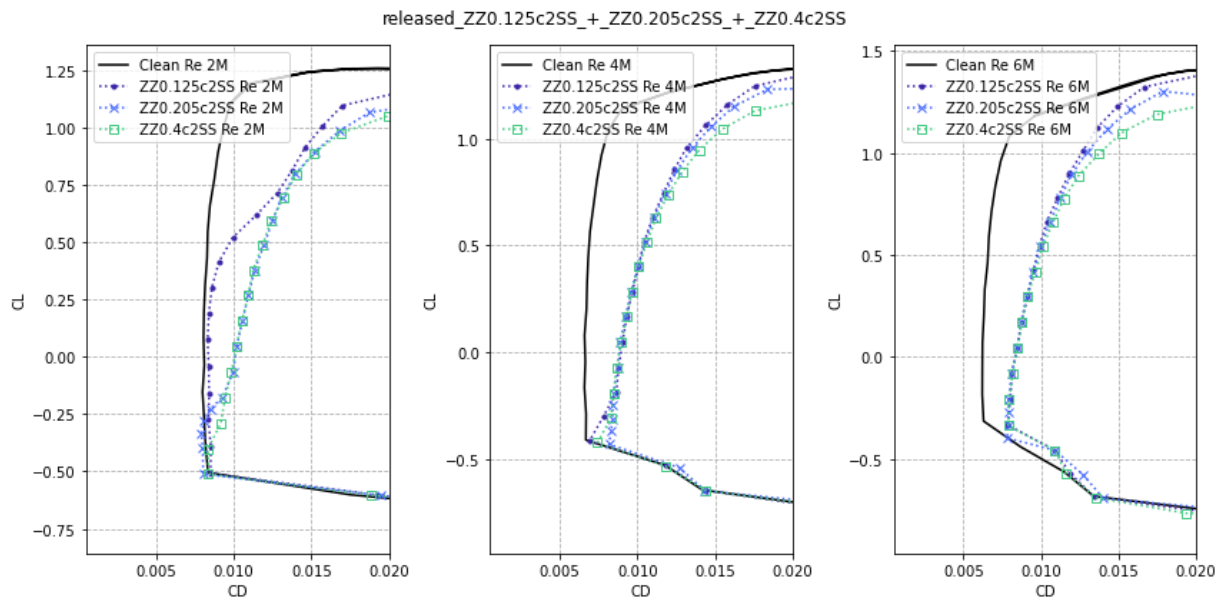
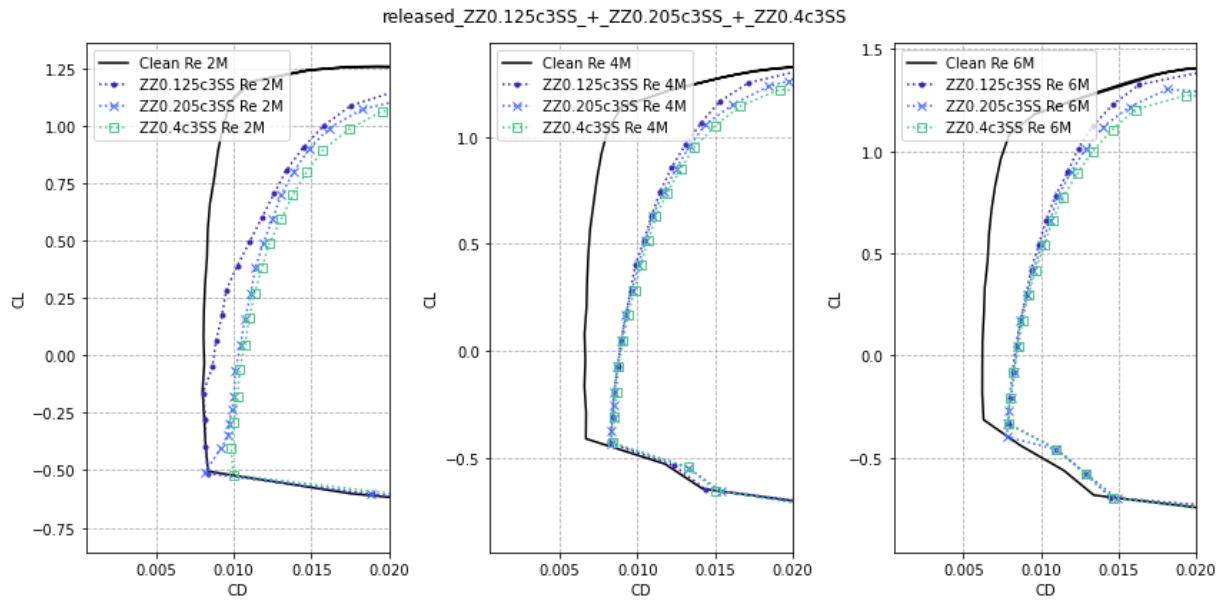
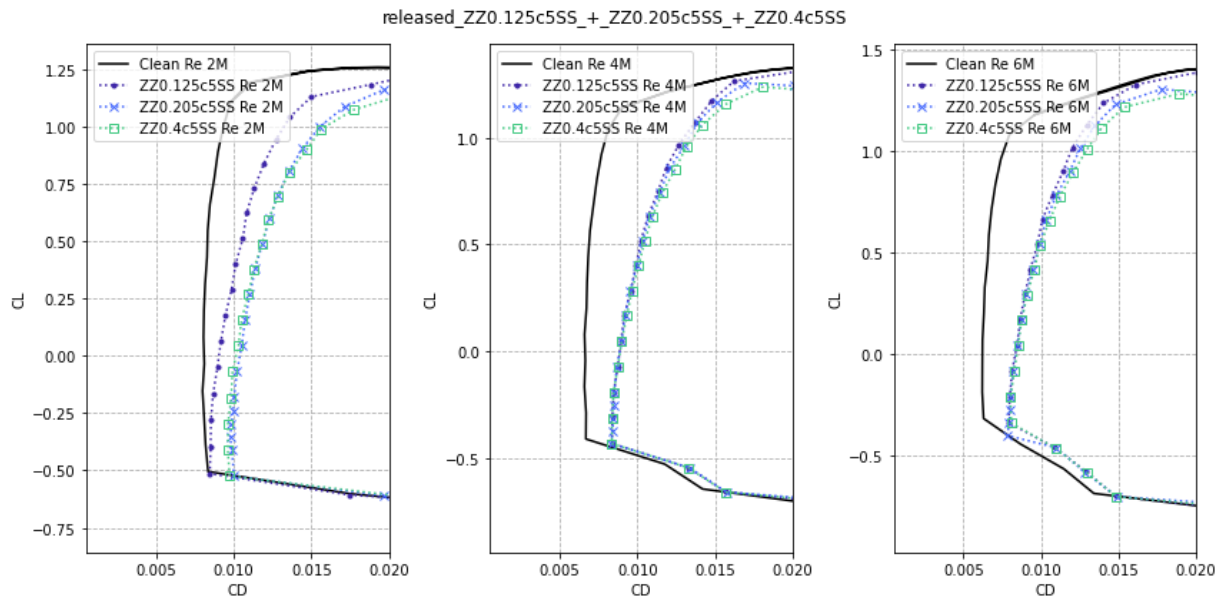


Figure A.4: CL over CD at  $x/c = 2\%$

**A.1.2. Region 2: Standard+**



**Figure A.5: CL over CD at  $x/c = 3\%$**



**Figure A.6: CL over CD at  $x/c = 5\%$**

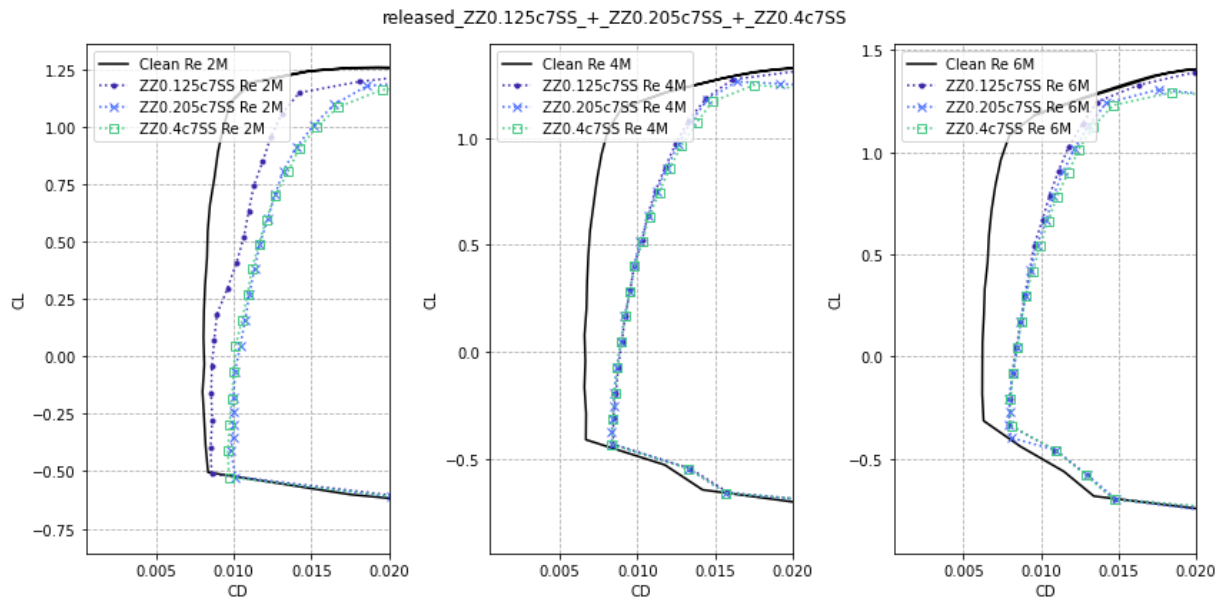


Figure A.7: CL over CD at  $x/c = 7\%$

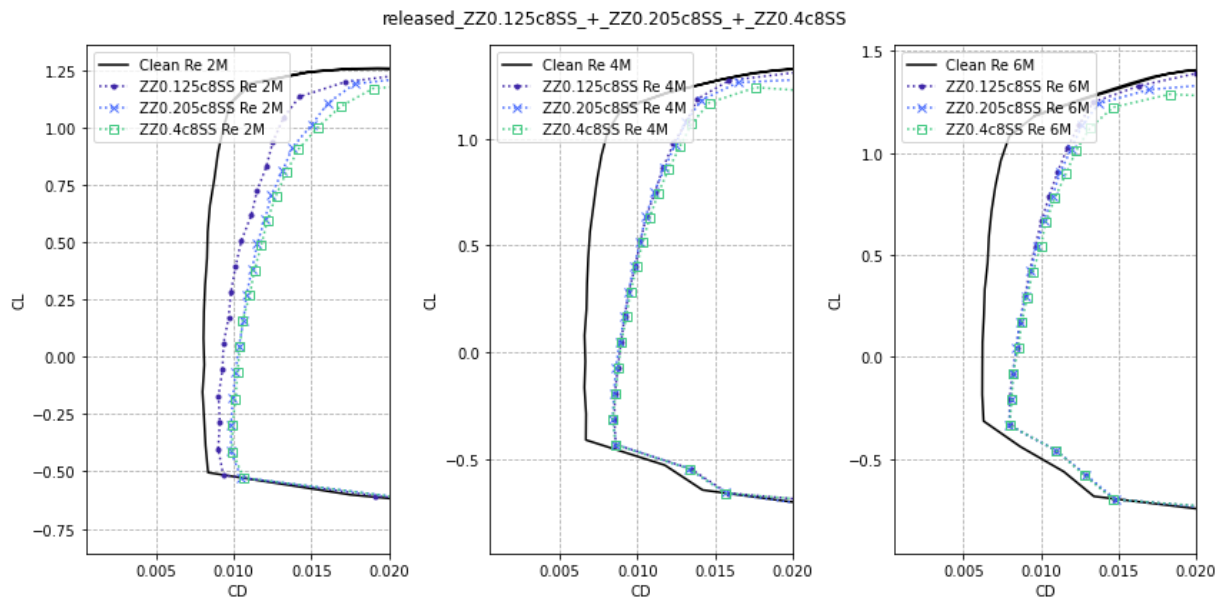
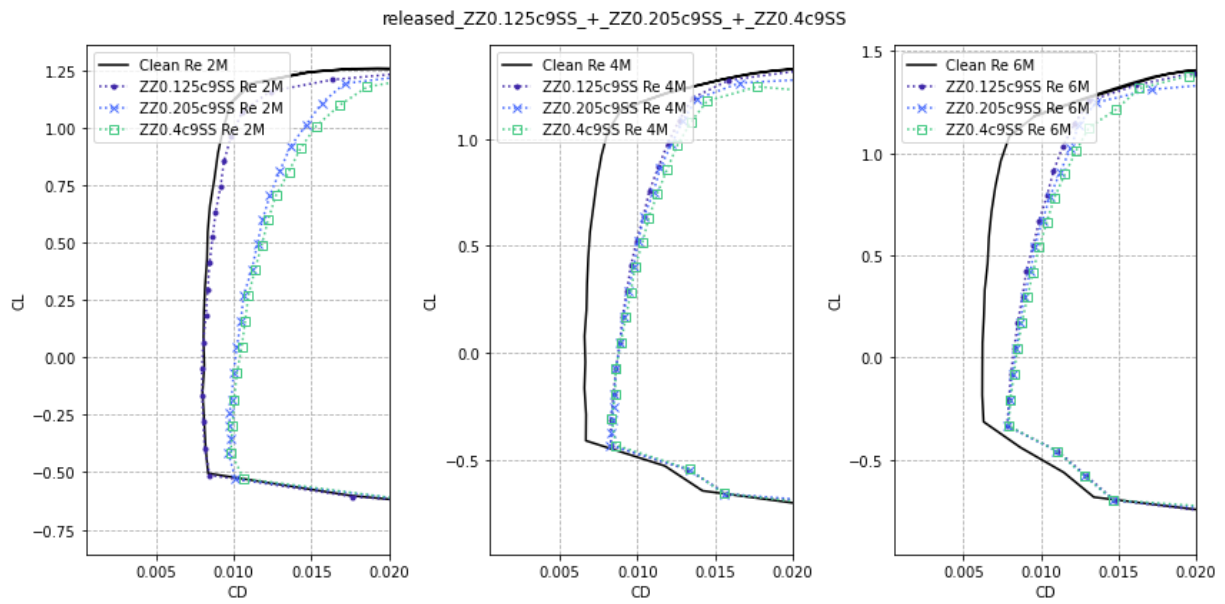
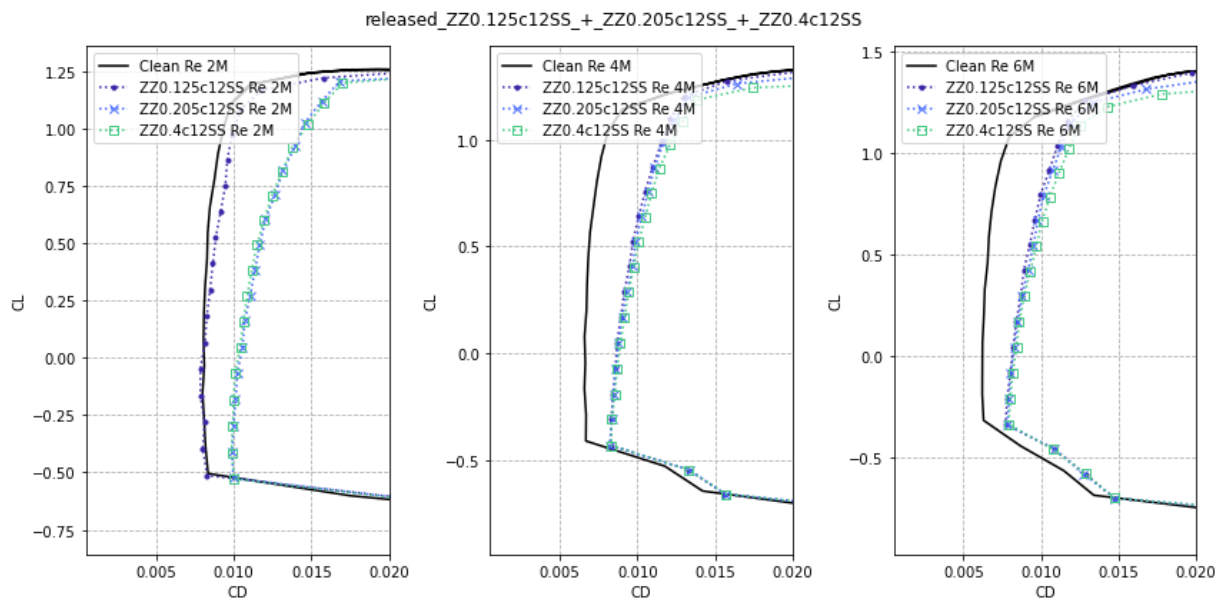


Figure A.8: CL over CD at  $x/c = 8\%$

**A.1.3. Region 3: Protection Tapes**



**Figure A.9: CL over CD at  $x/c = 9\%$**



**Figure A.10: CL over CD at  $x/c = 12\%$**

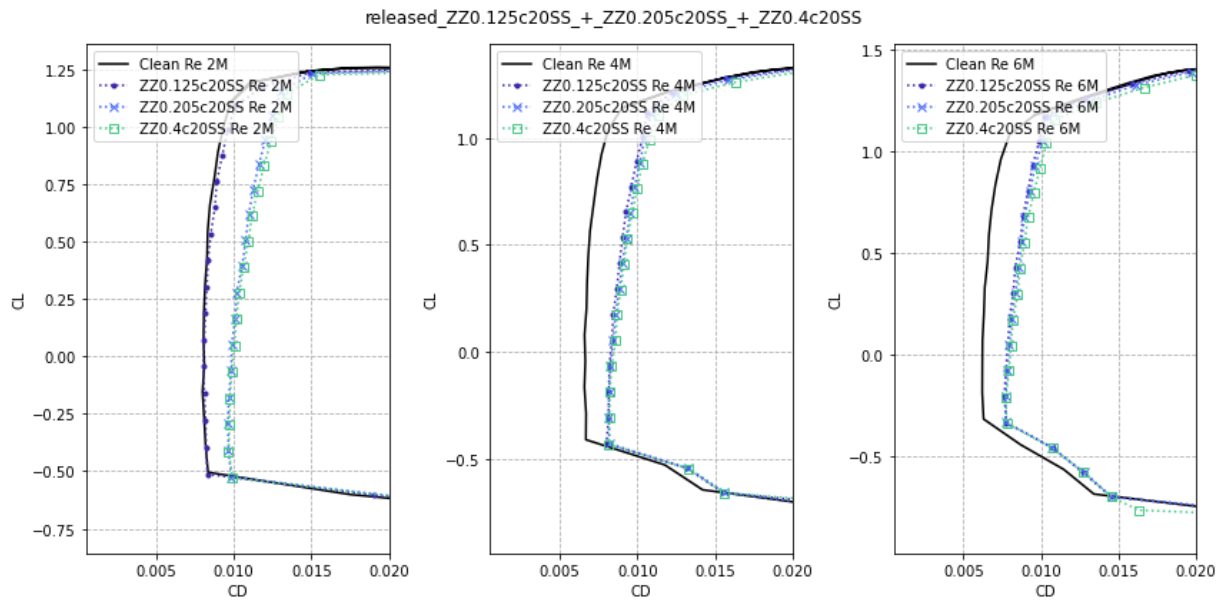


Figure A.11: CL over CD at  $x/c = 20\%$

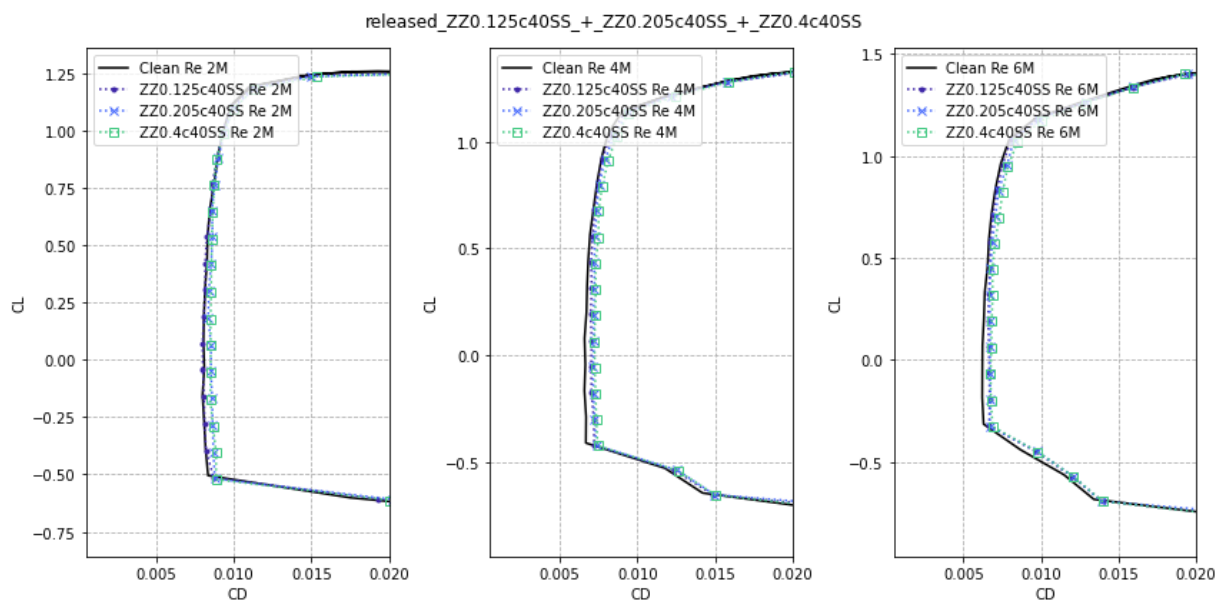


Figure A.12: CL over CD at  $x/c = 40\%$

**A.2. Polars**

For completion, more polar plots are presented here to allow availability of a larger quantity of results.

ZZT400 - Re6m

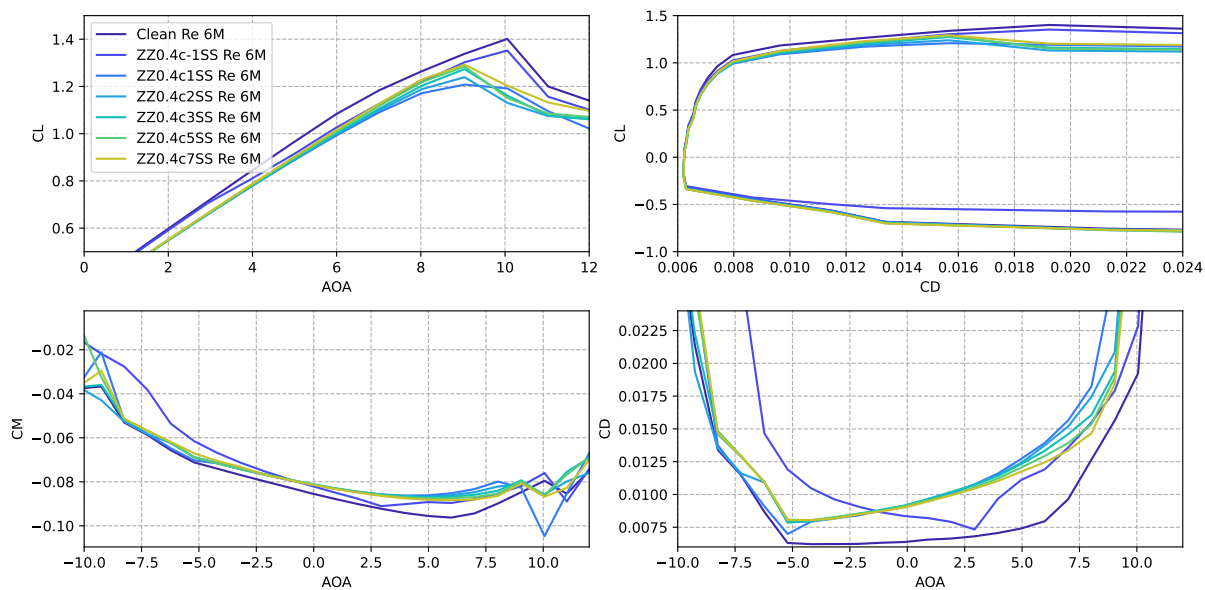


Figure A.13:  $C_L, C_D, C_M$  Polars for ZZT with  $400\mu m$  height and  $12mm$  width at  $Re=6m$  and for Locations= $[-1,1,2,3,5,7] \%x/c_{ss}$

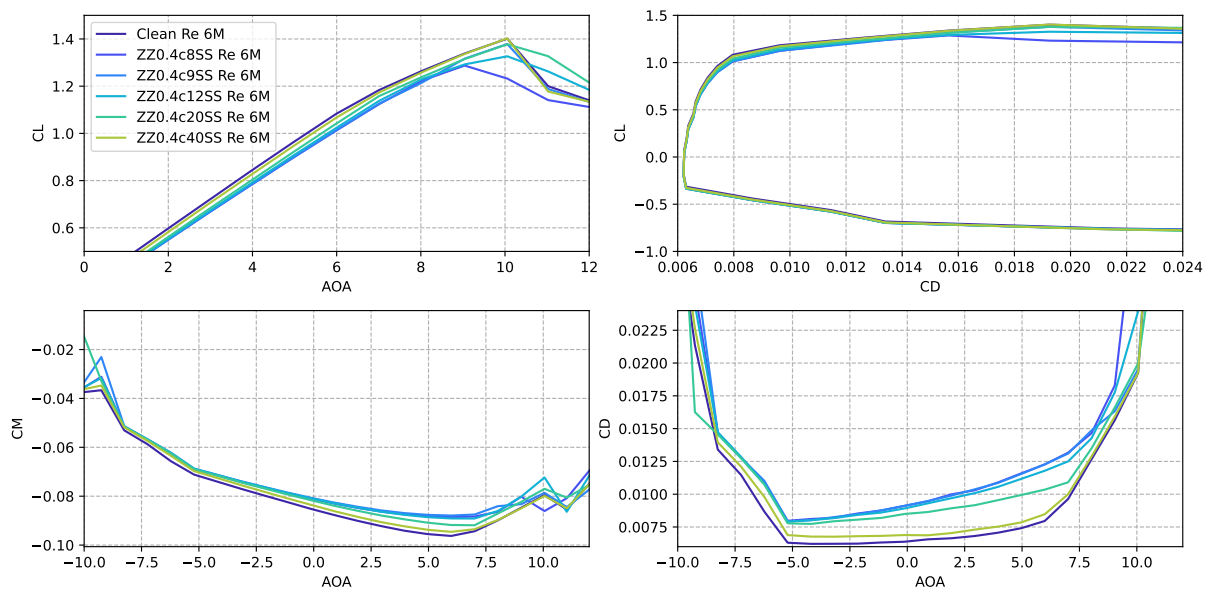


Figure A.14:  $C_L, C_D, C_M$  Polars for ZZT with  $400\mu m$  height and  $12mm$  width at  $Re=6m$  and for Locations= $[8,9,12,20,40] \%x/c_{ss}$

ZZT400 - Re4m

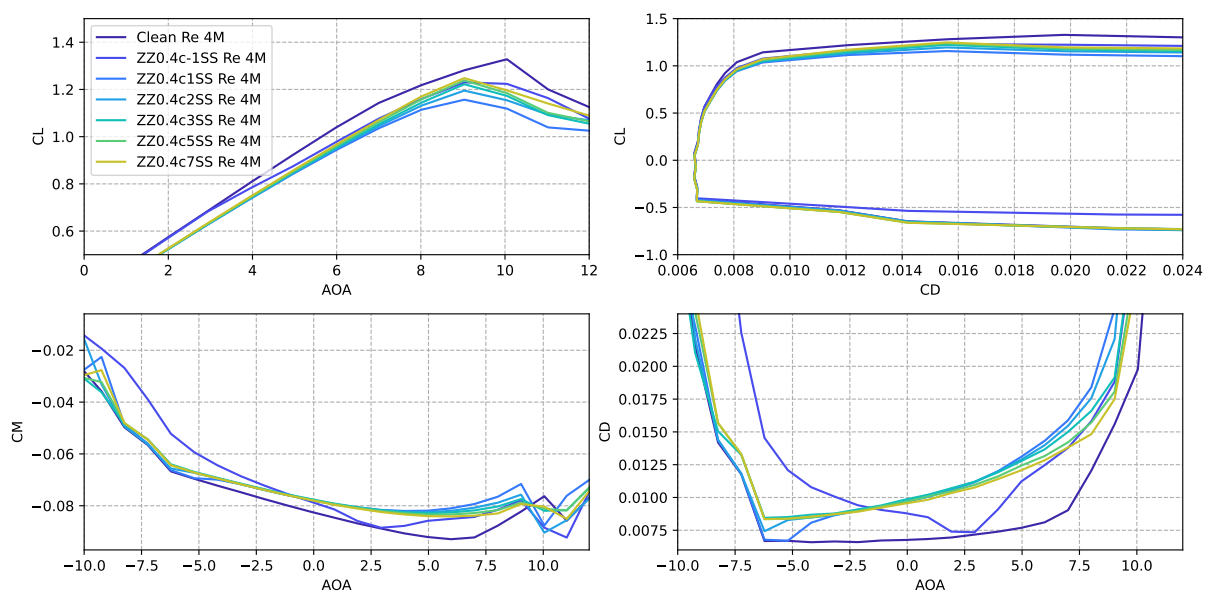


Figure A.15: CL,CD,CM Polars for ZZT with 400µm height and 12mm width at Re=4m and for Locations=[-1,1,2,3,5,7] %x/c<sub>ss</sub>

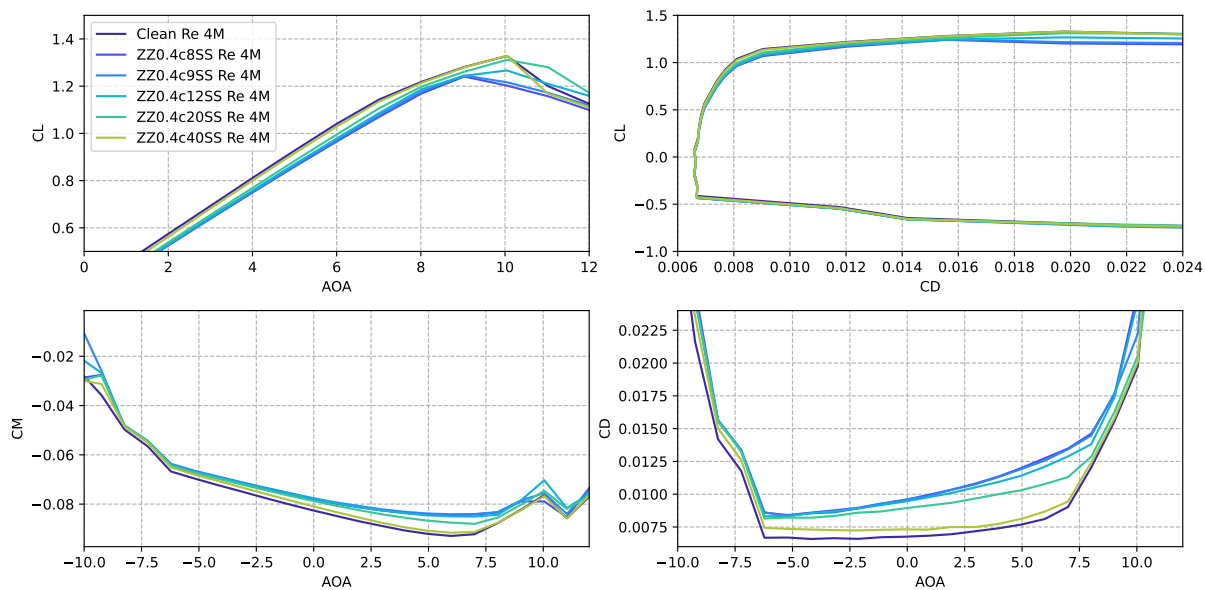
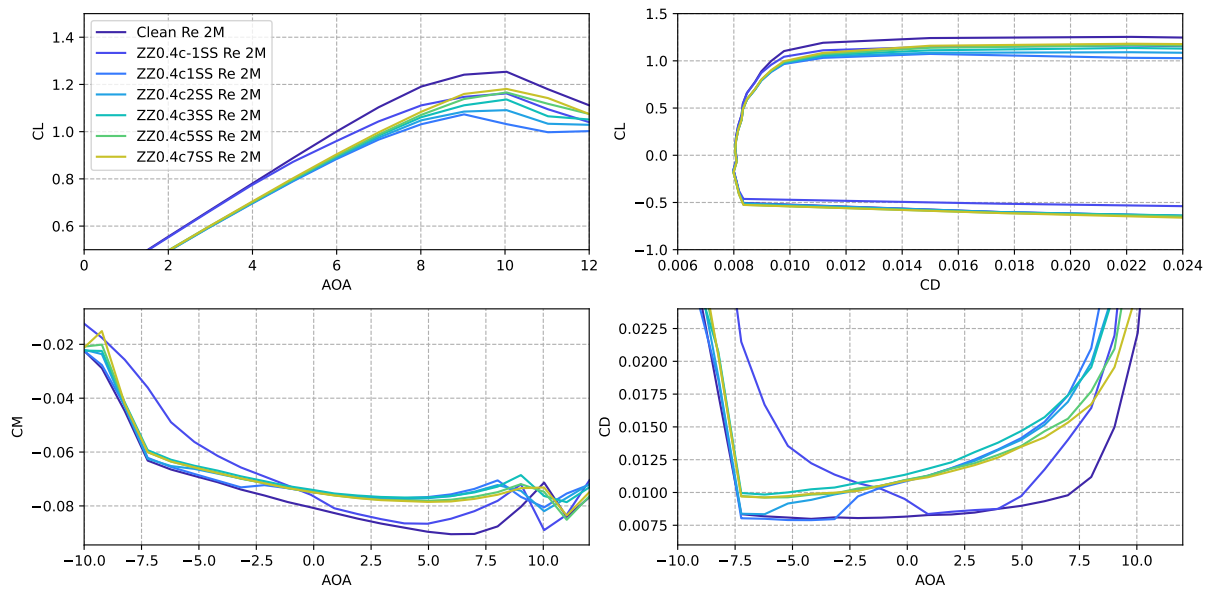
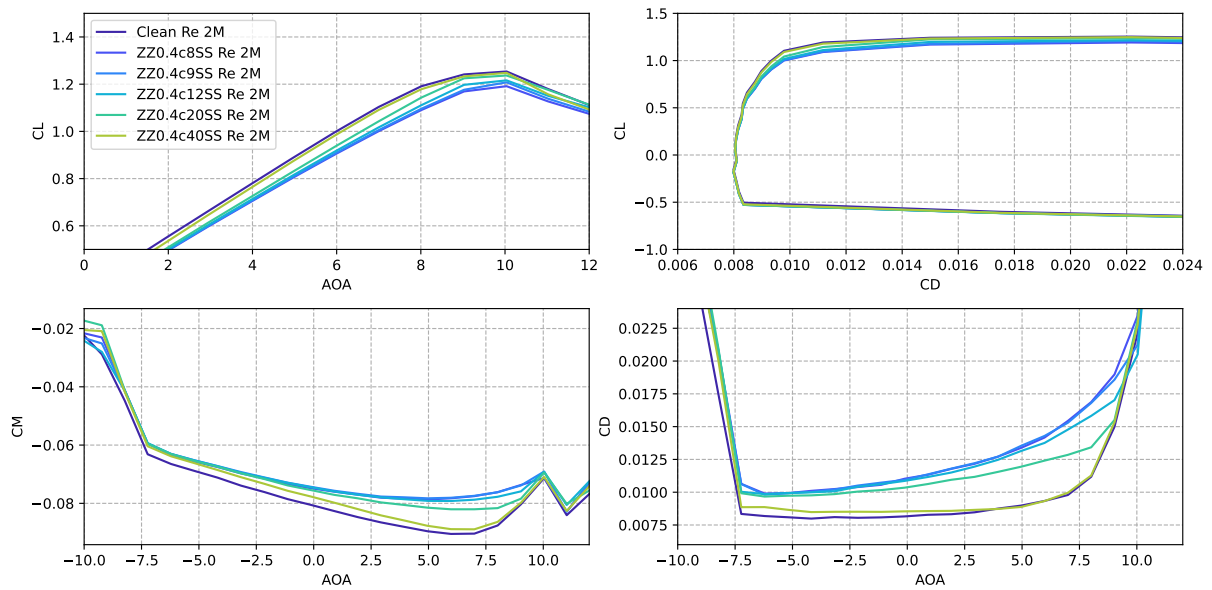


Figure A.16: CL,CD,CM Polars for ZZT with 400µm height and 12mm width at Re=4m and for Locations=[8,9,12,20,40] %x/c<sub>ss</sub>

**ZZT400 - Re2m**



**Figure A.17:** CL,CD,CM Polars for ZZT with  $400\mu m$  height and  $12mm$  width at  $Re=2m$  and for Locations= $[-1,1,2,3,5,7] \%x/c_{ss}$



**Figure A.18:** CL,CD,CM Polars for ZZT with  $400\mu m$  height and  $12mm$  width at  $Re=2m$  and for Locations= $[8,9,12,20,40] \%x/c_{ss}$

**ZZT205 - Re6m**

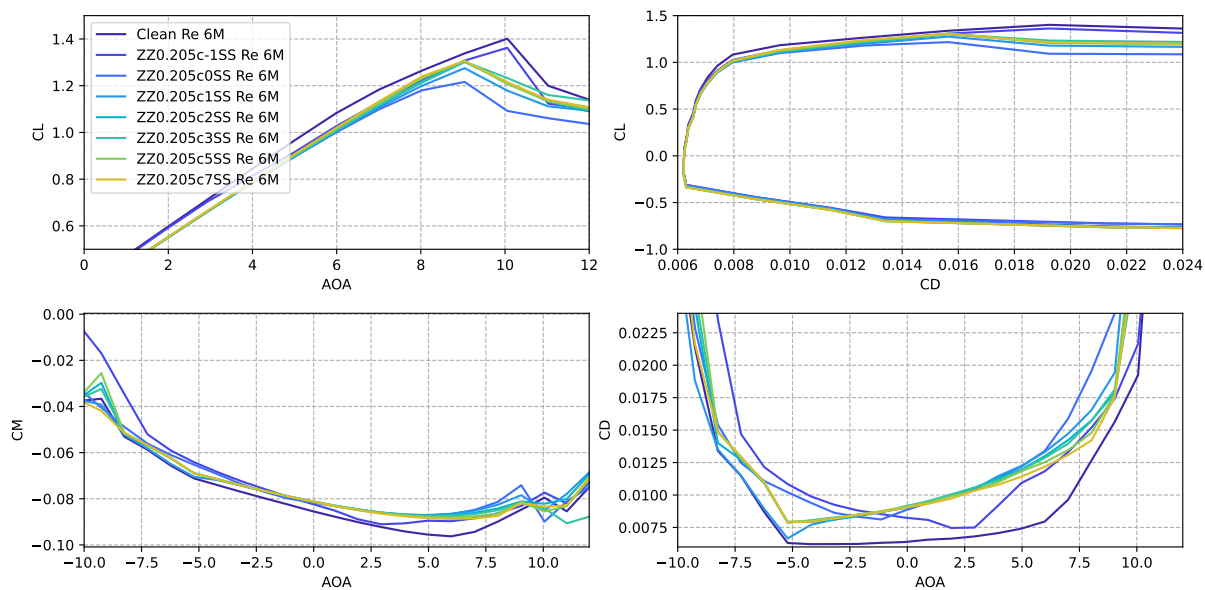


**Figure A.19:** CL,CD,CM Polars for ZZT with 205 $\mu$ m height and 12mm width at Re=6m and for Locations=[-1,0,1,2,3,5,7] % $x/c_{ss}$

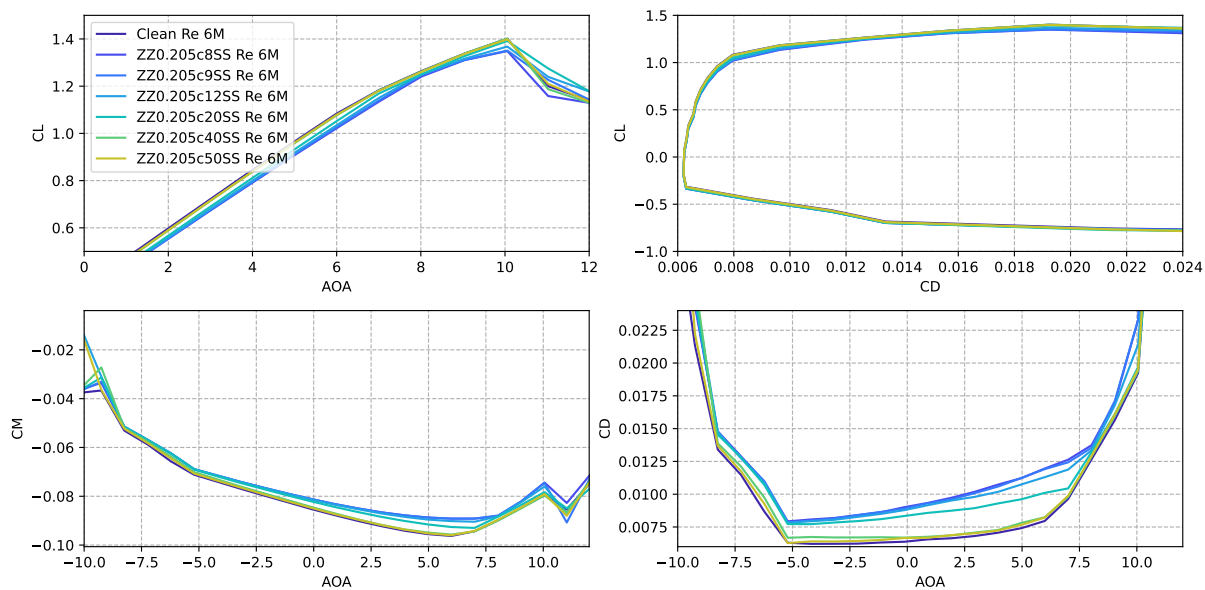


**Figure A.20:** CL,CD,CM Polars for ZZT with 205 $\mu$ m height and 12mm width at Re=6m and for Locations=[8,9,12,20,40,50] % $x/c_{ss}$

**ZZT205 - Re4m**

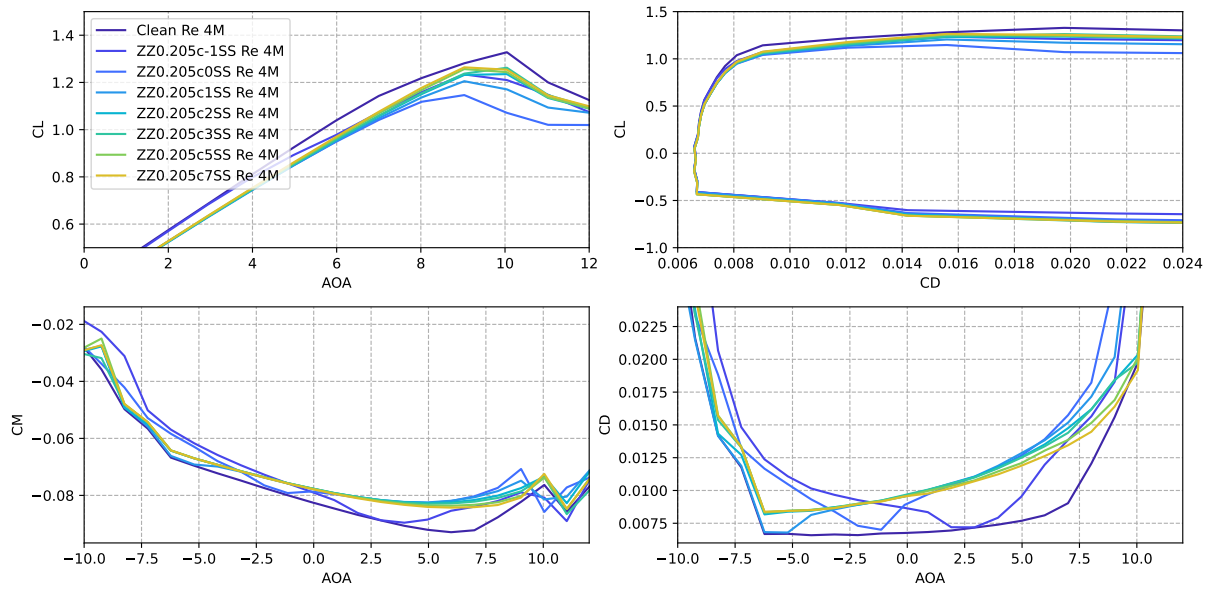


**Figure A.21:** CL,CD,CM Polars for ZZT with  $205\mu m$  height and  $12mm$  width at  $Re=4m$  and for Locations= $[-1,0,1,2,3,5,7] \%x/c_{ss}$

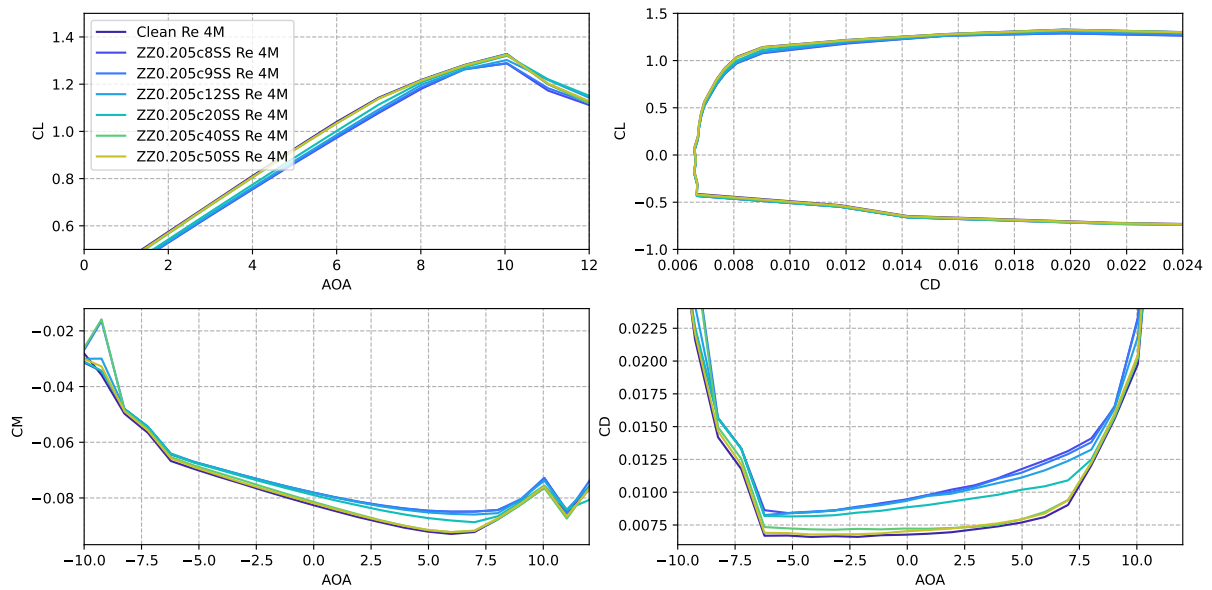


**Figure A.22:** CL,CD,CM Polars for ZZT with  $205\mu m$  height and  $12mm$  width at  $Re=4m$  and for Locations= $[8,9,12,20,40,50] \%x/c_{ss}$

**ZZT205 - Re2m**

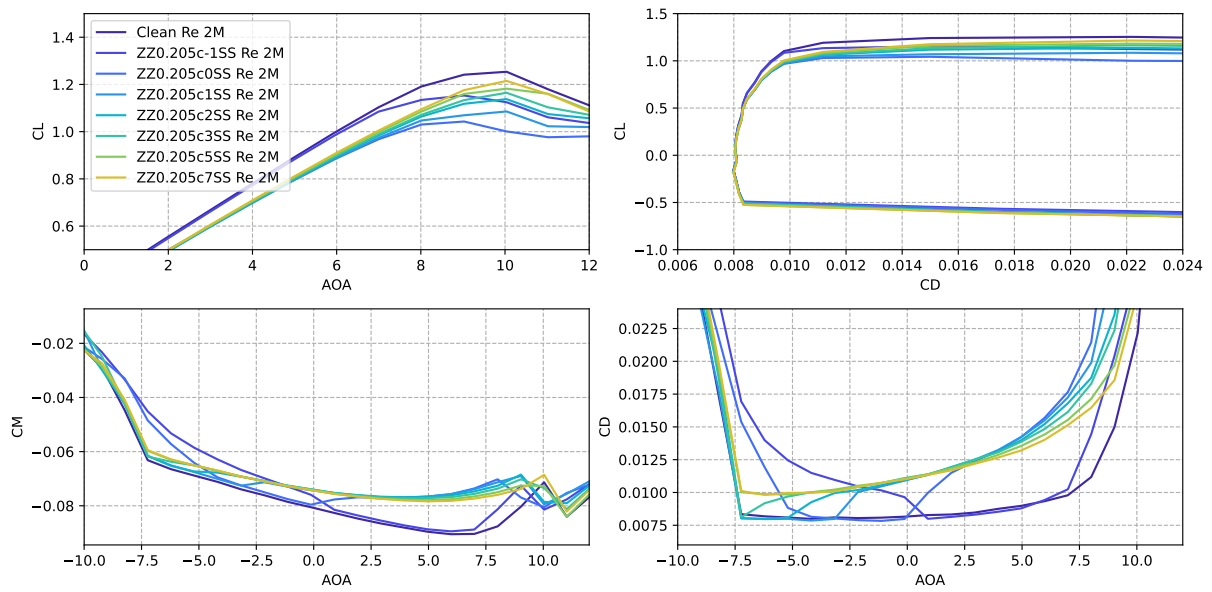


**Figure A.23:** CL,CD,CM Polars for ZZT with 205 $\mu$ m height and 12mm width at Re=2m and for Locations=[-1,0,1,2,3,5,7] % $x/c_{ss}$

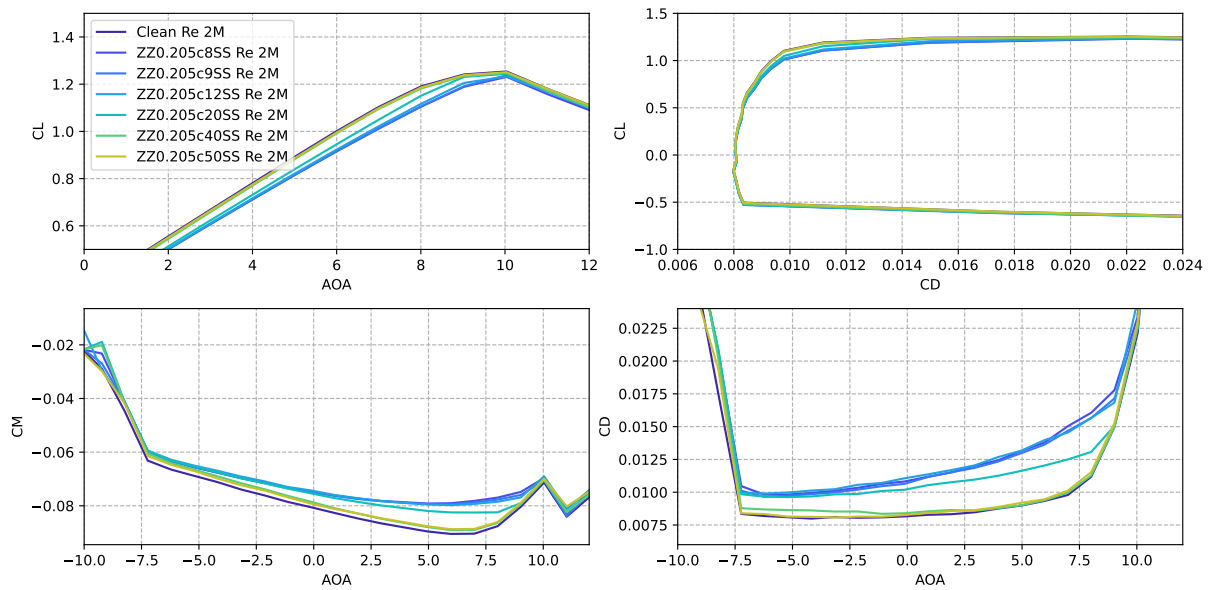


**Figure A.24:** CL,CD,CM Polars for ZZT with 205 $\mu$ m height and 12mm width at Re=2m and for Locations=[8,9,12,20,40,50] % $x/c_{ss}$

ZZT125 - Re6m

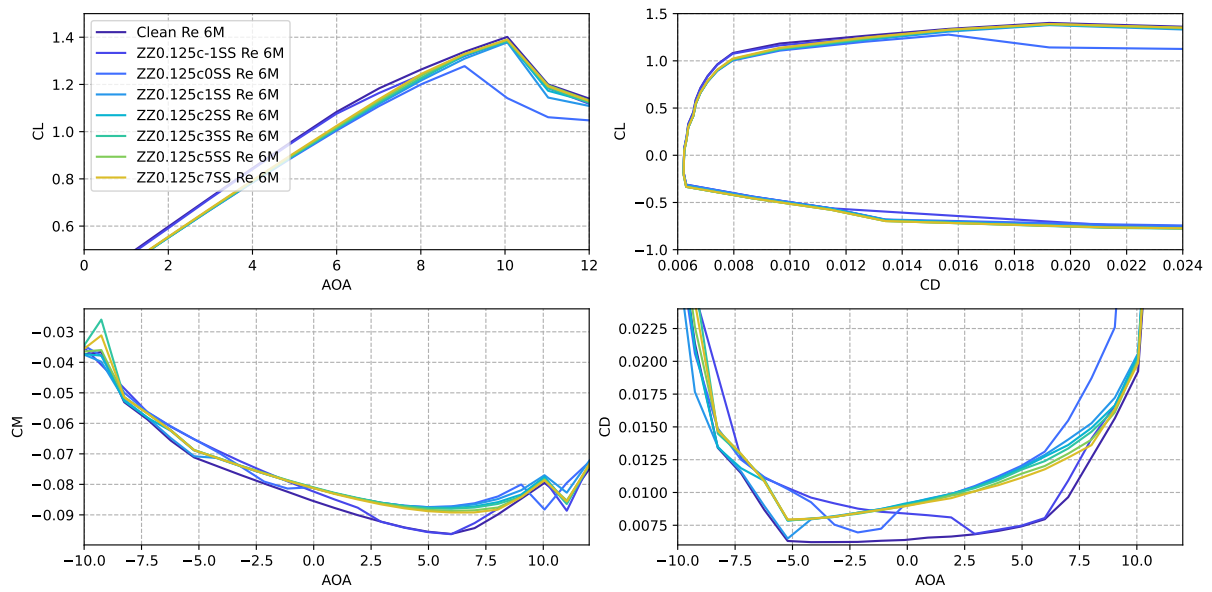


Figure A.25: CL,CD,CM Polars for ZZT with 125 $\mu$ m height and 12mm width at Re=6m and for Locations=[-1,0,1,2,3,5,7] % $x/c_{ss}$

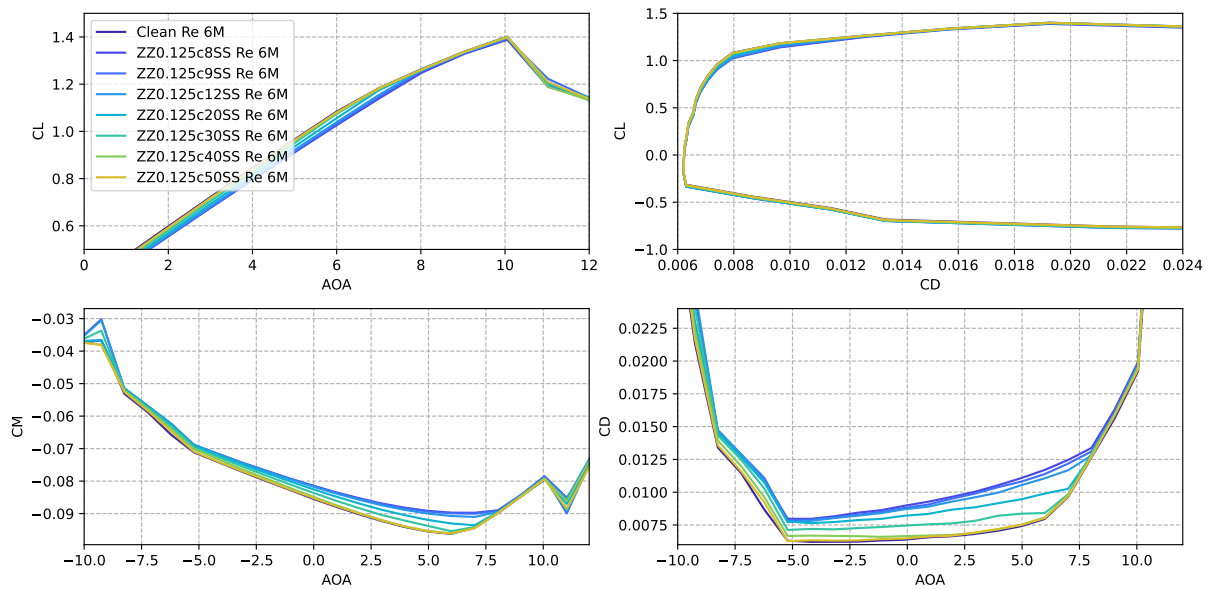
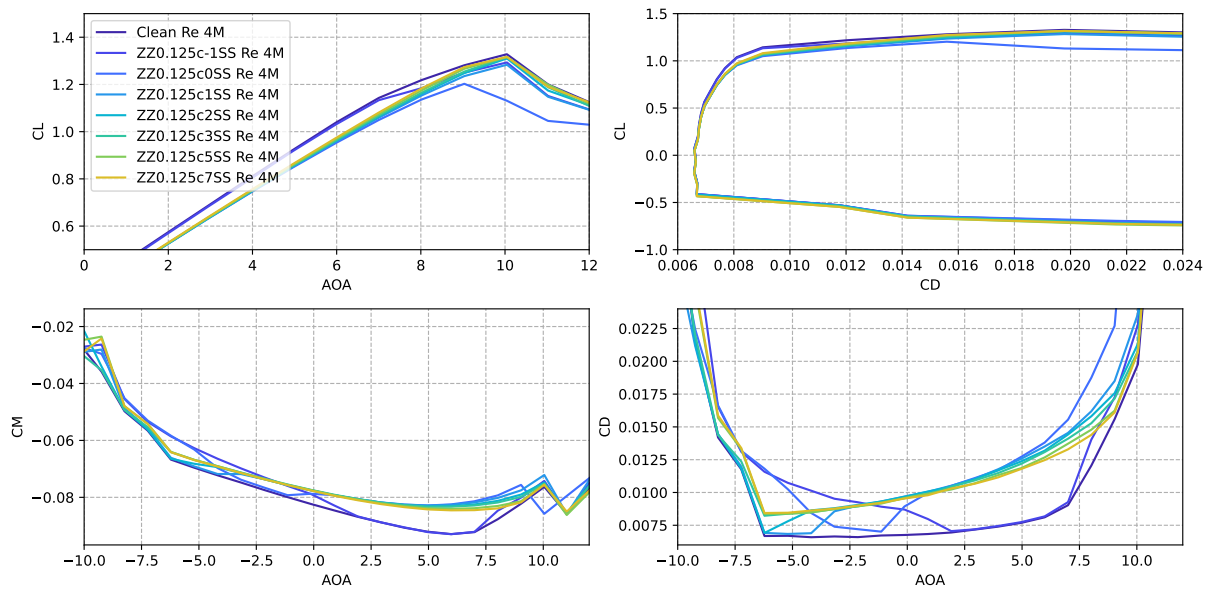
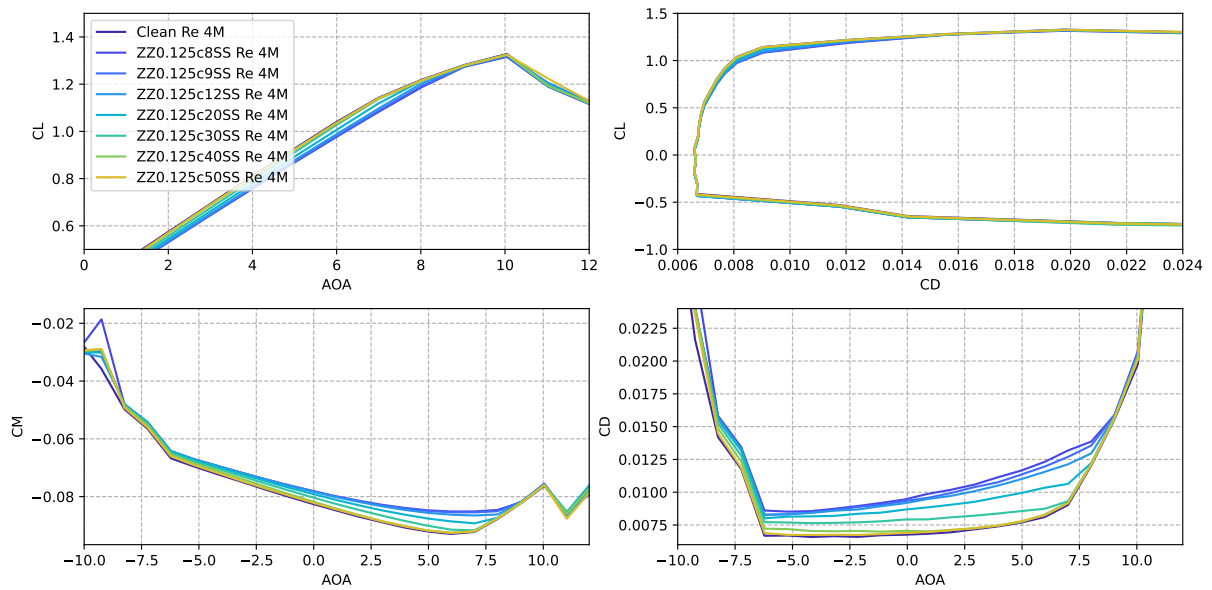


Figure A.26: CL,CD,CM Polars for ZZT with 125 $\mu$ m height and 12mm width at Re=6m and for Locations=[8,9,12,20,30,40,50] % $x/c_{ss}$

**ZZT125 - Re4m**



**Figure A.27:** CL,CD,CM Polars for ZZT with  $125\mu m$  height and  $12mm$  width at  $Re=4m$  and for Locations= $[-1,0,1,2,3,5,7] \%x/c_{ss}$



**Figure A.28:** CL,CD,CM Polars for ZZT with  $125\mu m$  height and  $12mm$  width at  $Re=4m$  and for Locations= $[8,9,12,20,30,40] \%x/c_{ss}$

**ZZT125 - Re2m**

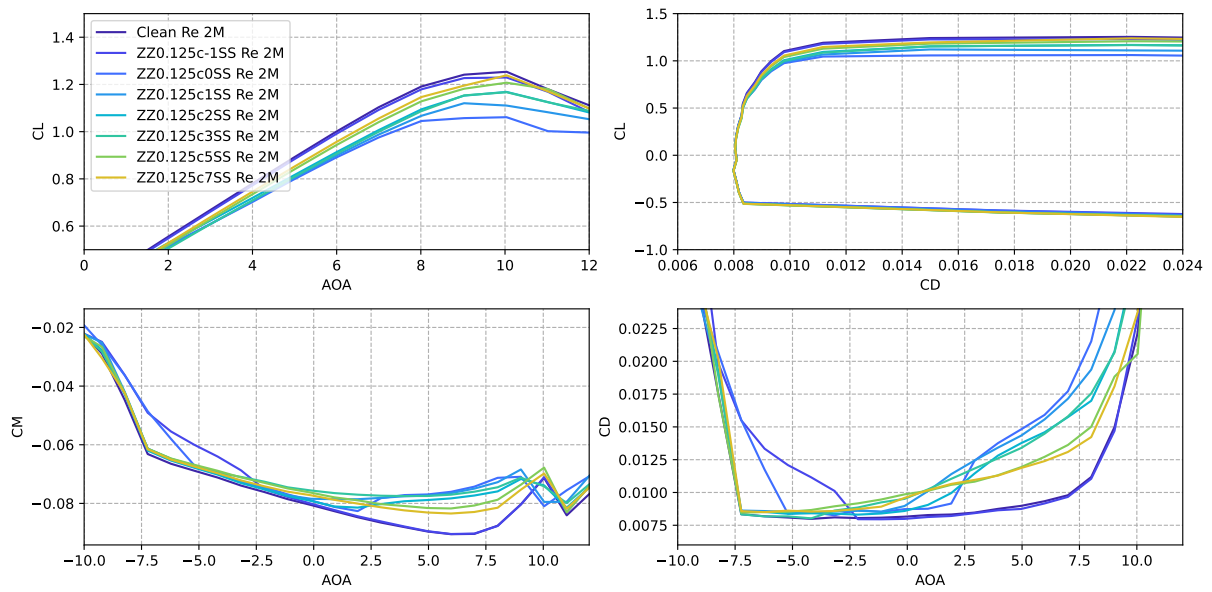


**Figure A.29:** CL,CD,CM Polars for ZZT with  $125\mu\text{m}$  height and  $12\text{mm}$  width at  $\text{Re}=2\text{m}$  and for Locations= $[-1,0,1,2,3,5,7] \%x/c_{ss}$

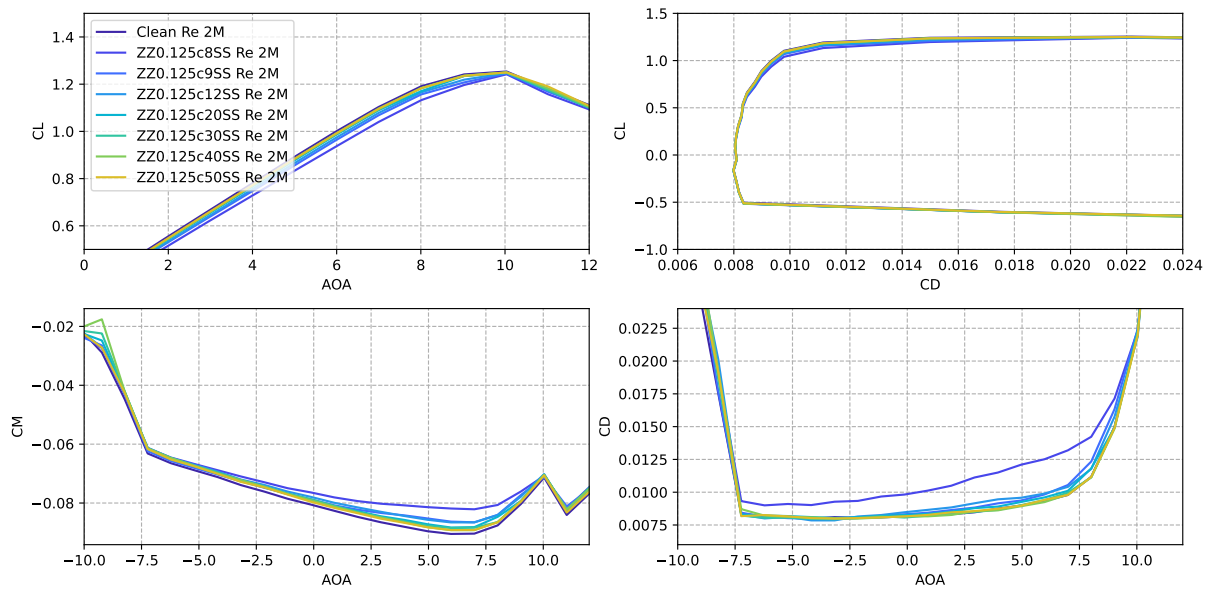


**Figure A.30:** CL,CD,CM Polars for ZZT with  $125\mu\text{m}$  height and  $12\text{mm}$  width at  $\text{Re}=2\text{m}$  and for Locations= $[8,9,12,20,30,40] \%x/c_{ss}$

### A.3. 3 Regions for $\Delta CP$

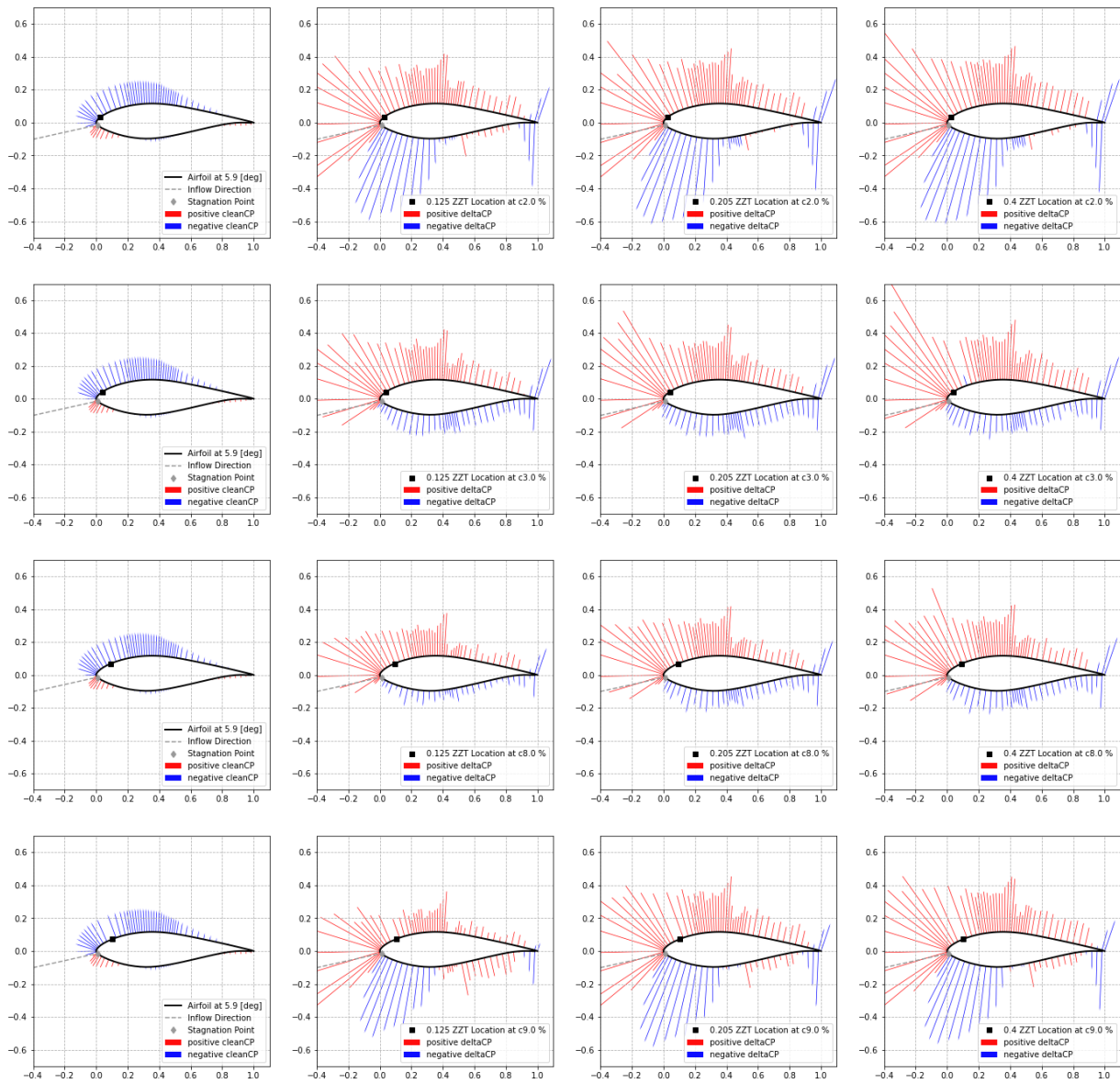


Figure A.31: 3 Regions at  $Re=2e6$  at  $\alpha = 6^\circ$

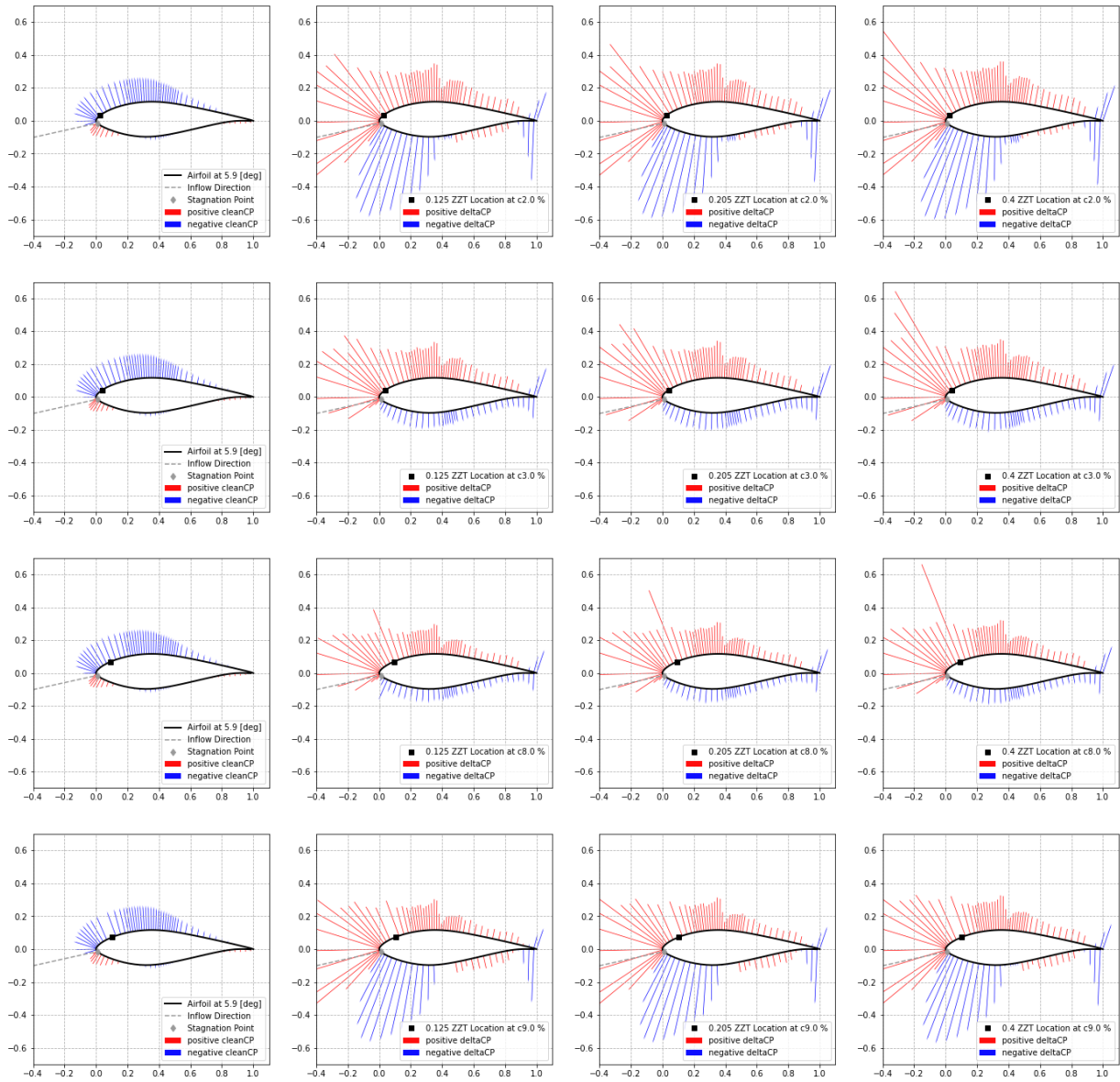


Figure A.32: 3 Regions at  $Re=4e6$  at  $\alpha = 6^\circ$

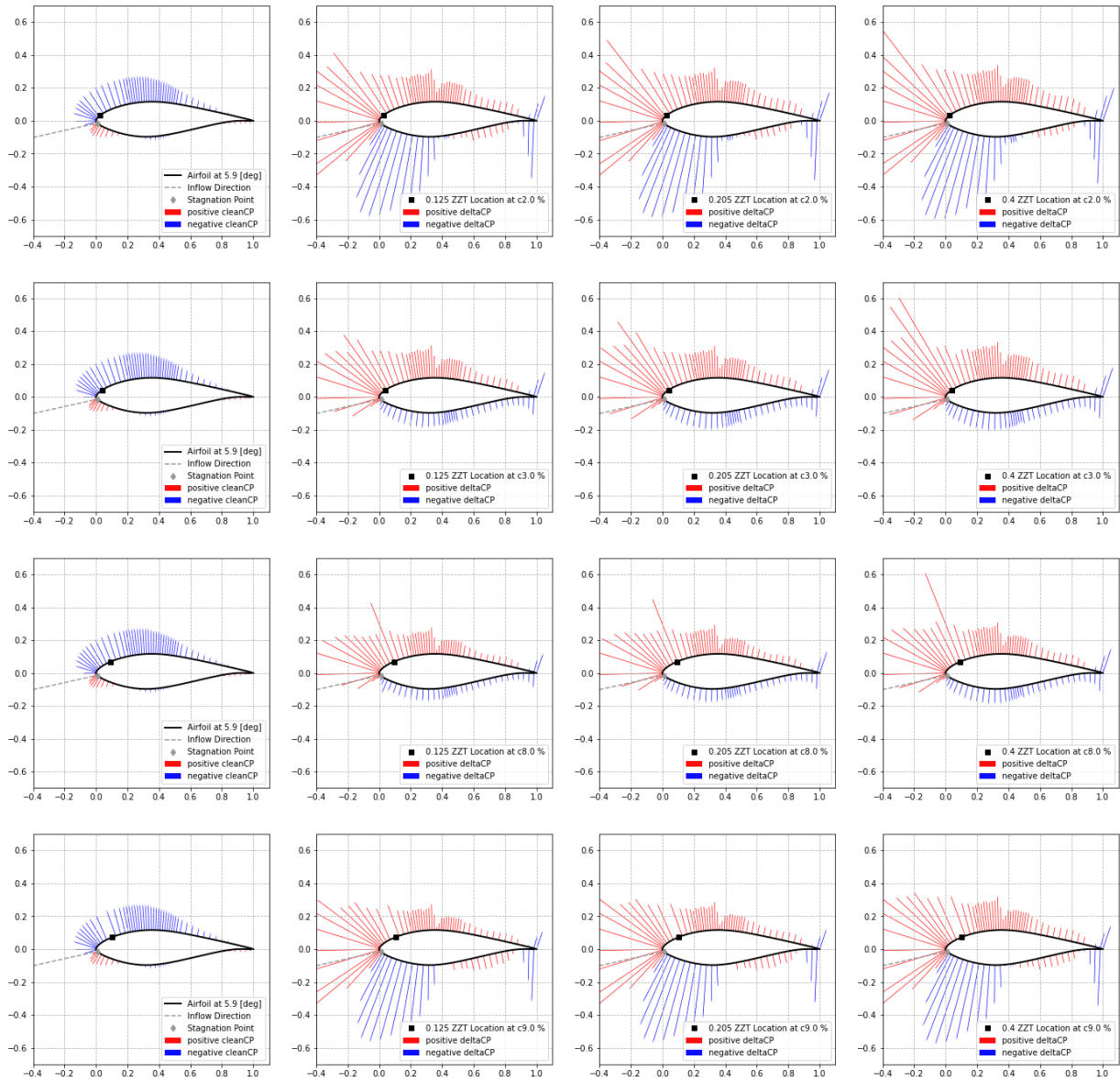


Figure A.33: 3 Regions at  $Re=6e6$  at  $\alpha = 6^\circ$

### A.4. FW vs BW Step

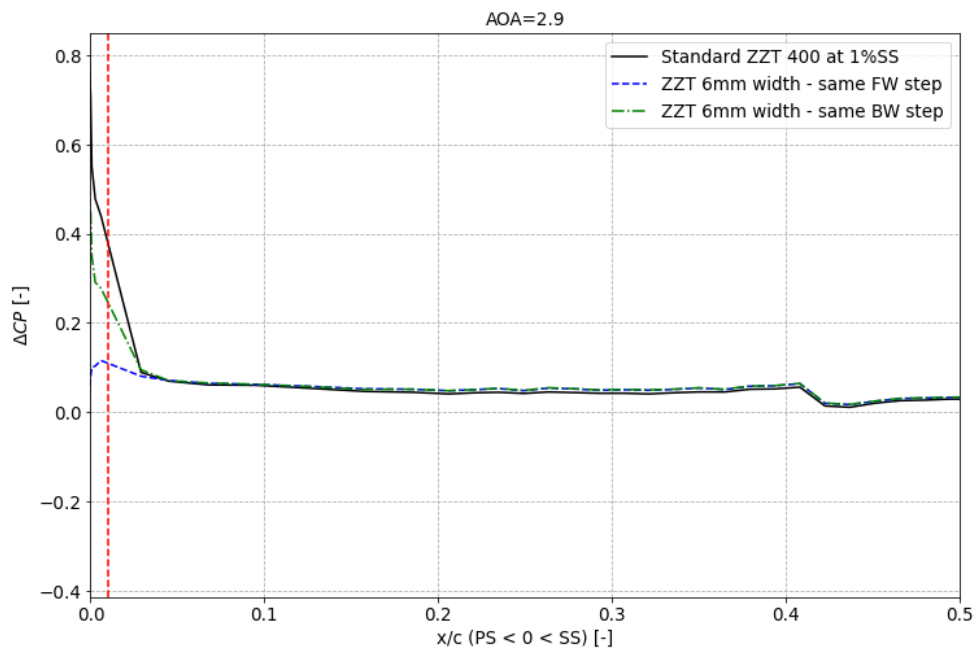


Figure A.34: Forward vs Backward step  $x/c=1\%$

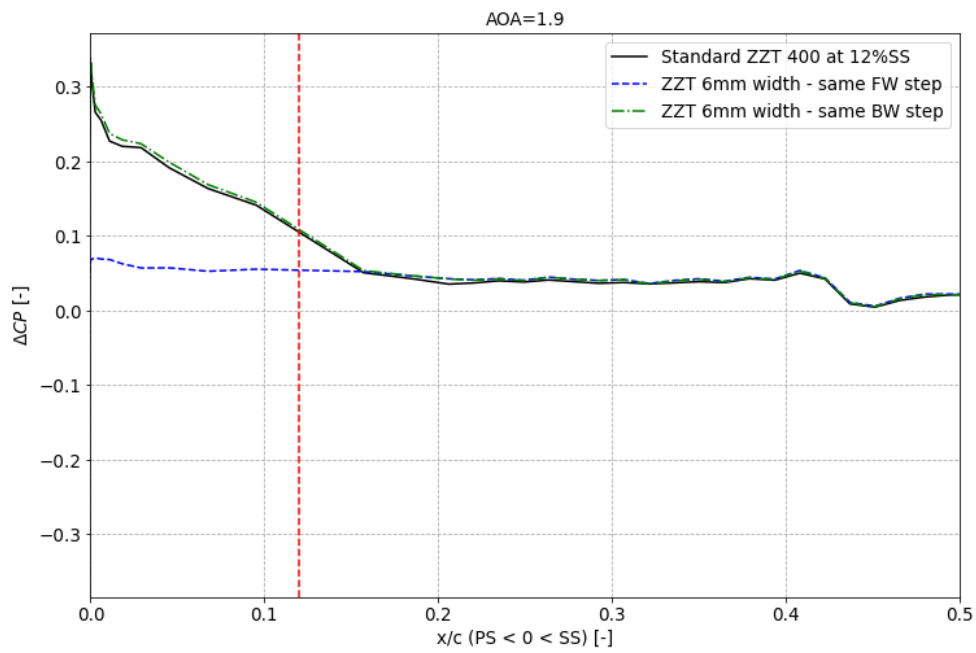


Figure A.35: Forward vs Backward step  $x/c=12\%$

### A.5. Reference Roughness

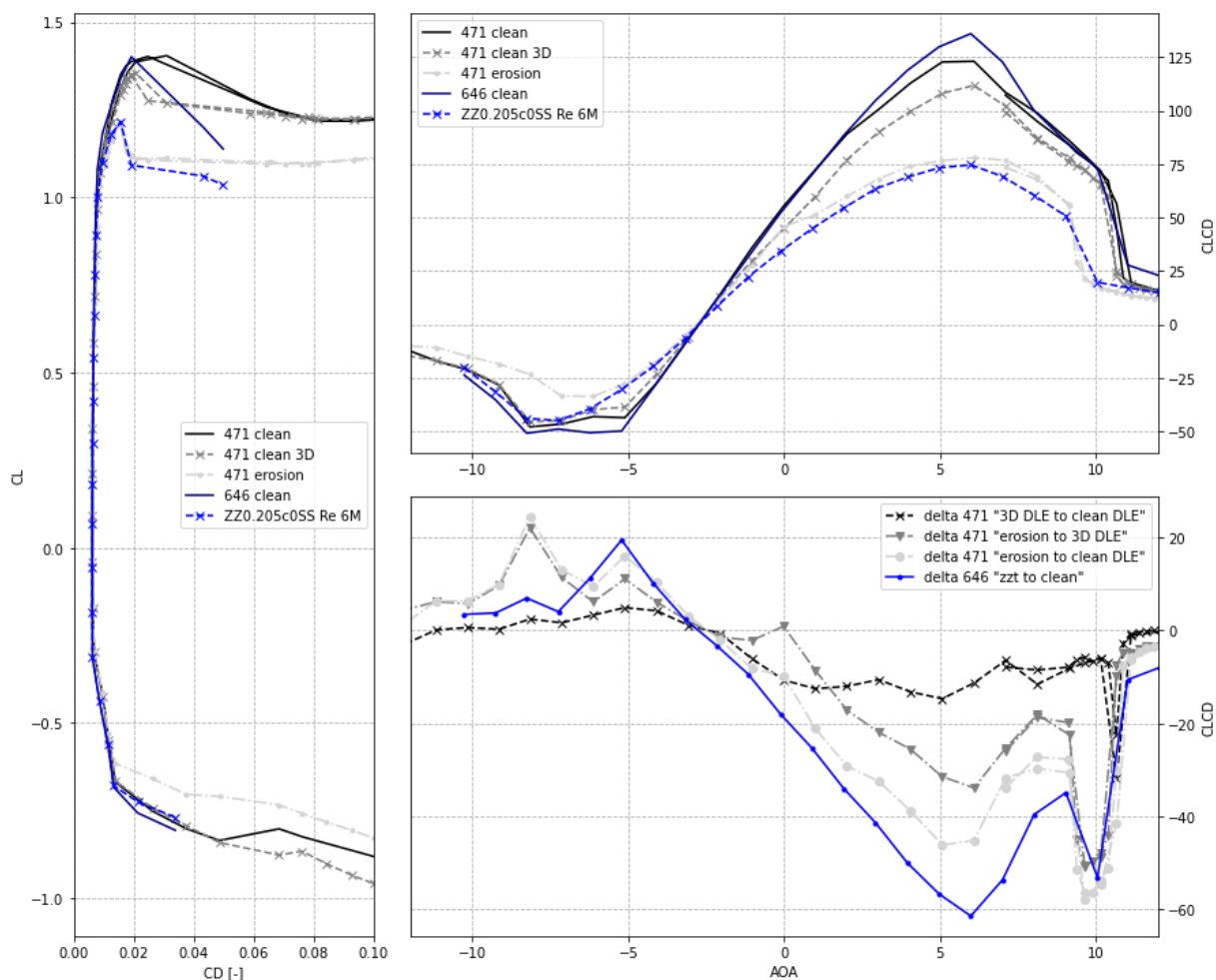


Figure A.36: DLE comparison ZZT205c0

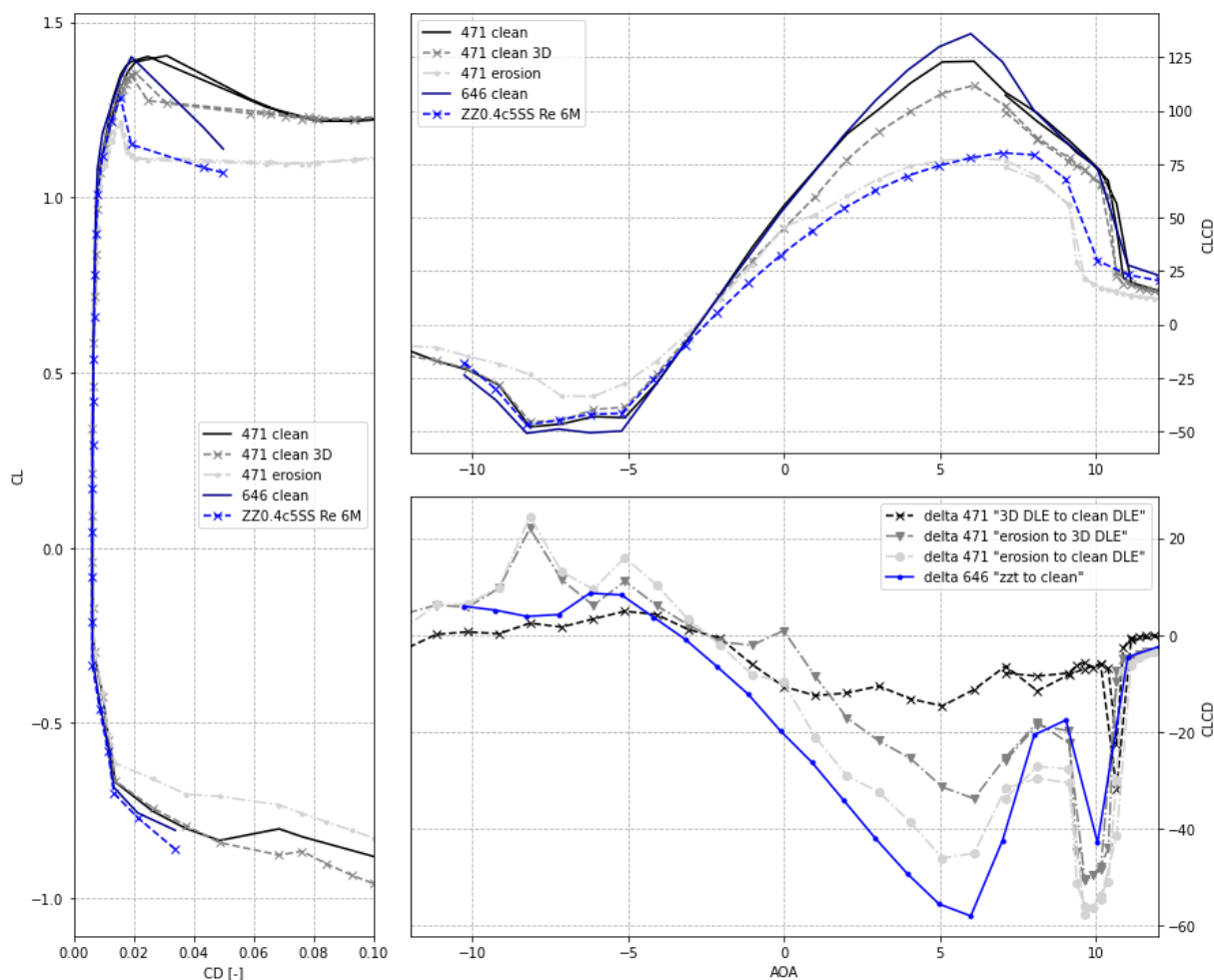


Figure A.37: DLE comparison ZZT400c5

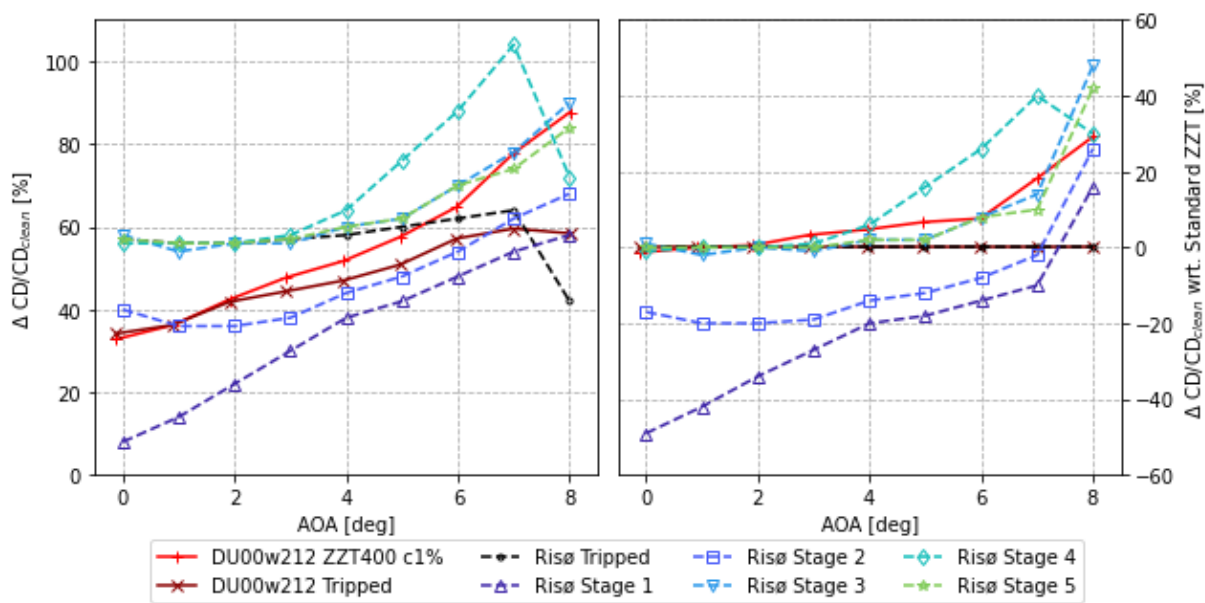


Figure A.38: CD comparison with Gaudern et al. [7] at Re=2e6

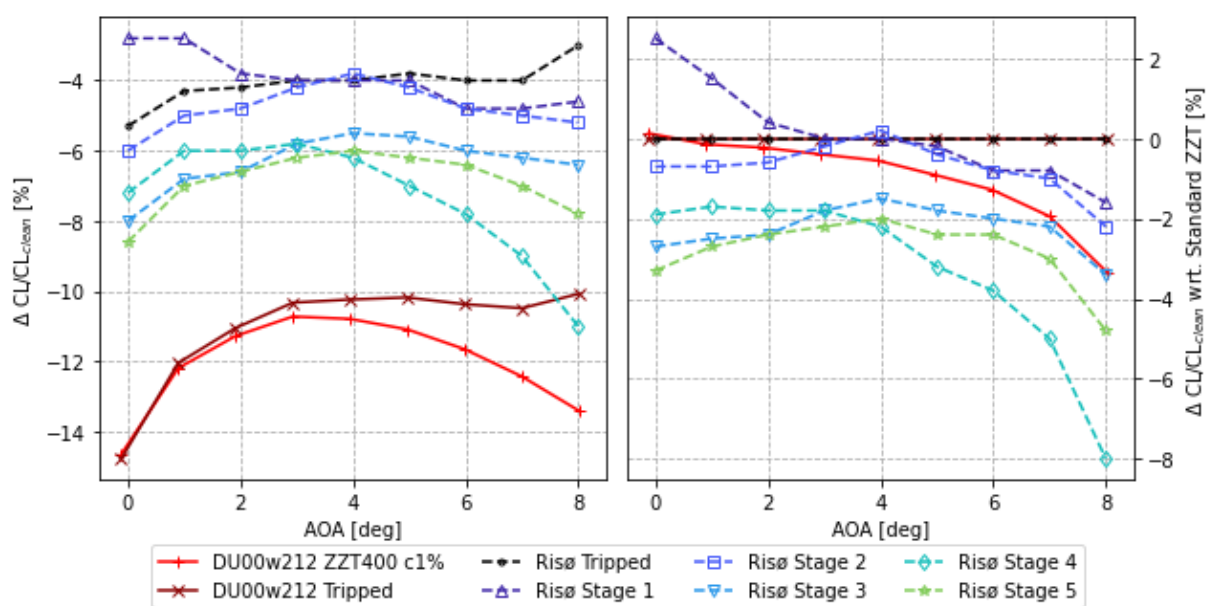


Figure A.39: CL comparison with Gaudern et al. [7] at Re=2e6

# References

- [1] M H Keegan, D H Nash, and M M Stack. “On erosion issues associated with the leading edge of wind turbine blades”. In: *Journal of Physics D: Applied Physics* 46.38 (Sept. 2013), p. 21. DOI: 10.1088/0022-3727/46/38/383001. URL: <https://doi.org/10.1088/0022-3727/46/38/383001>.
- [2] Mohammed G. Khalfallah and Aboelyazied M. Koliub. “Effect of dust on the performance of wind turbines”. In: *Desalination* 209.1 (2007). The Ninth Arab International Conference on Solar Energy (AICSE-9), Kingdom of Bahrain, pp. 209–220. ISSN: 0011-9164. DOI: <https://doi.org/10.1016/j.desal.2007.04.030>.
- [3] Christian Bak et al. “What is the critical height of leading edge roughness for aerodynamics?”. In: *Journal of Physics: Conference Series* 753.2 (Sept. 2016), p. 022023. DOI: 10.1088/1742-6596/753/2/022023.
- [4] Wind Europe. “Offshore wind energy 2022 mid-year statistics”. This report summarises offshore installations from 1 January 2022 to 30 June 2022. August 2022.
- [5] Thomas Hjort. “Innovation Zone: We have the Power - don't lose it (Vattenfall)”. Green Power Wind Energy Denmark 2022. 2022. URL: <https://greenpowerdenmark.dk/kalender/wind-energy-denmark-2022>.
- [6] Agrim Sareen, Chinmay A. Sapre, and Michael S. Selig. “Effects of leading edge erosion on wind turbine blade performance”. In: *Wind Energy* 17.10 (2014). Cited by: 171, pp. 1531–1542. DOI: 10.1002/we.1649.
- [7] N Gaudern. “A practical study of the aerodynamic impact of wind turbine blade leading edge erosion”. In: *Journal of Physics: Conference Series* 524.1 (June 2014), p. 012031. DOI: 10.1088/1742-6596/524/1/012031.
- [8] Trong Bui, David Oates, and Jose Gonzalez. “Design and evaluation of a new boundary-layer rake for flight testing”. In: *38th Aerospace Sciences Meeting and Exhibit*. DOI: 10.2514/6.2000-503.
- [9] Alexander Meyer Forsting et al. *LERAP: Leading Edge Repair and Performance. Commissioned by The Energy Innovation Cluster*. English. DTU Wind Energy I I-1212. DTU Wind and Energy Systems, 2022. DOI: 10.11581/DTU.00000264.
- [10] Michael F. Kerho and Michael B. Bragg. “Airfoil Boundary-Layer Development and Transition with Large Leading-Edge Roughness”. In: *AIAA Journal* 35.1 (1997), pp. 75–84. DOI: 10.2514/2.65. eprint: <https://doi.org/10.2514/2.65>. URL: <https://doi.org/10.2514/2.65>.
- [11] Chris Langel et al. “Analysis of the Impact of Leading Edge Surface Degradation on Wind Turbine Performance”. In: Jan. 2015, p. 13. DOI: 10.2514/6.2015-0489.
- [12] R.P.J.O.M. van Rooij and W.A. Timmer. “Roughness sensitivity considerations for thick rotor blade airfoils”. In: Cited by: 26. 2003. URL: <https://www.scopus.com/inward/record.uri?eid=2-s2.0-84894774439%5C&partnerID=40%5C&md5=b7843a172af207d95e26acd775c33934>.

- [13] Piet Verschuren and Hans Doorewaard. *Designing a Research Project*. second. Amsterdam: Eleven International Publishing, 2013.
- [14] Edward White et al. "Leading-Edge Roughness Effects on 63(3)-418 Airfoil Performance". In: *49th AIAA Aerospace Sciences Meeting including the New Horizons Forum and Aerospace Exposition*, pp. 1–13. DOI: 10.2514/6.2011-352.
- [15] Robert S. Ehrmann et al. "Realistic leading-edge roughness effects on airfoil performance". In: Cited by: 25; All Open Access, Green Open Access. 2013. DOI: 10.2514/6.2013-2800.
- [16] Emil Krog Kruse, Christian Bak, and Anders Smærup Olsen. "Wind tunnel experiments on a NACA 633-418 airfoil with different types of leading edge roughness". In: *Wind Energy* 24.11 (2021), pp. 1263–1274. DOI: <https://doi.org/10.1002/we.2630>.
- [17] O.S. Ozcakmak et al. "Inflow Turbulence and Leading Edge Roughness Effects on Laminar-Turbulent Transition on NACA 63-418 Airfoil". In: vol. 1037. 2. Cited by: 9; All Open Access, Bronze Open Access, Green Open Access. 2018. DOI: 10.1088/1742-6596/1037/2/022005.
- [18] M.R. Soltani, A.H. Birjandi, and M. Seddighi Moorani. "Effect of surface contamination on the performance of a section of a wind turbine blade". In: *Scientia Iranica* 18.3 (2011), pp. 349–357. ISSN: 1026-3098. DOI: <https://doi.org/10.1016/j.scient.2011.05.024>.
- [19] W.A. Timmer and A.P. Schaffarczyk. "The effect of roughness at high Reynolds numbers on the performance of aerofoil DU 97-W-300Mod". In: *Wind Energy* 7.4 (2004). Cited by: 68, pp. 295–307. DOI: 10.1002/we.136.
- [20] W.H Rae Barlow J.B. and A. Pope. "Low-Speed Wind Tunnel Testing". In: 3rd, pp. 328–366. DOI: ISBN:978-0-471-55774-6.
- [21] D. Althaus. "Der Laminarwindkanal des Instituts für Aerodynamik und Gasdynamik." German. In: (1980). Originalfassung 1964.
- [22] W.G. Vincent H.J. Allen. "Wall Interference in a Two-Dimensional-Flow Wind Tunnel with Consideration of the Effect of Compressibility". English. In: (1944).
- [23] Philippe Giguère and Michael S. Selig. "Aerodynamic effects of leading-edge tape on aerofoils at low Reynolds numbers". In: *Wind Energy* 2.3 (1999), pp. 125–136. DOI: [https://doi.org/10.1002/\(SICI\)1099-1824\(199907/09\)2:3<125::AID-WE23>3.0.CO;2-5](https://doi.org/10.1002/(SICI)1099-1824(199907/09)2:3<125::AID-WE23>3.0.CO;2-5).
- [24] Albert L Braslow. "Use of grit-type boundary-layer transition trips on wind-tunnel models". In: *NACA-TN-D-3579* (1966), pp. 1–19. URL: <https://ntrs.nasa.gov/citations/19660026829>.
- [25] J. P. Bons. "A Review of Surface Roughness Effects in Gas Turbines". In: *Journal of Turbomachinery* 132.2 (Jan. 2010). 021004. ISSN: 0889-504X. DOI: 10.1115/1.3066315.
- [26] Eugene C Braslow Albert L ; Knox. "Simplified Method for Determination of Critical Height of Distributed Roughness Particles for Boundary-layer Transition at Mach Numbers from 0 to 5". In: *NACA-TN-4363* (1958), pp. 1–19. URL: <https://ntrs.nasa.gov/citations/19930085292>.
- [27] P. S. Klebanoff and K. D. Tidstrom. "Mechanism by Which a Two-Dimensional Roughness Element Induces Boundary-Layer Transition". In: *The Physics of Fluids* 15.7 (July 1972), pp. 1173–1188. ISSN: 0031-9171. DOI: 10.1063/1.1694065.

- [28] Ponnampalam Balakumar and Prahladh S. Iyer. "Laminar to Turbulence Transition in Boundary Layers Due to Tripping Devices". In: *AIAA Scitech 2021 Forum*. DOI: 10.2514/6.2021-1948.
- [29] Michel Labib, Ruxandra Botez, and Andrei Popov. "Determination of the Transition Point on the Upper Surface of a Wing Airfoil". In: Apr. 2007.
- [30] Walter Tollmien et al. "Über Flüssigkeitsbewegung bei sehr kleiner Reibung". In: *Ludwig Prandtl Gesammelte Abhandlungen: zur angewandten Mechanik, Hydro- und Aerodynamik*. Ed. by F. W. Riegels. Berlin, Heidelberg: Springer Berlin Heidelberg, 1961, pp. 575–584. ISBN: 978-3-662-11836-8. DOI: 10.1007/978-3-662-11836-8\_43.
- [31] Snorri Gudmundsson. "Chapter 8 - The Anatomy of the Airfoil". In: *General Aviation Aircraft Design*. Ed. by Snorri Gudmundsson. Boston: Butterworth-Heinemann, 2014, pp. 235–297. ISBN: 978-0-12-397308-5. DOI: <https://doi.org/10.1016/B978-0-12-397308-5.00008-8>.
- [32] J. G. Schepers et al. "Final results from the EU project AVATAR: aerodynamic modelling of 10 MW wind turbines". English. In: vol. 1037. 2. IOP Publishing, 2018. DOI: 10.1088/1742-6596/1037/2/022013.
- [33] Marijn Leendert Willy Veraart. "Deterioration in aerodynamic performance due to leading edge rain erosion". In: *Master Thesis - EWEM at TUDelft and DTU (2017)*, pp. 1–120.

Technical  
University of  
Denmark

Frederiksborgvej, 339  
4000 Roskilde  
Tlf. 4525 1700

[www.vindenergi.dtu.dk](http://www.vindenergi.dtu.dk)